Conversion of Chlorinated Waste Streams from the Production of Polyvinyl Chloride over La-Based Catalysts

Aloysius W. A. M. van der Heijden

A.W.A.M. van der Heijden
Conversion of Chlorinated Waste Streams from the Production of Polyvinyl Chloride over La-Based Catalysts

ISBN: 978-90-8891-0388

Cover- en binnenwerk-layout door Lai Ting Tang
Drukkerij Proefschriftmaken.nl, Oisterwijk

Conversion of Chlorinated Waste Streams from the Production of Polyvinyl Chloride over La-Based Catalysts

De omzetting van gechloreerde afvalstromen afkomstig van de productie van polyvinylchloride over La-bevattende katalysatoren

(met een samenvatting in het Nederlands)

Proefschrift

ter verkrijging van de graad van doctor aan de Universiteit Utrecht op gezag van de rector magnificus, prof. dr. J.C. Stoof, ingevolge het besluit van het college voor promoties in het openbaar te verdedigen op woensdag 21 mei 2008 des middags te 12.45 uur

door

Aloysius Wilhelmus Antonius Maria van der Heijden

geboren op 14 juni 1980 te Bergeijk

A.W.A.M. van der Heijden
Conversion of Chlorinated Waste Streams from the Production of Polyvinyl Chloride over La-Based Catalysts

Promotor: Prof. dr. ir. B.M. Weckhuysen

Dit proefschrift werd mogelijk gemaakt met financiële steun van een VICI/NWO-CW subsidie

"I have learned more from my mistakes than from my successes"

Sir Humphrey Davy

Contents

1

Reactions Steps and Related Chlorinated Waste Streams in the Industrial Production of PVC: The Potential of La-based Catalysts for Chlorine Management

Chlorinated C_1 and C_2 hydrocarbons (CHC_{1-2}) are used in many applications. Particularly, the production of polyvinyl chloride (PVC), which accounts for one third of all chlorine consumption, is built up of several reaction steps involving chlorinated hydrocarbons (CHCs). In this introductory chapter, the catalytic conversion of chlorinated waste streams resulting from PVC production using basic oxides is reviewed. First, the use and environmental effects of chlorinated CHC_{1-2} are dealt with. In a second part, the reaction steps and the compounds involved in the production of C_2H_3Cl, which is the monomer for the production of PVC, are discussed. Finally, an overview is provided on the potential of basic oxides for the destruction of CHCs. Special emphasis will be on La_2O_3-based catalysts. The chapter ends with an outline and motivation of this PhD thesis.

Chapter 1

Introduction

Chlorine is one of the most important chemicals, which is used for the manufacturing of numerous commercial products. In 2004, chlorine production in whole Europe made an all time record of 10.35 million tons.[1] The largest part of the chlorine is used for the production of organic compounds; the production makes up for 85 % of the chlorine applications (Figure 1).[1] In fact, the polyvinyl chloride (PVC) industry is the main consumer of chlorine with more than one third of the chlorine production. Chlorination of organic molecules with chlorine results in activation of the molecules for reactions. This, combined with the fact that the raw material (sodium chloride) for chlorine is available in an almost unlimited amount, makes chlorine chemistry well-suited for large-scale synthesis.

The C-Cl bond in organic chlorinated molecules is covalent in nature. Nevertheless, the strong electronegative chlorine produces a polar component with a shift of the negative charge in the direction of the chlorine: $R_3C^{\partial+}$-$Cl^{\partial-}$. The energy of the C-Cl bond is relatively low; the manner of dissociation can be heterolytic (ionic) and homolytic (radical), as shown in Reaction Eqs. (1) and (2), respectively.[2]

$$R_3C\text{-}Cl \rightarrow R_3C^+ + Cl^- \quad (1)$$

$$R_3C\text{-}Cl \rightarrow R_3C\bullet + Cl\bullet \quad (2)$$

This can be used to replace the chlorine in a chlorinated molecule by a different atom or functional group. Thus chlorinated hydrocarbons (CHCs) can be used as components for a whole variety of synthesis reactions and intermediates. Scheme 1 shows the molecular structures of chlorinated methanes, ethanes, ethenes and oxygen-containing organic compounds.

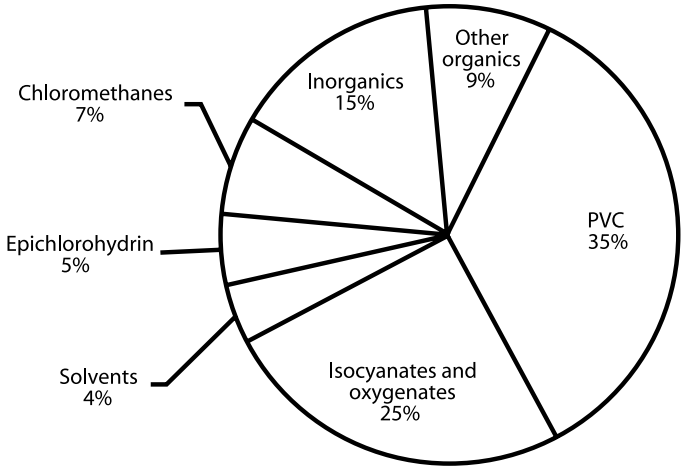

Figure 1. Overview of the European chlorine applications in 2004.[1]

The potential of La-based catalysts for chlorine management

a *Chlorinated methanes*


tetrachloromethane (carbon tetrachloride)


trichloromethane


dichloromethane


chloromethane

b *Chlorinated ethanes*


hexachloroethane


pentachloroethane


1,1,2,2-tetra-chloroethane


1,1,1,2-tetra-chloroethane


1,1,2-trichloroethane


1,1,1-trichloroethane


1,2-dichloroethane


1,1-dichloroethane


chloroethane

c *Chlorinated ethenes*


tetrachloroethene


trichloroethene


trans-1,2-dichloroethene


cis-1,2-dichloroethene


1,1-dichloroethene


chloroethene

d *Oxygen- and Chlorine-containing compounds*

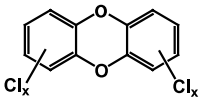
polychlorodibenzo-1,4-dioxin

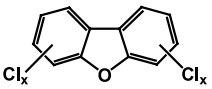
polychlorodibenzofuran


carbonyl chloride


formyl chloride

Scheme 1. Molecular structures and IUPAC names of chlorinated (a) methanes, (b) ethanes, (c) ethenes and (d) some oxygen-containing organic compounds.

Chapter 1

Chlorinated C_1 and C_2 (CHC_{1-2}) are especially useful for industrial chemical reactions. This is illustrated by the various uses of the CHC_{1-2}, shown in Table 1. Several compounds are used for the production of polymers. C_2H_3Cl and 1,1-$C_2H_2Cl_2$ are used as monomers for the synthesis of PVC and polyvinylidene chloride (PVDC), respectively. This is illustrated by Reaction Eqs. (3) and (4). In addition, 1,1-$C_2H_2Cl_2$ is used as a copolymer of C_2H_3Cl, acetonitrile, methacrylonitrile and methacrylate. CH_3Cl is also used as a main reactant to produce silicon polymers via the Rochow synthesis.[2]

Table 1. Main applications or uses of chlorinated CHC_{1-2} compounds.[2]

Chemical formula	**Uses / Application**
CCl_4	• Process agent • Chemical intermediate
$CHCl_3$	• Production of HCFC 22
CH_2Cl_2	• Paint stripper • Aerosol spray propellant • Degreaser • Blowing agent for polyurethane foam
CH_3Cl	• Silicone polymer production • Intermediate in drug manufacturing • Methylating agent
1,1,2-$C_2H_3Cl_3$	• Metal degreasing • Production of HCFC 141b and 142b
1,1-$C_2H_4Cl_2$	• Precursor for trichloroethanes
1,2-$C_2H_4Cl_2$	• C_2H_3Cl production • Extracting agent • Solvent
CH_5Cl	• Ethylating agent
C_2Cl_4	• Dry cleaning solvent • Metal degreasing • Textile finishing, dying and extracting processes
C_2HCl_3	• Metal degreasing • Extractant • Degreasing in textile industry • Solvent formulation for rubbers, paint strippers and paints • Intermediate in dye, colour, HCFC and HFC production
1,1-$C_2H_2Cl_2$	• PVDC production • Copolymer of C_2H_3Cl, acetonitrile, methacrylonitrile and methacrylate
C_2H_3Cl	• PVC production

$$n\ CH_2{=}CHCl \rightarrow -(CH_2\text{-}CHCl)_n- \quad (3)$$

$$n\ CHCl{=}CHCl \rightarrow -(CHCl\text{-}CHCl)_n- \quad (4)$$

Other $CHC_{1\text{-}2}$ are used as a building block in industrial organic reactions. CH_3Cl is used as an intermediate in drug manufacturing. It is also used as a methylating agent, and similarly C_2H_5Cl is used as an ethylating agent. $CHCl_3$ and 1,1,1-$C_2H_3Cl_3$ are used for the production of refrigerants. 1,2-$C_2H_4Cl_2$ is converted into vinyl chloride by dehydrochlorination via thermal cracking and is therefore also important for the production of PVC. The $CHC_{1\text{-}2}$ are also widely used because of their ability to dissolve organic compounds and their volatility; they are used as degreaser, industrial solvent, blowing agent, propellant, paint stripper, extractant and dry cleaning agent.

Once, $CHC_{1\text{-}2}$ were used in many commercial applications, e.g. as refrigerants, spray can propellants, insecticides and pesticides. However, in the last decades their toxic properties and effect on the environment have become better understood. Table 2 shows that, except for 1,1,1-$C_2H_3Cl_3$, all compounds listed are either known or at least suspected carcinogens.[3, 4] The Indiana Relative Chemical Hazard (IRHC) score is used to classify the effect of a compound on human health, ecosystems and environmental health generally.[5] All CHCs listed in Table 2 have relatively high IRCH scores. Therefore, restrictions on the use and emission of several $CHC_{1\text{-}2}$ have been made to reduce the concentrations in water and air worldwide.[6, 7] Particularly, the production and processing of carbon tetrachloride and 1,1,1-$C_2H_3Cl_3$ are severely restricted by the Montreal Protocol as well as by the Intergovernmental Panel on Climate Change.[8, 9] As a result of regulation and introduction of chlorine-free alternatives, the use of $CHC_{1\text{-}2}$ in commercial applications has greatly reduced. Therefore, the use of $CHC_{1\text{-}2}$ is almost entirely attributed to industrial applications.

Table 2. Carcinogenicity and IRCH score of common chlorinated $CHC_{1\text{-}2}$. The Indiana Relative Chemical Hazard (IRCH) Score indicates how a chemical compares with others in terms of its capacity to impact human health, ecosystems, or environmental health generally. The IRCH scores of $COCl_2$ and CO_2 are provided as reference.

Chemical Formula	Carcinogenic	IRCH Score
CCl_4	Yes	42
$CHCl_3$	Yes	36
CH_2Cl_2	Yes	30
CH_3Cl	Suspected	30
1,1,1-$C_2H_3Cl_3$	No	37
1,1-$C_2H_4Cl_2$	Yes	24
1,2-$C_2H_4Cl_2$	Yes	39
C_2H_5Cl	Yes	37
C_2Cl_4	Yes	38
C_2HCl_3	Yes	41
1,1-$C_2H_2Cl_2$	Suspected	41
C_2H_3Cl	Yes	49
$COCl_2$	No	37
CO_2	No	4

Ironically, the same quality that makes CHCs a favourite for industrial organic chemists, is also the reason for environmental concern and call for a ban on chlorine.[10] The high electron affinity of chlorine makes CHCs effective building blocks for the synthesis of molecular structures. On the other hand, the electron affinity stabilizes some chemical structures, which are not broken down and remain in the atmosphere when emitted. They are then able to reach the stratosphere resulting in ozone depletion. Other compounds, e.g. polychlorinated dioxins and furans (Scheme 1d), combine persistence with accumulation in fat tissue, where they can build up to toxic levels.[11] Even CHCs that are not persistent themselves, can decompose into harmful products.

The two-faced character of chlorine is best seen in the production of PVC. The high demand for PVC also results in the formation of large quantities of $CHC_{1\text{-}2}$ as by-products. These by-products have to be destroyed to prevent emission and, consequently, the previously mentioned environmental effects. This introductory chapter starts with an overview of the C_2H_3Cl production process, focusing on the chemical reactions, products and process conditions. Next, the catalytic destruction of CHCs over basic oxides is reviewed. The focus will be on La_2O_3-based materials. The chapter ends with an outline and motivation of the PhD thesis.

Vinyl Chloride Monomer Production: Reactions, Products and Process Conditions

PVC is the second most used plastic in the world after polyethyene (PE). In Europe, more than one third of all chlorine is used to sythesize this product and the annual production of PVC has steadily increased in the last decade.[1] C_2H_3Cl is the main reactant for the industrial synthesis of PVC. The production of C_2H_3Cl is built up out of several steps.[2] An overview is given in Figure 2.

The first step is the chlorination of ethylene into 1,2-$C_2H_4Cl_2$; this is done by either direct chlorination or oxychlorination. Next, the crude 1,2-$C_2H_4Cl_2$ is purified and the by-products are separated into fractions. The purified 1,2-$C_2H_4Cl_2$ is then thermally cracked to C_2H_3Cl. A final purification step yields C_2H_3Cl which is stored and/or used for polymerization into PVC. In this purification step, HCl and 1,2-$C_2H_4Cl_2$ are recovered and the remaining by-products are separated. The by-product mixture contains many $CHC_{1\text{-}2}$, which are not commercially attractive for recovery and are processed as waste. In what follows, we will discuss the different reaction steps in more detail.

Chlorination / Oxychlorination of Ethylene into 1,2-$C_2H_4Cl_2$

In the direct chlorination reaction, chlorine is used to convert ethylene into 1,2-$C_2H_4Cl_2$ (Reaction Eq. (5)). Figure 3 shows the diagram of an industrial reactor used for the direct chlorination of ethylene into 1,2-$C_2H_4Cl_2$.[12-14] This is a bubble-column with external loop used

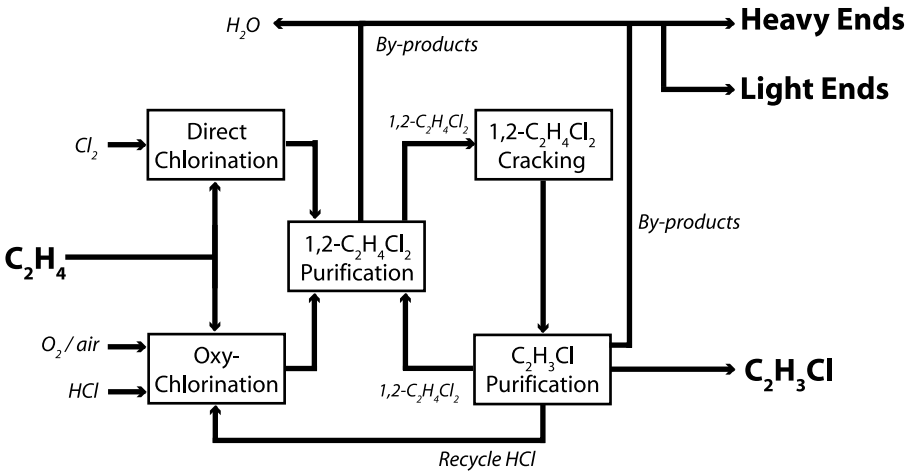

Figure 2. Schematic overview of the C_2H_3Cl production process.

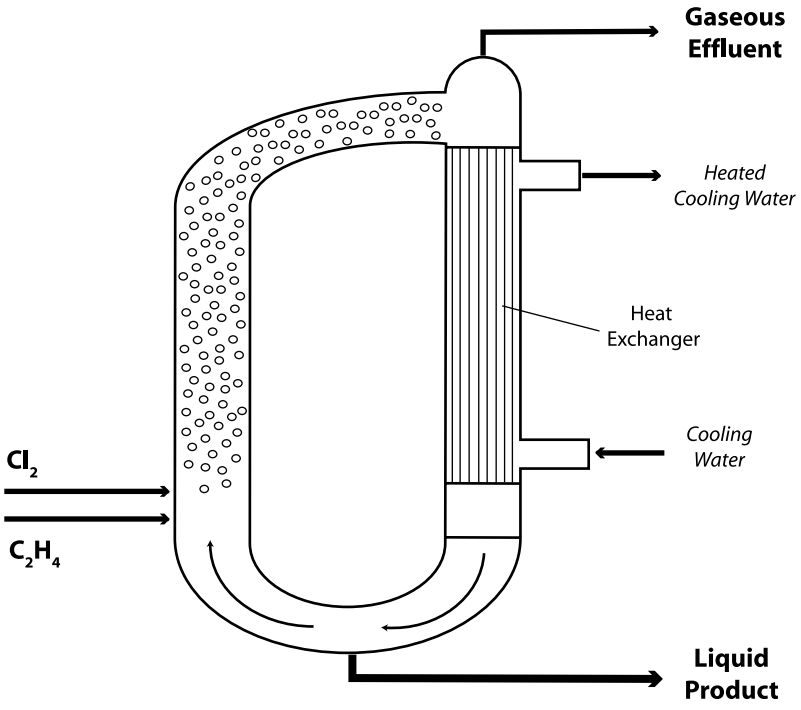

Figure 3. Diagram of a bubble-column reactor with external loop used for the industrial production of $1,2\text{-}C_2H_4Cl_2$ via the direct chlorination of ethylene.

for low-temperature chlorination, which is applied in 70 % of the licenses issued for this process. Ethylene and chlorine are both in gaseous state and are fed to the reactor. Here, they dissolve and diffuse in liquid 1,2-$C_2H_4Cl_2$. In the liquid phase the exothermic reaction of chlorine and ethylene occurs, increasing the temperature. The difference in density between the heterogenic phase and thermal-exchange zones enables the recirculation of the liquid phase. In this way, the reaction temperature (50-70 °C) can be controlled by means of the heat exchanger. The main by-product is 1,1,2-trichloroethane, which is formed according to Reaction Eq. (6). A useful catalyst is $FeCl_3$, which is soluble in the reaction medium and favours the selectivity towards 1,2-$C_2H_4Cl_2$ production. High temperature direct chlorination utilizes the reaction heat to distill the 1,2-$C_2H_4Cl_2$. However, it is less selective than the low temperature process, even though the energy input is lower.

$$C_2H_4 + Cl_2 \rightarrow 1,2\text{-}C_2H_4Cl_2 \quad (5)$$

$$1,2\text{-}C_2H_4Cl_2 + Cl_2 \rightarrow 1,1,2\text{-}C_2H_3Cl_3 + HCl \quad (6)$$

For the synthesis of 1,2-$C_2H_4Cl_2$, oxychlorination (Reaction Eq. (7)) is often combined with direct chlorination to re-use HCl gas formed in the production of C_2H_3Cl. In this reaction, $CuCl_2$, supported on γ-alumina, is used as catalyst. The catalytic reaction mechanism follows a three step redox mechanism; 1) chlorination of ethylene by reduction of $CuCl_2$ (Reaction Eq. (8)), 2) oxidation of CuCl into an oxychloride (Reaction Eq. (9)) and 3) re-chlorination of the oxychloride into $CuCl_2$ (Reaction Eq. (10)).[15]

$$C_2H_4 + 2\ HCl + \tfrac{1}{2}\ O_2 \rightarrow 1,2\text{-}C_2H_4Cl_2 + H_2O \quad (7)$$

$$C_2H_4 + 2\ CuCl_2 \rightarrow 1,2\text{-}C_2H_4Cl_2 + 2\ CuCl \quad (8)$$

$$2\ CuCl + \tfrac{1}{2}\ O_2 \rightarrow Cu_2OCl_2 \quad (9)$$

$$Cu_2OCl_2 + 2\ HCl \rightarrow 2\ CuCl_2 + H_2O \quad (10)$$

The reaction is performed at 220-260 °C and 5-6 bar using both air and oxygen in fluid- or fixed-bed reactors.[16, 17] The main reaction is accompanied by various side reactions. Ethylene undergoes complete and incomplete combustion to give CO and CO_2, as illustrated by Reaction Eqs. (11) and (12).[18] In addition, several CHCs are formed in side-reactions.

$$C_2H_4 + 3\ O_2 \rightarrow 2\ CO_2 + 2\ H_2O \quad (11)$$

$$C_2H_4 + 2\ O_2 \rightarrow 2\ CO + 2\ H_2O \quad (12)$$

Apart from water, the contaminants mainly consist of CHCs. Table 3 shows the composition of crude 1,2-$C_2H_4Cl_2$ composed of both direct chlorination and oxychlorination reactor effluent.[19] Even though the reaction is highly selective towards 1,2-$C_2H_4Cl_2$ (~98 %), the production scale results in the formation of large quantities of by-products. The crude 1,2-$C_2H_4Cl_2$ mixture is purified using azeotropic distillation.[20] This enables the separation of compounds with small differences in boiling point. Two distillation fractions remain, the so-called light ends and heavy ends.

Table 3. Analysis of crude 1,2-$C_2H_4Cl_2$ obtained from direct chlorination and oxychlorination reactor effluent.[19]

Chemical formula	Concentration (wt%)	Contaminants only (wt%)
Product 1,2-$C_2H_4Cl_2$	98.35	-
Light ends		46.7
2-C_2H_4ClOH	0.09	5.4
CCl_4	0.11	6.6
$CHCl_3$	0.06	3.6
1,1-$C_2H_4Cl_2$	0.02	1.2
C_2H_5Cl	0.48	28.7
c-1,2-$C_2H_2Cl_2$	0.01	0.6
t-1,2-$C_2H_2Cl_2$	0.01	0.6
Heavy ends		53.3
1,1,2-$C_2H_3Cl_3$	0.50	29.9
CCl_3CHO	0.38	22.8
2,2-$C_2H_3Cl_2OH$	0.01	0.6

Thermal Cracking of 1,2-$C_2H_4Cl_2$ into C_2H_3Cl

The industrial synthesis of C_2H_3Cl is mainly based on the thermal decomposition (cracking) of 1,2-$C_2H_4Cl_2$ in a non-catalytic gas phase reaction (Reaction Eq. (13)).[2] The reaction is endothermic and occurs via a first order free radical chain mechanism. The reaction temperature is 500-550 °C and the pressure is kept at 20-30 bar. Figure 4 displays the schematic diagram of an 1,2-$C_2H_4Cl_2$ cracking furnace. The reactor, equipped with a burner, is designed for plug-flow conditions with tubes placed in the convective zone of the furnace.[2]

$$1,2\text{-}C_2H_4Cl_2 \rightarrow C_2H_3Cl + HCl \quad (13)$$

The liquid 1,2-$C_2H_4Cl_2$ is evaporated in the upper part of the furnace at 200 °C. Cracking takes place in the hotter lower part of the reactor. 1,2-$C_2H_4Cl_2$ cracking is typically carried out at 50-60 % conversion.[21] Therefore, the main constituents are 1,2-$C_2H_4Cl_2$, C_2H_3Cl and HCl. In addition, numerous gas phase by-products are formed in small amounts. Apart from the gaseous effluent, tars and coke are formed as by-products.

The crude C_2H_3Cl is cooled and quenched to remove HCl, which can be re-used in the oxychlorination process. In a second distillation column, C_2H_3Cl is drawn off as the main product. From the bottom of the column low-boiling products are removed first by distillation. In the last distillation tower, 1,2-$C_2H_4Cl_2$ is separated from the other CHCs and is recycled to the cracker via the 1,2-$C_2H_4Cl_2$ purification step. In Table 4, the reaction mixture composition resulting from the thermal cracking of 1,2-$C_2H_4Cl_2$ is shown. In this reaction,

several chlorinated CHC_{1-2} are formed, which are also divided into the light and heavy ends fraction. Moreover, several hydrocarbons are formed as a result of the radical reactions.

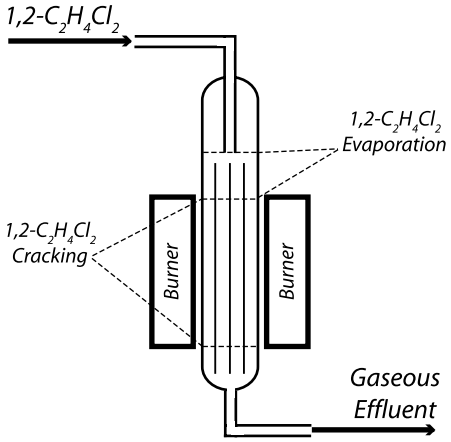

Figure 4. Diagram of an 1,2-$C_2H_4Cl_2$ cracking furnace used for the industrial preparation of C_2H_3Cl via thermal dehydrochlorination of 1,2-$C_2H_4Cl_2$.

Table 4. Reactor effluent analysis of 1,2-$C_2H_4Cl_2$ cracking pulse experiment.[21]

Chemical formula	Concentration (mol%)	Contaminants only (mol%)
Product	51.99	
HCl	25.93	-
C_2H_3Cl	26.05	-
Light ends	0.32	2.18
CH_3Cl	0.11	0.77
C_2H_5Cl	0.02	0.14
CH_2Cl_2	0.02	0.12
1,1-$C_2H_2Cl_2$	0.15	1.04
c-1,2-$C_2H_2Cl_2$	0.02	0.11
Heavy ends	0.03	0.20
C_4H_5Cl	0.03	0.20
Other by-products	14.30	97.61
CH_4	0.52	3.54
C_2H_4	12.47	85.15
C_2H_2	0.27	1.84
C_2H_6	0.04	0.30
C_2H_4O	0.60	4.06
C_4H_6/C_4H_4	0.40	2.71

Destruction of Light and Heavy Ends

Because of the previously discussed effects and the restrictions on the emission, the CHC_{1-2} have to be disposed of efficiently. However, CHCs are generally heat-resistant. Moreover, the CHC_{1-2} are able to react into dioxins (Scheme 1d) when heated to a temperature around 400-500 °C. Therefore, the light and heavy ends formed during the production of C_2H_3Cl are incinerated at >1000 °C.[22] Although this process is highly efficient (99 %), it is costly as a result of the high temperature. In addition, incineration leads to the loss of feedstock. Currently, incineration is commonly used for the disposal of light and heavy ends. However, to reduce the costs for the conversion of these waste streams and enable recycling of the compounds new techniques are investigated. Catalytic conversion of the CHC_{1-2} using a heterogeneous catalyst possesses great potential due to the practical applicability to industrial waste streams. However, chlorine is a known poison to numerous catalyst materials, which makes catalytic reactions with chlorinated compounds difficult or even cumbersome. In what follows, a state of the art of the catalytic destruction of CHCs over basic oxides is provided, especially focusing on La_2O_3-based materials.

Catalytic Conversion of CHCs: Catalytic Destruction and Destructive Adsorption over Lanthanide Oxide-Based Materials

Catalytic destruction can be divided in three reaction types: catalytic oxidation, hydrogenolysis and steam reforming. Catalytic oxidation is similar to traditional incineration techniques:[23] the substrate reacts with oxygen, although catalytic oxidation proceeds at lower temperature (300-550 °C). By complete oxidation, CO_2, H_2O, Cl_2 and HCl are formed exclusively, as shown in Reaction Eq. (14), because HCl and Cl_2 are equilibrated via the Deacon reaction (Reaction Eq. (15)). Catalysts for this reaction are noble metals[24-32] and transition metal oxides[33-40], which are supported by various materials, such as SiO_2, Al_2O_3, TiO_2, carbon[41], zeolites[42-46] and cordierites.[47, 48] Unsupported pillared clays, perovskites and zeolites are also active catalysts for catalytic oxidation.[49, 50] This reaction is hindered by side-reactions, involving chlorination of the catalyst and formation of CHCs.[51]

$$C_xH_yCl_z + (^{(y-z)}/_4 + x)\ O_2 \rightarrow x\ CO_2 + z\ HCl + {}^{(y-z)}/_2\ H_2O \quad (14)$$

$$Cl_2 + H_2O \rightarrow 2\ HCl + ½\ O_2 \quad (15)$$

Hydrogenolysis is the reaction in which C-Cl bonds are broken under formation of HCl in the presence of hydrogen at temperatures mostly below 200 °C (Reaction Eq. (16)). Pd and Pt catalysts, supported on SiO_2, Al_2O_3, TiO_2, ZrO_2 and carbon, are the most active for this reaction.[52-56] This technique offers several advantages, including the recycling of the reaction products. However, it is not used often, because of the fast deactivation of the catalyst by chlorine poisoning and coke formation.

$$C_xH_yCl_z + {}^z/_2\ H_2 \rightarrow C_xH_{y+z/2} + {}^z/_2\ HCl \quad (16)$$

Catalytic steam reforming of CHCs is a process which uses steam to remove chlorine from CHCs. This reaction yields HCl and oxygenated products, such as CO and CO_2. Two groups of catalyst materials can be distinguished: supported noble metals and supported metal oxides.[57-62] Support materials are SiO_2, Al_2O_3 and TiO_2. The temperature range is between 400 and 750 °C. Similar to the other catalytic systems, the catalyst is progressively poisoned by the CHCs and can slowly be regenerated by treatment with steam. It was found, however, that basic oxides are active and stable materials for the catalytic reforming of CHCs. The next section will deal with the catalytic destruction of chlorinated methanes over basic oxides, focusing on lanthanide oxides.

Destructive Adsorption and Catalytic Destruction of CCl_4 over Basic Oxides

Basic metal oxides, such as alkaline earth metal oxides and lanthanide oxides, can convert CHCs into oxygenated products, while they undergo transformation into the corresponding metal chlorides. This reaction is known as destructive adsorption and was pioneered by Klabunde and co-workers.[63-68] The reaction proceeds by adsorption of the gas phase CHC at the catalytic surface of the metal oxide. The chlorine atoms of the CHC are transferred to the solid and, in exchange, lattice oxygen is donated to the gas phase molecule. Most studies have been done on the destructive adsorption of CCl_4 over metal oxides, because it only possesses C-Cl bonds (Reaction Eq. (17)) and is therefore a model reactant. It was found that increased basicity of the metal oxide results in higher efficiency of destructive adsorption of CCl_4. Moreover, the chlorination of the metal oxides is accompanied by the formation of intermediate oxychloride phases.[69]

$$M_x^{y+}O_{y\,.\,x/2} + {}_{y\,.\,x/4}CCl_4 \rightarrow xM^{y+}Cl_y + {}_{y\,.\,x/4}CO_2 \quad (17)$$

The destructive adsorption behaviour for CCl_4 of several alkaline earth oxides and lanthanide oxides at 300 °C is shown in Figure 5.[69, 70] The following trend in activity is observed: BaO > SrO > La_2O_3 > Pr_2O_3 > Nd_2O_3 >> CaO ≈ MgO. The hypothesis that this process could be made catalytic by regeneration of lattice oxygen was investigated by the regeneration of the materials with steam according to Reaction Eq. (18). This equation is illustrated for different materials by Figure 6.[71-73] The regeneration of the alkaline earth metal oxides, especially for BaO and SrO, is difficult. The ability to regenerate lattice oxygen appears to increase with decreasing basicity for the alkaline earth metal oxides. The rare earth metal oxides show a higher regeneration capacity, with Pr_2O_3 and Nd_2O_3 nearly fully regenerated after 4 h of steam treatment. The dechlorination of La_2O_3 is slightly slower than for the other rare earth metal oxides.

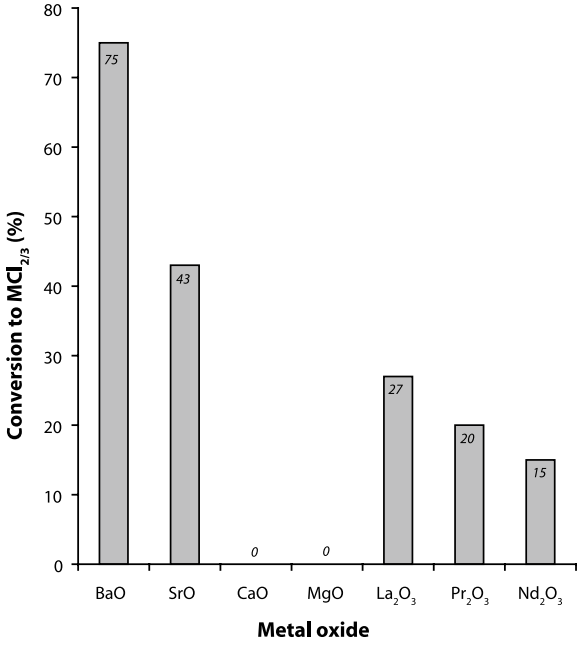

Figure 5. Destructive adsorption of CCl_4 on earth alkaline and lanthanide oxides at 300 °C. The efficiency of the process (%) is expressed as the percentage of the metal oxide transformed into the metal chloride after injecting 250 µl CCl_4 in a He stream for a molar ratio of 20 (CCl_4 : metal oxide).[69, 70]

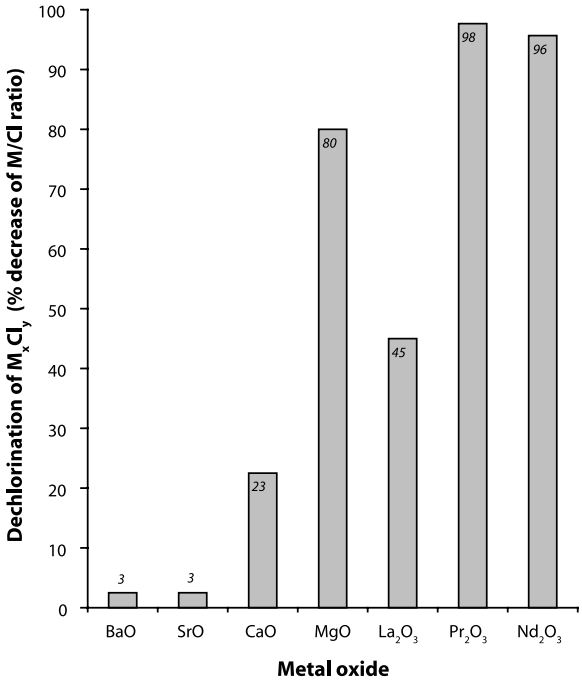

Figure 6. Dechlorination of earth alkaline and lanthanide oxides at 300 °C in the presence of steam for 4 h. The efficiency of the process is expressed as the Cl/M ratio before (grey) and after (black) dechlorination.[71]

$$xM^{y+}Cl_y + {}_{x\,.\,y/2}H_2O \rightarrow M_x^{y+}O_{y\,.\,x/2} + {}_{x\,.\,y}HCl \quad (18)$$

Thus, different behaviour is observed for the separate destructive adsorption and dechlorination reaction over basic metal oxides. An over amount of steam was added to the CCl_4 feed to verify whether a net catalytic reaction is possible (Reaction Eq. (19)) and to determine the relative activities of the materials. The conversion for the catalytic destruction of CCl_4 after 7 h time on stream over the metal oxide series is shown in Figure 7.[71-73] La_2O_3 and Pr_2O_3 were found to have the best combination of activity for destructive adsorption and in situ regeneration of the catalyst.

$$CCl_4 + 2\ H_2O \rightarrow CO_2 + 4\ HCl \quad (19)$$

The metal oxides were supported on γ-Al_2O_3 to increase the destruction capacity of the catalyst by increasing the catalytic surface area. The conversion after 7 h on stream over the supported metal oxide catalysts is shown in Figure 8.[71-73] The supported La_2O_3 catalyst possesses a high destruction capacity compared to other catalytic systems.[71-74] The catalyst was also tested for a substantial time on stream and was found to be highly stable for the catalytic conversion of CCl_4 (Figure 9).[71-73] Because of the promising results, La_2O_3 was chosen as a catalyst material for further study of the conversion of CHCs.

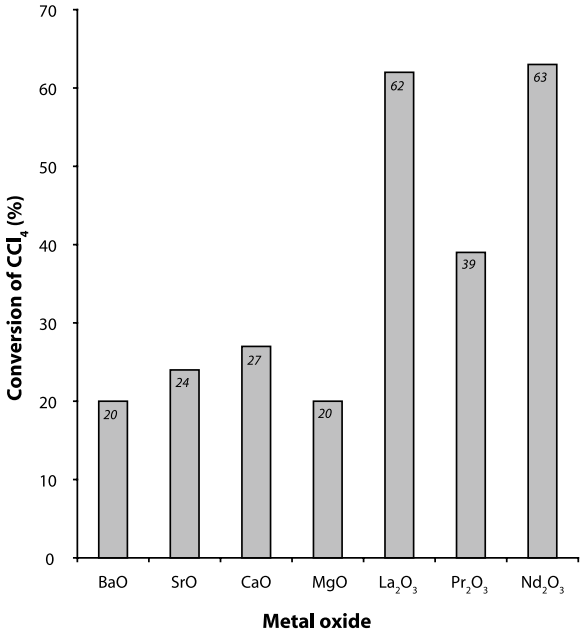

Figure 7. Conversion of CCl_4 and H_2O to CO_2 and HCl after 7 h on stream at 350 °C over alkaline oxides and lanthanide oxides (H_2O/CCl_4 = 61).[71]

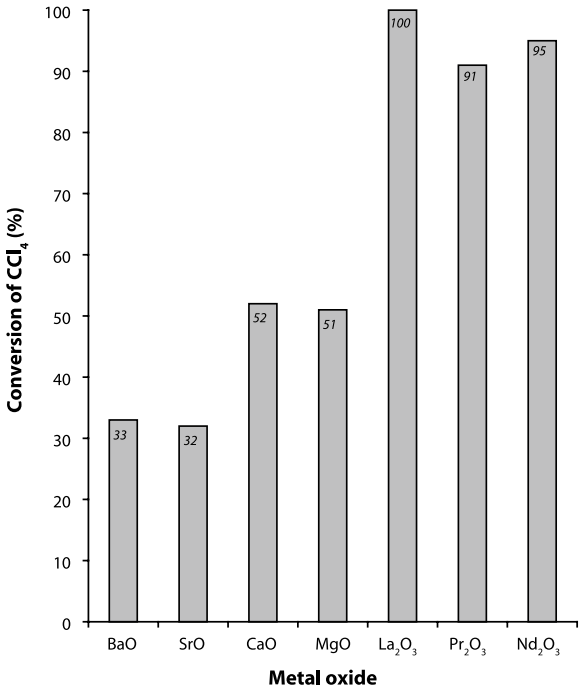

Figure 8. Conversion of CCl_4 and H_2O to CO_2 and HCl after 7 h on stream at 350 °C over alkaline oxides and lanthanide oxides supported on γ-Al_2O_3 (H_2O/CCl_4 = 61).[71]

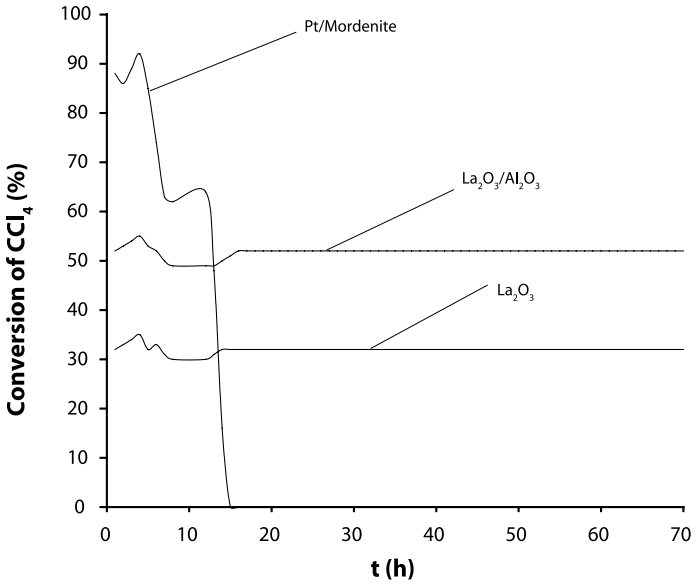

Figure 9. Long-term stability of La_2O_3, 11.7 wt% La_2O_3/Al_2O_3 and Pt/mordenite during the conversion of CCl_4 at 300 °C (H_2O/CCl_4 = 61).[71]

Behaviour of La_2O_3-based Catalysts during Conversion of CCl_4

The pure La_2O_3 catalyst was characterized with Raman spectroscopy during the steam reforming of CCl_4.[71, 72] The Raman spectra of the catalyst reveal the bulk phase composition of the catalyst as a function of time and position in the reactor (Figure 10).[71, 72] Initially, only bands assigned to La_2O_3 are observed at 106, 190 and 408 cm^{-1}. After 8 h, other bands appear in the spectrum at 438, 334, 210, 186 and 122 cm^{-1}, indicating partial conversion of the bulk phase into LaOCl according to Reaction Eq. (20). Even though the bulk phase composition changed, full conversion was still maintained. When only LaOCl was observed in the Raman spectra after 24 h of reaction, full conversion was still obtained. This means that, in addition to La_2O_3, LaOCl is also a highly active phase. Typical bands of $LaCl_3$ at 208 and 183 cm^{-1} arise after 36 h, indicating a second conversion of the bulk phase of LaOCl into $LaCl_3$ (Reaction Eq. (21)). The bands due to LaOCl, however, remain present in the spectra even after 48 h time-on-stream. In summary, the chlorination of the catalyst first proceeds via a fast reaction, converting La_2O_3 into LaOCl. This is followed by a more gradual transformation of LaOCl into $LaCl_3$. This process resembles destructive adsorption, but in this case the added steam delays the chlorination of the catalyst. A higher H_2O/CCl_4 ratio can further delay the chlorination of the catalyst material, as illustrated in Table 5.[71]

Raman spectroscopy provides insight into the changes in the bulk phase composition of the catalyst. Therefore, the catalyst was also analyzed before and after reaction with X-ray photoelectron spectroscopy (XPS) to determine the extent of chlorination of the catalytic surface.[71, 72] The O/La and Cl/La ratios that were found from the XPS spectra are shown in Table 6. There is a significant difference between the Raman and XPS results; more chlorine is present in the bulk phase than on the catalytic surface. This is explained by the fact there is bulk diffusion of chlorine atoms from the surface to the centre of the catalyst particle. This results in more chlorinated bulk phase and more oxygenated catalytic surface. The

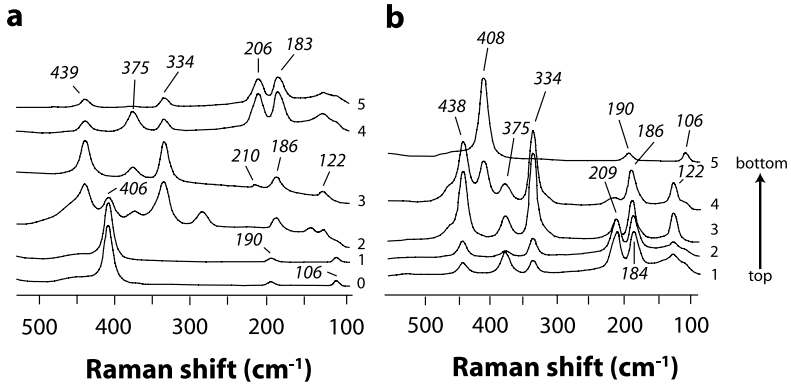

Figure 10. Raman spectra of La_2O_3 during the reaction of CCl_4 with H_2O (H_2O/CCl_4 = 61) at 350 8C: A) after 0) 0, 1) 8, 2) 16, 3) 24, 4) 36, and 5) 48 h on stream; and B) reactor mapping from 1 (top) to 5 (bottom) after 36 h on stream.[71, 72]

migration of the chlorine and oxygen atoms in the catalyst particle is schematically shown in Figure 11.[71]

$$La_2O_3 + ½\ CCl_4 \rightarrow 2\ LaOCl + ½\ CO_2 \quad (20)$$
$$LaOCl + ½\ CCl_4 \rightarrow LaCl_3 + ½\ CO_2 \quad (21)$$

Table 5. Bulk phase composition during the catalytic destruction of CCl_4 over La_2O_3 as investigated with Raman spectroscopy.[71]

Hours time-on-stream	Molar ratio H_2O/CCl_4		
	10	**61**	**360**
0	La_2O_3	La_2O_3	La_2O_3
2	LaOCl	La_2O_3	La_2O_3
8	$LaCl_3$	La_2O_3 + LaOCl	La_2O_3
16	$LaCl_3$	LaOCl	LaOCl
24	$LaCl_3$	LaOCl + $LaCl_3$	LaOCl
36	$LaCl_3$	LaOCl + $LaCl_3$	LaOCl

Table 6. O/La and Cl/La ratio of the catalyst as a function of time-on-stream for the catalytic destruction of CCl_4 over La_2O_3 (H_2O/CCl_4 = 61).[71, 72]

Hours time-on-stream	O/La	Cl/La	Phase composition based on XPS ratios
0	-	-	100 % La_2O_3
2	0.32	0	100 % La_2O_3
8	0.31	0	93 % La_2O_3 + 7 % LaOCl
16	0.27	0.91	64 % La_2O_3 + 36 % LaOCl
24	0.19	1.12	8 % La_2O_3 + 92 % LaOCl
36	0.15	4.40	67 % LaOCl + 33 % $LaCl_3$

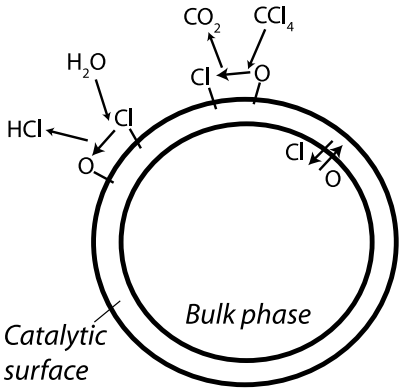

Figure 11. Bulk diffusion of chlorine atoms from the surface to the centre of the catalyst particle combined with regeneration and chlorination of the surface.[71]

Mechanism of Catalytic Destruction over La_2O_3-based Materials

Two reaction mechanisms were investigated for the catalytic destruction of CCl_4: 1) destructive adsorption of CCl_4 and 2) the dechlorination reaction with steam. The results of Density Functional Theory (DFT) calculations indicate that destructive adsorption proceeds via step-wise donation of chlorine to the catalytic surface.[71, 72] The reaction is built up from several elementary steps:

$$CCl_4 + La^{3+}(surf.) + O^{2-}(surf.) \rightarrow La^{3+}Cl^{-}(surf.) + CCl_3O^{-}(surf.) \quad (22)$$
$$La^{3+}Cl^{-}(surf.) + CCl_3O^{-}(surf.) \rightarrow La^{3+}Cl^{-}Cl^{-}(surf.) + COCl_2 \quad (23)$$
$$COCl_2 + La^{3+}(surf.) + O^{2-}(surf.) \rightarrow La^{3+}Cl^{-}(surf.) + COClO^{-}(surf.) \quad (24)$$
$$La^{3+}Cl^{-}(surf.) + COClO^{-}(surf.) \rightarrow La^{3+}Cl^{-}Cl^{-}(surf.) + CO_2 \quad (25)$$

As CCl_4 approaches the surface, the carbon atom becomes activated by a basic lattice oxygen site. Simultaneously, a chlorine atom is drawn towards two La^{3+} Lewis acid sites. The C-Cl bond is elongated and eventually the chlorine atom is transferred to the lattice, bridged between the two La atoms. The remaining fragment is present on the surface as an O-CCl_3 species (Reaction Eq. (22)). This reaction step is predicted to be exothermic as shown in the energy diagram in Figure 12. Next, the O-CCl_3 species donates a chlorine atom to the lattice and removes an oxygen atom from the solid (Reaction Eq. (23)). This reaction step is similar to the first removal of a chlorine atom and results in the formation of phosgene. Phosgene is re-adsorbed and can again donate two chlorine atoms to the surface in exchange for an

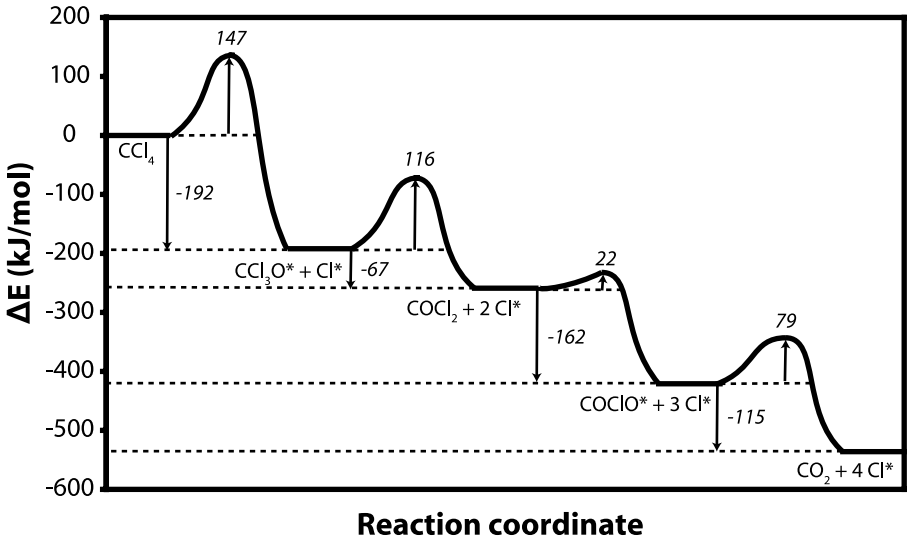

Figure 12. Energy diagram for CCl_4 decomposition on La_2O_3 (001). Reference energy is defined as CCl_4 + 2 H_2O + La_2O_3.[71]

oxygen atom (Reaction Eq. (24) and (25)). All reaction steps are exothermic and the first step (Reaction Eq. (22)) is predicted to be the rate-determining step in the destructive adsorption of CCl_4.

The calculations were repeated for the destructive adsorption of CCl_4 over LaOCl (001).[71] The reaction occurs via the same mechanism of step-wise donation of chlorine to the surface. The reaction energetics, on the other hand, are significantly different. Both the barrier for the formation of O-CCl_3 (Reaction Eq. (22)) and $COCl_2$ (Reaction Eq. (23)) are lower than for La_2O_3 at 73 and 24 kJ/mol, respectively. The barrier for steam dechlorination increases from around 180 to 506 kJ/mol compared to the reaction over La_2O_3. These calculations suggest the catalytic destruction of CCl_4 consists of two self-accelerating reactions; the dechlorination reaction rate is expected to accelerate with decreasing catalyst chlorine content, whereas the destructive adsorption reaction rate is expected to accelerate with increasing chlorine content. Therefore, an optimal catalyst composition may exist, which balances both reactions.

Because the chlorination of the bulk phase during reaction was observed with Raman spectroscopy, calculations were performed on the diffusion of chlorine atoms on the surface and into the bulk.[71] The chlorine atom is not limited to the position of the original oxygen atom. It was found that the barrier for surface diffusion is estimated at approximately 80 kJ/mol. The diffusion of chlorine atoms into the bulk is an endothermic process by 68 kJ/mol and results in migration of subsurface oxygen to the catalytic surface. The estimated activation energy is 208 kJ/mol, which is larger than for any of the destructive adsorption reaction steps. This means that the diffusion of chlorine into the bulk becomes the rate-determining step when no steam is added to the feed.

DFT calculations were also performed on the dechlorination of $LaCl_3$.[71, 72] The reactions are all predicted to be endothermic (Figure 13). Two reaction pathways are predicted, namely a step-wise hydroxyl formation and a subsequent dehydroxylation (Reaction Eqs. (26)-(28)), or by the reaction of surface chlorine and a hydroxyl group (Reaction Eqs. (26) and (29)). The latter reaction occurs at increased surface chlorine coverage. However, no significant differences in energetics were found with varying amounts of surface chlorine for the dechlorination steps of $LaCl_3$.

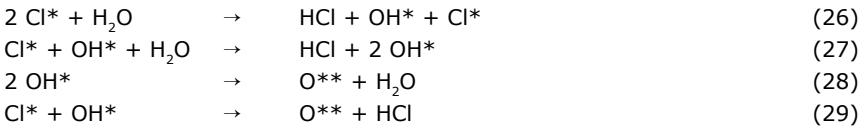

2 Cl* + H_2O	→	HCl + OH* + Cl*	(26)
Cl* + OH* + H_2O	→	HCl + 2 OH*	(27)
2 OH*	→	O** + H_2O	(28)
Cl* + OH*	→	O** + HCl	(29)

The catalytic destruction of CCl_4 was performed on La_2O_3 and LaOCl samples and the gas phase composition was monitored with in situ infrared spectroscopy (IR).[75] It was found that the initial temperature of reaction is lower for LaOCl than for La_2O_3 (Figure 14). The initial temperature of reaction is not influenced by the amount of sample used. This means that the LaOCl phase is more active than La_2O_3 rather than possessing more active sites.

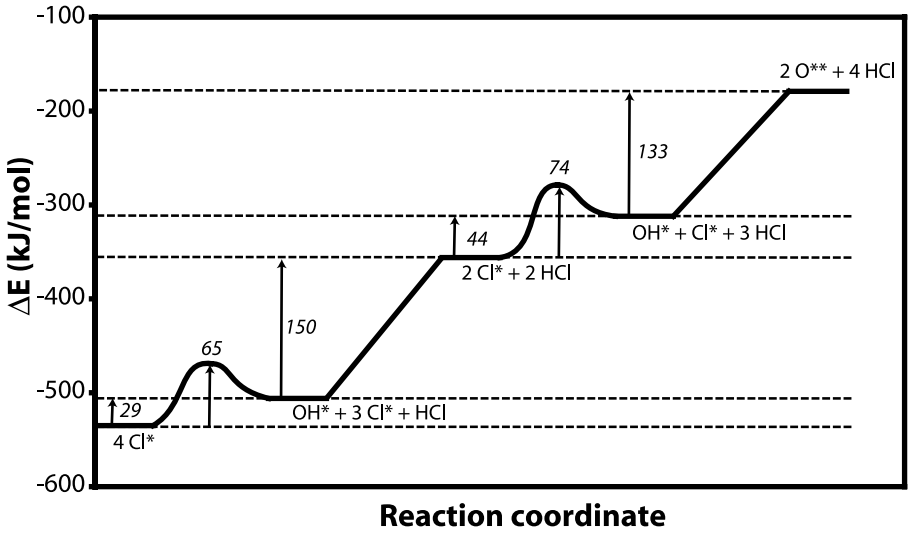

Figure 13. Energy diagram for removal of surface chlorine with steam on La_2O_3 (001). The reference energy is defined as $CCl_4 + H_2O + La_2O_3$.[71]

The calculations indicate that the rate-determining step is the dissociation of CCl_4 over an acid-base pair, resulting in the donation of a chlorine atom to the surface and the formation of O-CCl_3. The La^{3+} Lewis acid site initializes the split and the basic oxygen site stabilizes the remaining CCl_3 fragment. Therefore, the acid-base properties of the catalyst are expected to be of major influence on its activity for the destructive adsorption and catalytic destruction of CCl_4.

Acid-Base Properties of La_2O_3-based Catalysts

The acid-base properties of La_2O_3, LaOCl and $LaCl_3$ have been investigated using DFT calculations and IR probing with CO, pyridine, dimethylpyridine (DMP) and CO_2.[76] The adsorption of CO on the catalyst materials occurs at low temperature (77 K), and results in a shift of the CO vibrational frequencies for the adsorbed CO compared to the gas phase. The shift is a measure for Lewis acidity of the La^{3+} sites (Figure 15). The following trend in Lewis acidity was observed: La_2O_3 < LaOCl < $LaCl_3$. This Lewis acidity trend is confirmed by DFT estimates on CO adsorption and Lowest Unoccupied Molecular Orbital (LUMO) energies. The stronger basic molecules pyridine and DMP adsorb primarily on Brønsted acidic sites. In the case of LaOCl and $LaCl_3$ the probe molecules become protonated. By combining the probing experiment with pyridine and DMP with temperature programmed desorption, the same trend in acid strength was found as for the Lewis acid strength (Figure 16). The results for the Lewis and Brønsted acidity of the La-based materials are summarized in Table 7.

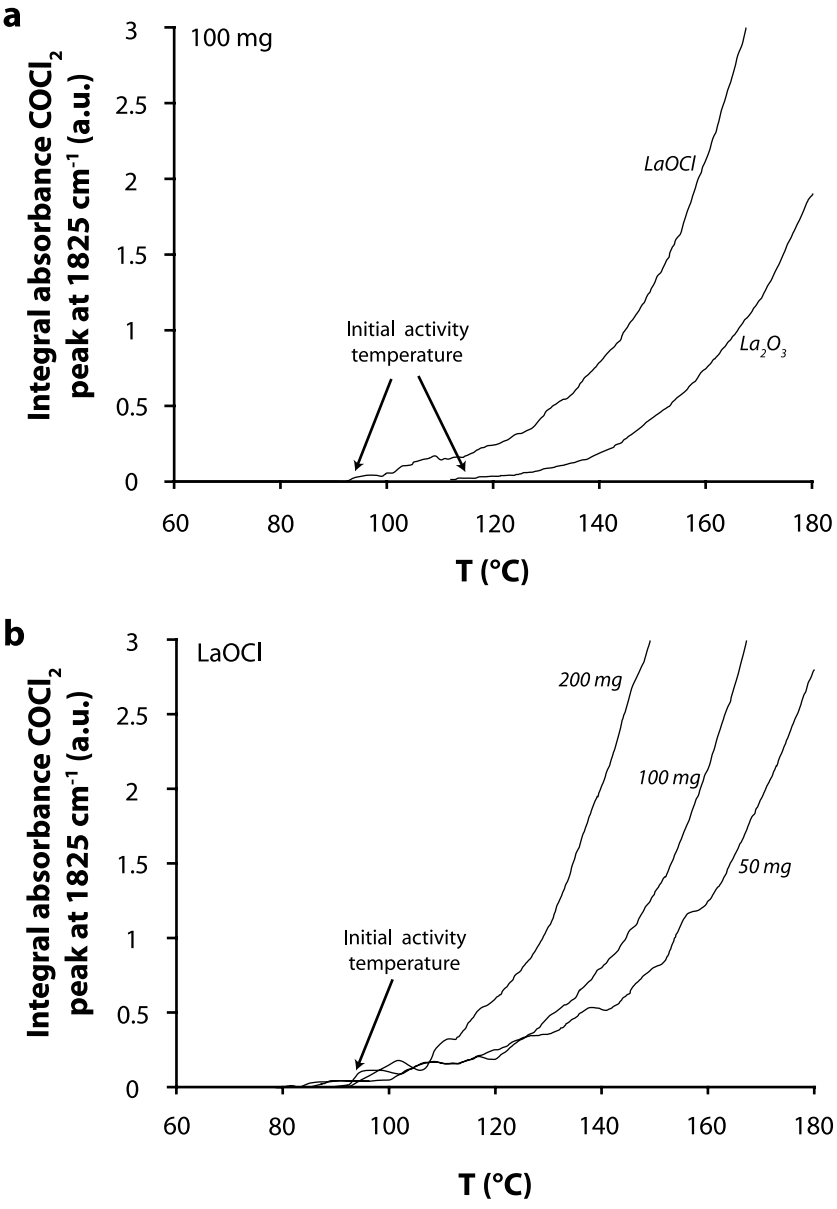

Figure 14. Results of temperature-programmed reaction between CCl_4 and catalyst material wafer, during which the gas phase monitored with IR (a) Comparison of La_2O_3 and LaOCl 100 mg wafers. (b) Comparison of 50, 100, and 200 mg wafers of LaOCl.[75]

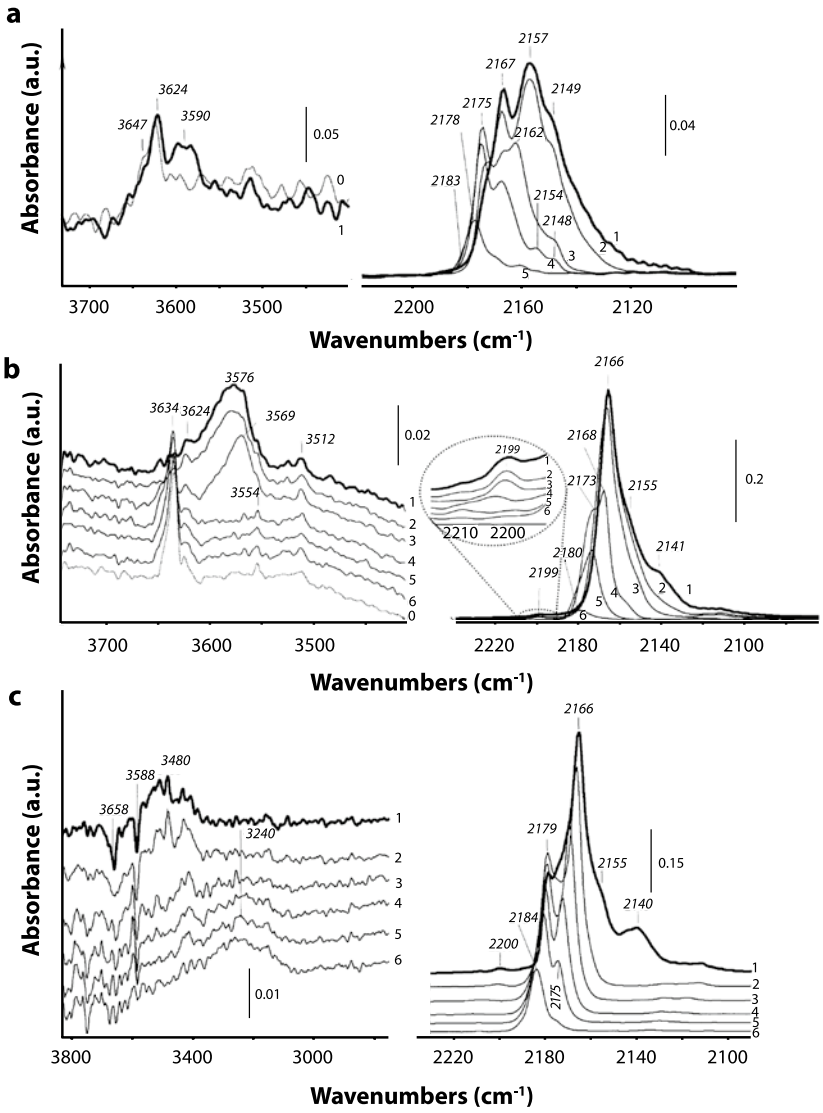

Figure 15. FTIR spectra of CO adsorbed at -196 °C (a) on La_2O_3 pretreated at 800 °C: 0, before adsorption; 1, 10.6 mbar CO in equilibrium; 2, evacuation of gas-phase CO to 1.3 $.10^{-4}$ mbar; 3, evacuation for 3 min at 1.3 $.10^{-4}$ mbar; 4, evacuation for 5 min at 1.3 $.10^{-5}$ mbar; 5, evacuation for 7 min at 1.3 $.10^{-5}$; and 6, evacuation for 15 min at 1.3 $.10^{-5}$ mbar. (b) On LaOCl pretreated at 550 °C: 0, before adsorption; 1, 10.6 mbar CO in equilibrium; 2, evacuation of gas-phase CO to 1.3 $.10^{-4}$ mbar; 3, evacuation for 30 s at 1.3 $.10^{-4}$ mbar; 4, evacuation for 5 min at 1.3 $.10^{-5}$ mbar; 5, evacuation for 15 min at 1.3 $.10^{-5}$ mbar; and 6, evacuation for 20 min at 1.3 $.10^{-5}$ mbar. (c) CO adsorbed at -196 °C on $LaCl_3$ pretreated at 550 °C: 1, 10.6 mbar CO in equilibrium; 2, evacuation of gas-phase CO to 1.3 $.10^{-4}$ mbar; 3, evacuation for 3 min at 1.3 $.10^{-4}$ mbar; 4, evacuation for 7 min at 1.3 $.10^{-5}$ mbar; 5, evacuation for 10 min at 1.3 $.10^{-5}$ mbar; and 6, evacuation for 20 min at 1.3 $.10^{-5}$ mbar. Spectrum before CO adsorption was subtracted in the CO spectral region.[76]

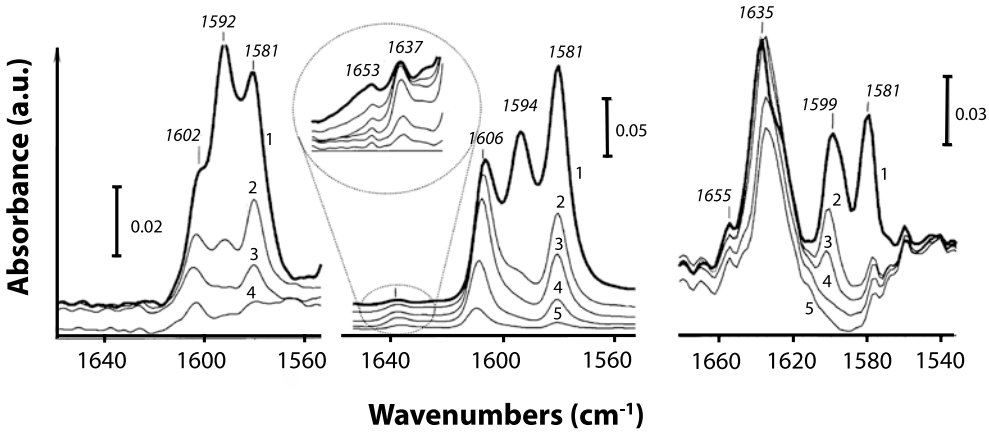

Figure 16. IR spectra of 2,6-dimethylpyridine DMP adsorbed at RT on a, La_2O_3; b, LaOCl; and c, $LaCl_3$: 1, 1.3 mbar in equilibrium; 2, evacuation of gas-phase DMP at RT; 3, evacuation to 1.3 .10^{-3} mbar at RT; 4, evacuation at 100 °C; and 5, evacuation at 200 °C.[76]

Table 7. Evaluation of Lewis and Brønsted acidity of La_2O_3, LaOCl and $LaCl_3$.[76]

	La_2O_3	**LaOCl**	**$LaCl_3$**
Brønsted Acidity			
$\Delta\nu$(OH) experimental high CO coverage, cm^{-1}	-34	-58	-107
	La_2O_3 (001)	LaOCl (001)	$LaCl_3$ (100)
Computational model surface	na	-38	-107
$\Delta\nu$(OH) calculated with H-bonded CO, cm^{-1}	na	1702	1524
ΔE for OH^-(surf) → O^{2-}(surf) + H^+ at 0.25 ML, kJ/mol			
Lewis Acidity			
ν(CO) experimental low CO coverage, cm^{-1}	2178	2180	2184
ν(CO) experimental high CO coverage, cm^{-1}	2167, 2175 (sh.)	2166, 2173 (sh.)	2166, 2179 (sh.)
Computational model surface	La_2O_3 (001)	LaOCl (001)	$LaCl_3$ (100)
ν(CO) calculated at 0.25 ML, cm^{-1}	2153	2157	2170
ΔE for CO adsorption at 0.25 ML, kJ/mol	-23	-28	-37
LUMO energy, kJ/mol (Lower energy indicates stronger Lewis acidity)	-177	-208	-297

na = not applicable, sh. = shoulder

CO_2 was used as a probe molecule in combination with IR to evaluate the strength of the basic oxygen sites, because it readily reacts to form carbonates when adsorbed on a basic oxygen site.[76] Carbonates were indeed formed upon adsorption of CO_2 on La_2O_3 and LaOCl. On $LaCl_3$ no significant carbonate formation was observed, indicating an absence of oxygen adsorption sites on $LaCl_3$. The carbonates on La_2O_3 were assigned as polydentate and bulk species, whereas bridged carbonates dominated the spectrum of CO_2 adsorbed on LaOCl. The experiments show that carbonates are formed more readily on La_2O_3 than on

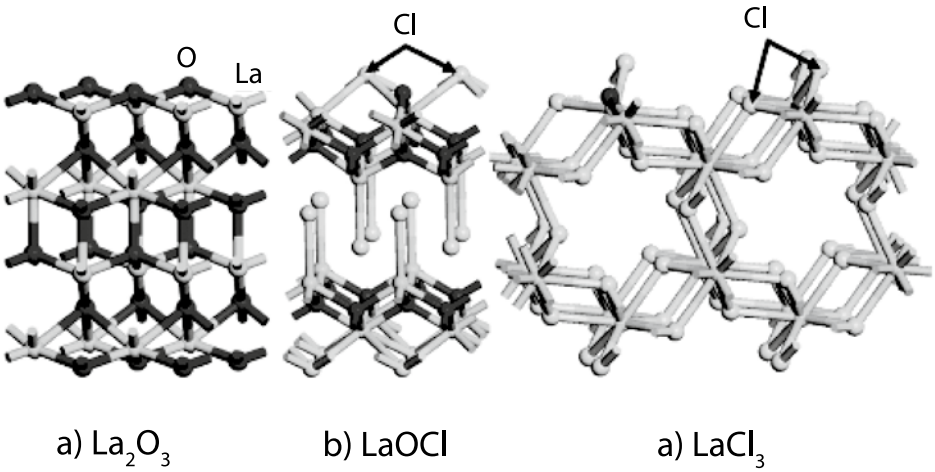

Figure 17. Unit cells of (a) La_2O_3(001), (b) LaOCl(001), and (c) $LaCl_3$(100) used in the construction of infinite periodic models for performing DFT calculations. Arrows indicate chlorine atoms that can be substituted for an oxygen atom to obtain an additional equivalent surface oxygen site on LaOCl and $LaCl_3$.[76]

LaOCl, which suggests the oxygen adsorption sites are more basic on the former. However, the accurate determination of basicity of the La-based materials is hindered by the formation of different types of carbonates on each material.

The unit cells of the surface models that were used in the DFT calculations are shown in Figure 17. The energetics of the initial reaction step over La_2O_3, LaOCl and $LaCl_3$ (partially dechlorinated surface) were calculated, as shown in Figure 18. The activation energy for the initial breaking of a C-Cl bond, which is considered the rate-determining step, follows the trend: La_2O_3 > $LaCl_3$ (partially dechlorinated surface) > LaOCl. The calculations suggest that the La^{3+} Lewis acid site initializes the reaction by elongating the C-Cl bond until chlorine is donated to the surface. The fact that LaOCl is a more active phase than La_2O_3 indicates that a different surface composition directly influences the activity. These two deductions are in agreement with the trend in Lewis acidity that was found from the IR probing results. However, a real connection between CHC destruction activity and the acid-base properties of the La-based catalysts is still missing.

Catalytic Destruction of $CHCl_3$ and CH_2Cl_2 in the Presence of Steam

CCl_4 is a model compound that only possesses C-Cl bonds, so the behaviour of C-H bond containing chlorinated C_1 (CHC_1) may differ from the reaction with CCl_4. Moreover, the chlorinated waste mixtures (light ends) also contain other chlorinated methanes, such as $CHCl_3$ and CH_2Cl_2. Therefore, γ-Al_2O_3-supported and unsupported La_2O_3 catalyst were tested for the catalytic destruction of $CHCl_3$ and CH_2Cl_2.[71, 73]

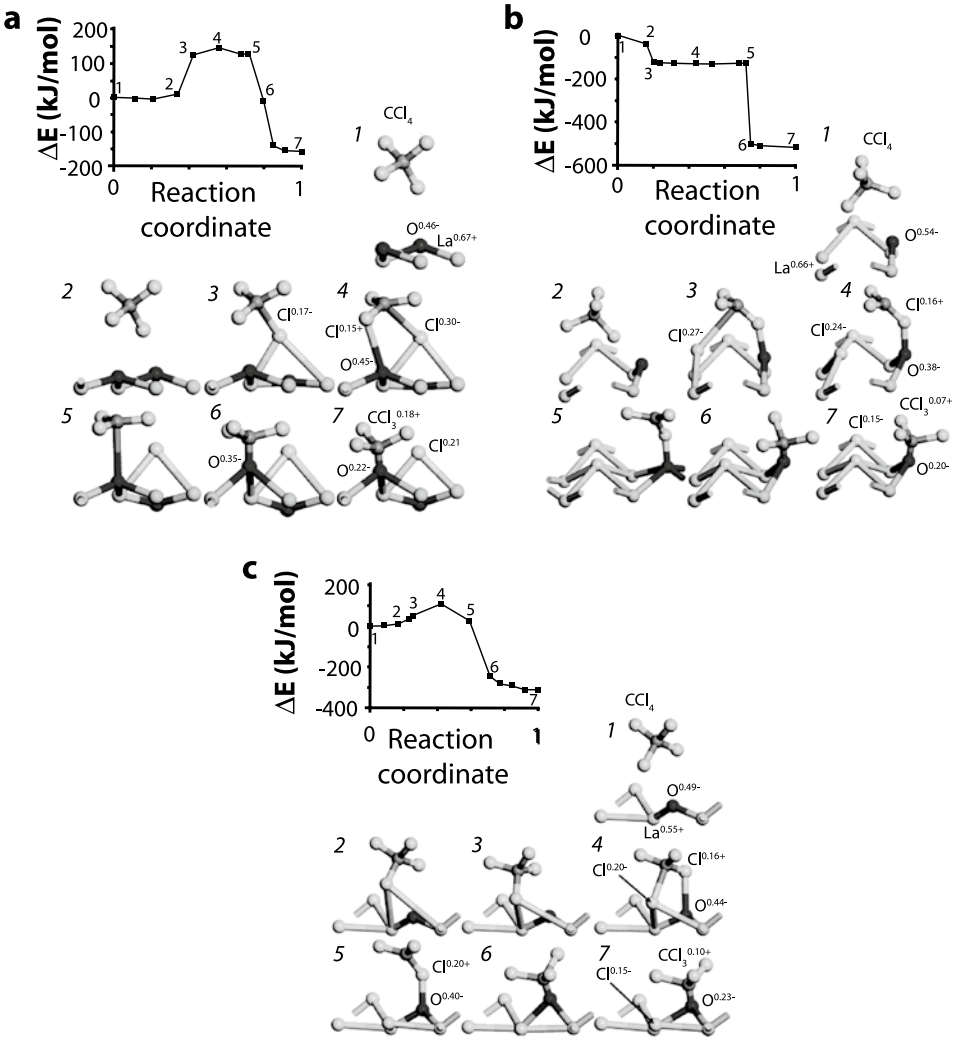

Figure 18. Energy diagram and schematic representation of the reaction pathway for the initial step in CCl_4 decomposition over (a) La_2O_3 (001), (b) LaOCl (001) and (c) $LaCl_3$ (100). Numbers next to element symbols specify partial Hirshfeld charges on atoms and molecular fragments.[76]

The activity results on the bulk catalyst show that the main difference with the catalytic destruction of CCl_4 was the formation of CO as the main product for both $CHCl_3$ and CH_2Cl_2.[71, 73] Trace amounts of CO_2 were also observed. The conversion after 7 h time-on-stream at 350 °C for all reactants over La-based catalysts is shown in Table 8. The conversion decreases with an increasing chlorine content of the reactant. This difference was attributed to the increasing number of C-H bonds (E_b = 411 kJ/mol) in the reactant, which is more difficult to break than the C-Cl bond (E_b = 327 kJ/mol). The fact that CO is formed and not CO_2, is thought to be a result of the direct composition of the reaction intermediate according to Reaction Eqs. (30)-(33). This is, however, a hypothesis and should be considered with care, because no CH_2O, CHClO and H_2 were detected at any time. Minor coke formation was also observed in the reactions with $CHCl_3$ and CH_2Cl_2 in contrast to the reaction with CCl_4.

$$CHCl_3 + O^{2-}(surf.) + La^{3+}(surf.) \rightarrow CHClO + La^{3+}Cl^{-}Cl^{-}(surf.) \quad (30)$$

$$CHClO \rightarrow CO + HCl \quad (31)$$

$$CH_2Cl_2 + O^{2-}(surf.) + La^{3+}(surf.) \rightarrow CH_2O + La^{3+}Cl^{-}Cl^{-}(surf.) \quad (32)$$

$$CH_2O \rightarrow CO + H_2 \quad (33)$$

When γ-Al_2O_3-supported catalysts were used, the conversion was higher than for the bulk catalysts because of the increased surface area.[71, 73] Moreover, in the case of CH_2Cl_2 the product distribution is completely different from that of the unsupported catalyst. CH_3Cl was also formed as a major product, which indicates that there must be two reaction mechanisms: one over La_2O_3 and one over the support. The nature of these reaction mechanisms was not investigated further, however. In summary, La-based catalysts are also active for the catalytic destruction of H-containing CHC_1. The reactions of $CHCl_3$ and CH_2Cl_2 over La_2O_3 resemble the catalytic destruction of CCl_4 (Reaction Eqs. (34) and (35)), but different products and activities were found.

Table 8. Catalytic activity (conversion in %) of bulk La_2O_3, LaOCl and $LaCl_3$ for CCl_4, $CHCl_3$ and CH_2Cl_2 destruction after 7 h on stream in the presence of steam at 350 °C. The reported activity of $LaCl_3$ materials should be considered with care since hydrated $LaCl_3$ easily transforms during heating in the reactor into LaOCl, so the activity of $LaCl_3$ could be partially due to the presence of LaOCl instead of $LaCl_3$.[73]

Compound	CCl_4	$CHCl_3$	CH_2Cl_2
La_2O_3	62	34	15
LaOCl	60	26	14
$LaCl_3$	5	24	11

$$CHCl_3 + H_2O \rightarrow CO + 3\ HCl \quad (34)$$

$$CH_2Cl_2 + H_2O \rightarrow CO + H_2 + HCl \quad (35)$$

Motivation and Outline of the PhD thesis

Catalytic conversion is a suitable method to lower the energy consumption of the destruction of the light and heavy ends during C_2H_3Cl production. In addition, the CHC_{1-2} could potentially be recycled into feedstock or fuel. Chlorine and chlorine-containing compounds are, however, known to be poisonous to many catalyst materials. Therefore, the challenge lies more in finding a suitable stable catalyst rather than a more active or selective catalyst. La_2O_3-based catalysts are not only resistant to chlorine poisoning, but incorporation of chlorine ions into the lattice of the catalyst is in fact a way to tune activity and selectivity. This PhD thesis illustrates the versatility of La_2O_3-based compounds as potential catalysts in chlorine-mediated organic reactions.

Chapter 2 deals with the relationship between activity and acid-base properties of La-based catalysts. La_2O_3 and LaOCl were extensively characterized, making use of X-ray diffraction, X-ray photoelectron spectroscopy, Raman spectroscopy and IR spectroscopy, while their acid-base properties were probed with CO, CO_2 and methanol. As a result, it was possible to explain the difference in the reactivity of the catalysts towards CCl_4 in terms of difference in Lewis acid strength and density.

Chapter 3 provides a general reaction scheme for the destructive adsorption of the CHC_1 series, namely CCl_4, $CHCl_3$, CH_2Cl_2 and CH_3Cl. In addition, the relationship between the composition of the catalyst and the observed activity and selectivity is discussed. In situ IR spectroscopy and GC analysis were used to monitor the reaction. As a result, fundamental insight is obtained into the intermediates of destructive adsorption when applying La_2O_3-based materials to convert mixtures of CHC_1. This is of high relevance when destroying the light ends in industrial waste streams.

In **Chapter 4**, it is shown that La_2O_3-based materials are also a catalyst for the dehydrochlorination of chlorinated ethanes. Elimination of HCl over the catalyst materials results in the formation of a C=C bond. The dehydrochlorination of several chlorinated ethanes, namely C_2H_5Cl, 1,2-$C_2H_4Cl_2$ and 1,1,2-$C_2H_3Cl_3$, was performed as a function of time and temperature. The reactor effluent in flow-gas experiments was continuously analyzed with GC. Moreover, before and after reaction, the catalytic surface and bulk phase of the catalyst material was characterized using XPS and XRD, respectively. The dehydrochlorination of 1,1,2-$C_2H_3Cl_3$ was also performed as a function of temperature, while the gas phase was analyzed using IR. The results illustrate how the chlorination degree of the catalyst material directly influences the selectivity in the dehydrochlorination reaction. This reaction is not only interesting for the conversion of chlorinated ethanes in waste streams, but could also be applied to enable selective cracking of 1,2-$C_2H_4Cl_2$ into C_2H_3Cl under less costly conditions.

Chapter 5 discusses $LaCl_3$ as a catalyst for the hydrogen-chlorine exchange reaction between CH_2Cl_2 and CCl_4 into $CHCl_3$. This is the first time that the activation of C-Cl and C-H bonds is performed catalytically without the presence of oxygen atoms. In this reaction, the reactants are run over a fully chlorinated catalyst in order to prevent destructive adsorp-

tion. Both bulk phase and carbon nanofiber-supported $LaCl_3$ catalysts are used. The reaction was monitored in a flow-gas experiment as a function of temperature and time using GC. In addition, DFT calculations were performed on the H-Cl exchange reaction between CCl_4 and CH_2Cl_2 to gain insight into the reaction steps. The exchange of H and Cl between CHCs under oxygen-free conditions is a new catalytic process and may be applicable for the selective conversion of chlorinated waste compounds, but it could also be used for the selective activation of hydrocarbons, such as methane or ethane.

In **Chapter 6**, the potential of the La-based materials for the conversion of CHC_{1-2} is explored in a series of flow-gas experiments. A mixture of chlorinated methanes and ethanes are converted over La_2O_3-based materials to verify whether the dehydrochlorination and destructive adsorption can occur simulta-neously in one reactor, as would be case for the light ends waste mixtures. Also, CCl_4 is tested as an alternative chlorinating agent for HCl in the conversion of methane into CH_3Cl. The low economic value of CCl_4 in comparison to HCl would make the process economically more favourable and serve as a route for the disposal of the undesirable CCl_4. Finally, a combination of La_2O_3 and SAPO-34 material was used as a test-case for the one-pot conversion of chlorinated waste compounds into products, such as fuel or chemical intermediates. CH_2Cl_2 was used as reactant and was converted via destructive adsorption over La_2O_3 into CH_3OH, which is consecutively converted into hydrocarbons via the methanol-to-olefin reaction over SAPO-34.

Chapter 7 consists of a summary of this PhD thesis and a look into the future. It provides the main conclusions as well as some comments with respect to future research on this topic.

References

1. Eurochlor Industry Review 2004-2005. To be found under http://www.eurochlor.org/.
2. R. Bartsch, C. L. Curlin, T. F. Florkiewicz, B. Lüke, H.-R. Minz, T. Navin, R. Scannell, P. Schmittinger, E. Zelfel, *Chlorine: Principles and Industrial Practice,* VCH: Weinheim, 2000.
3. State of California Environmental Protection Agency, *Chemicals Known to the State to Cause Cancer or Reproductive Toxicity,* Cal/EPA Secretariat: Sacramento, 2007.
4. U.S. Environmental Protection Agency Superfund Chemical Data Matrix. To be found under http://www.epa.gov/superfund/sites/npl/hrsres/tools/scdm.htm.
5. D. A. Whaley, *Development of a Worker Hazard Score for Individual Chemicals,* Indiana Pollution Prevention and Safe Materials Institute School of Civil Engineering, Purdue University: Morgantown, 1996.
6. U.S. Environmental Protection Agency, *The Clean Air Act of 1990, a Primer on Consensus Building,* Government Printing Office: Washington, D.C., 1990.
7. F. Pedersen, J. Falck, *Environmental Hazard Classification - Classification of selected substances as dangerous for the environment; NORDBAS2 software program,* TemaN-

ord, Nordic Council of Ministers: Copenhagen, 1997.
8. Ozone Secretariat United Nations Environment Programme, *Handbook for the Montreal Protocol on Substances that Deplete the Ozone Layer,* Secretariat of The Vienna Convention for the Protection of the Ozone Layer &The Montreal Protocol on Substances that Deplete the Ozone Layer: Nairobi, 2006.
9. International Panel on *Climate Change, Climate Change: The IPCC Scientific Assessment,* World Meteorological Organization/United Nations Environment Programme: Cambridge, 1990. S.
10. I. Amato, *Science* **1993,** 261, 152.
11. Safe, *Environ. Health Persp.* **1992,** 100, 259.
12. J. A. Orejas, *Chem. Eng. Sci.* **1999,** 54, 5299.
13. P. Schwarzmaier, I. Mielke, US 6235953, 2001
14. S. Wachi; Y. Ariki, H. Oshima, US 4873384, 1989.
15. C. Lamberti, C. Prestipino, F. Bonino, L. Capello, S. Bordiga, G. Spoto, A. Zecchina, S. D. Moreno, B. Cremaschi, M. Garilli, A. Marsella, D. Carmello, S. Vidotto, G. Leofanti, *Angew. Chem. Int. Ed.* **2002,** 41, 2341.
16. M. N. Newmann, *Encyclopedia of Polymer Science and Engineering,* Wiley: New York, 1985; Vol. 17.
17. J. S. Naworski, E. S. Evil, *Applied Industrial Catalysis,* Academic Press: New York, 1983; Vol. 1.
18. S. A. Kurta, I. M. Mykytyn, M. V. Khaber, *Russ. J. Appl. Chem.* **2005,** 78, 1110.
19. L. Schmidhammer, P. Hirschmann, H. Patsch, R. Strasser, US 4754088, 1988.
20. B. P. Guedes, M. F. Feitosa, L. S. Vasconcelos, A. B. Araújo, R. P. Brito, *Sep. Purif. Technol.* **2007,** 56, 270.
21. J. A. Incavo, *Ind. Eng. Chem. Res.* **1996,** 35, 931.
22. J. Erb, *Enivron. Prog.* **1993,** 12, 243.
23. M. Wilde, K. Anders, *Chem. Tech.* **1994,** 46, 316.
24. J. R. Gonzalez-Velasco, A. Aranzabal, R. Lopez-Fonseca, R. Ferret, J. A. Gonzalez-Marcos, *Appl. Catal. B* **2000,** 24, 33.
25. A. Gervasini, C. Pirola, V. Ragaini, *Appl. Catal. B* **2002,** 38, 17.
26. M. Bonarowska, A. Malinowski, W. Juszczyk, Z. Karpinski, *Appl. Catal. B* **2001,** 30, 187.
27. G. C. Bond, N. Sadeghi, *J. Appl. Chem. Biotechnol.* **1975,** 25, 241.
28. R. W. van den Brink, P. Mulder, R. Louw, *Catal. Today* **1999,** 54, 101.
29. A. A. Klinghoffer, J. A. Rossin, *Ind. Eng. Chem. Res.* **1992,** 31, 481.
30. J. M. Toledo, J. Corella, A. Sanz, *Environ. Prog.* **2001,** 20, 167.
31. A. Musialik-Piotrowska, K. Syczewska, *Catal. Today* **2002,** 73, 333.
32. M.-Y. Wey, W.-Y. Yang, H.-C. Huang, J.-C. Chen, *J. Air Waste Managem. Assoc.* **2002,** 52, 198.
33. M. M. R. Feijen-Jeurissen, J. J. Jorna, B. E. Nieuwenhuys, G. Sinquin, C. Petit, J. P. Hindermann, *Catal. Today* **1999,** 54, 65.

34. C.-C. Kim, S.-K. Ihm, *J. Chem. Eng. Jpn.* **2001,** 34, 143.
35. A. M. Padilla, J. Corella, J. M. Toledo, *Appl. Catal. B* **1999,** 22, 107.
36. S. D. Yim, K. H. Chang, D. J. Koh, I.-S. Nam, Y. G. Kim, *Catal. Today* **2000,** 63, 215.
37. Y. Liu, M. Luo, Z. Wei, Q. Xin, P. Ying, C. Li, *Appl. Catal. B* **2001,** 29, 61.
38. L. Storaro, R. Ganzerla, M. Lenarda, R. Zanoni, A. J. Lopez, P. Olivera-Pastor, E. R. Castellon, *J. Mol. Catal. A* **1997,** 115, 329.
39. F. Solymosi, J. Rasko, E. Papp, A. Oszko, T. Bansagi, *Appl. Catal. A* **1995,** 131, 55.
40. M. Kulazynski, J. G. van Ommen, J. Trawczynski, J. Walendziewski, *Appl. Catal. B* **2002,** 36, 239.
41. S. C. Petrosius, R. S. Drago, V. Young, G. C. Grunewald, *J. Am. Chem. Soc.* **1993,** 115, 6131.

42. R. Rachapudi, P. S. Chintawar, H. L. Greene, *J. Catal.* **1999,** 185, 58.
43. J. I. Gutiérrez-Ortiz, R. Lopez-Fonseca, U. Aurrekoetxea, J. R. Gonzalez-Velasco, *J. Catal.* **2003,** 218, 148.
44. S. Karmakers, H. L. Greene, *J. Catal.* **1994,** 148, 524.
45. R. Lopez-Fonseca, S. Cibrián, J. I. Gutiérrez-Ortiz, J. R. Gonzalez-Velasco, *Stud. Surf. Sci. Catal.* **2002,** 142, 847.
46. S. Chatterjee, H. L. Greene, Y. J. Park, *J. Catal.* **1992,** 138, 179.
47. J. J. Spivey, *Ind. Eng. Chem. Res.* **1987,** 26, 2165.
48. V. de Jong, M. K. Cieplik, W. A. Reints, F. Fernandez-Reino, R. Louw, *J. Catal.* **2002,** 211, 355.
49. G. Sinquin, J. P. Hindermann, C. Petit, A. Kiennemann, *Catal. Today* **1999,** 54, 107.
50. G. Sinquin, J. P. Hindermann, C. Petit, A. Kiennemann, *Appl. Catal. B* **1999,** 27, 105.
51. B. K. Hodnett, *Heterogeneous Catalytic Oxidation: Fundamental and Technological Aspects of the Selective and Total Oxidation of Organic Compounds.* Wiley: New York, 2000.
52. W. Juszczyk, A. Malinowski, Z. Karpinski, *Appl. Catal. A* **1998,** 166, 311.
53. F. D. Kopinke, K. Mackenzie, R. Köhler, *Appl. Catal. B* **2003,** 44, 15.
54. W. D. Rhodes, K. Lázár, V. I. Kovalchuk, J. L. d'Itri, *J. Catal.* **2002,** 211, 173.
55. Y. Ukisu, T. Miyadera, *Appl. Catal. B* **2003,** 40, 141.
56. D. R. Luebke, L. S. Vadlamannati, V. I. Kovalchuk, J. L. d'Itri, *Appl. Catal. B* **2002,** 35, 211.
57. G. C. Bond, F. Rosa, *Catal. Lett.* **1996,** 39, 261.
58. J. D. Ortega, J. T. Richardson, M. V. Twigg, *Appl. Catal. B* **1997,** 12, 339.
59. N. Couté, J. D. Ortega, J. T. Richardson, M. V. Twigg, *Appl. Catal. B* **1998,** 19, 175.
60. K. Intarajang, J. T. Richardson, *Appl. Catal. B* **1999,** 22, 27.
61. U. Weiss, M. P. Rosynek, J. H. Lunsford, *Chem. Commun.* **2000,** 5, 405.
62. N. Couté, J. T. Richardson, *Appl. Catal. B* **2000,** 26, 265.
63. P. D. Hooker, K. J. Klabunde, *Environ. Sci. Tech.* **1994,** 28, 1243.
64. O. Koper, Y.-X. Li, K. J. Klabunde, *Chem. Mater.* **1993,** 5, 500.

65. O. Koper, I. Lagadic, K. J. Klabunde, *Chem. Mater.* **1997,** 9, 2481.
66. K. J. Klabunde, A. Khaleel, D. Park, *High. Temp. Mater. Sci.* **1995,** 33, 99.
67. Y. Jiang, S. Decker, C. Mohs, K. J. Klabunde, *J. Catal.* **1998,** 180, 24.
68. I. V. Mishakov, A. F. Bedilo, R. M. Richards, V. V. Chesnokov, A. M. Volodin, V. I. Zaikovskii, R. A. Buyanov, K. J. Klabunde, *J. Catal.* **2002,** 206, 40.
69. B. M. Weckhuysen, G. Mestl, M. P. Rosynek, T. R. Krawietz, J. F. Haw, J. H. Lunsford, *J. Phys. Chem. B* **1998,** 102, 3773.
70. B. M. Weckhuysen, M. P. Rosynek, J. H. Lunsford, *Phys. Chem. Chem. Phys.* **1999,** 1, 3157.
71. P. van der Avert. Catalytic destruction of chlorinated hydrocarbons over lanthanide oxides. Katholieke Universiteit Leuven, Leuven, 2003.
72. P. van der Avert, S. G. Podkolzin, O. V. Manoilova, H. de Winne, B. M. Weckhuysen, *Chem. Eur. J.* **2004,** 10, 1637.
73. P. Van der Avert, B. M. Weckhuysen, *Phys. Chem. Chem. Phys.* **2004,** 6, 5256.
74. P. van der Avert, B. M. Weckhuysen, *Angew. Chem. Int. Ed.* **2002,** 41, 4730.
75. S. G. Podkolzin, O. V. Manoilova, B. M. Weckhuysen, *J. Phys. Chem. B* **2005,** 109, 11634.
76. O. V. Manoilova, S. G. Podkolzin, B. Tope, J. Lercher, E. E. Stangland, J. M. Goupil, B. M. Weckhuysen, *J. Phys. Chem. B* **2004,** 108, 15770.

2

Destructive Adsorption of CCl_4 over La-Based Solids: Linking Activity to Acid-Base Properties

In previous research it was found that La_2O_3-based catalysts offer the best combination of activity and stability for the catalytic destruction of chlorinated C_1 (CHC_1). In this chapter, the synthesis and physicochemical properties of La_2O_3, LaOCl and $LaCl_3$ are discussed. The chapter starts with an introduction and hypothesis regarding the link between acid-base properties and activity of La_2O_3-based materials for the destructive adsorption of CHC_1. Next, the experimental method of catalyst preparation and characterization using X-ray diffraction (XRD), X-ray photoelectron spectroscopy (XPS), scanning electron microscopy (SEM), N_2-physisorption, temperature programmed desorption (TPD) of CO_2, infrared (IR) and Raman spectroscopy are provided. Also, the experimental setups for the activity measurements and the IR probing experiments used throughout this PhD thesis are presented. Two factors were found to be of influence on the activity of La_2O_3-based materials for the destructive adsorption of CCl_4; the strength of the Lewis acid site and the availability of lattice oxygen. A higher degree of chlorination results in stronger Lewis acid sites and hence, higher intrinsic activity. However, a certain number of O atoms is needed to maintain activity. Therefore, an optimum combination of the acid-base pair is expected to exist in a suitable catalytic material.

Introduction

As discussed in Chapter 1, in previous work it has been shown that of all basic oxides, La_2O_3-based catalysts possess the optimal combination of activity and regeneration for the destructive adsorption and catalytic destruction of chlorinated hydrocarbons.[1-4] La_2O_3 is not the most basic of the metal oxides, so basicity is not only of influence. The activity for destructive adsorption is higher, for example, in BaO. In fact, the high destructive capacity of La_2O_3 lies in the regeneration potential with steam. This reaction relies heavily on the mobility of lattice oxygen atoms.

La_2O_3-based materials have high oxygen mobility and La^{3+} has been used as a dopant to increase oxygen mobility in catalysts.[5] This mobility is important for the regeneration of lattice oxygen. Oxygen atoms from water are converted into lattice oxygen at the catalytic surface of the solid under formation of HCl. Bulk phase conversion from $LaCl_3$ into LaOCl was detected, however, indicating that the diffusion of oxygen in the lattice is significant.[1, 3, 4] Therefore, destructive adsorption, which results in chlorination of the catalyst, should be investigated in order to gain fundamental understanding on the conversion of CHCs over La-based catalysts.

It was found that La_2O_3 and LaOCl are active for the destructive adsorption of CCl_4, although the latter is the more active phase.[6] From previous density functional theory (DFT) calculations, in combination with IR probing experiments, a general trend was observed: surface basicity decreases in the order La_2O_3 > LaOCl > $LaCl_3$.[6, 7] However, a real connection between CHC_1 destruction activity and the acid-base properties of the La-based catalysts is still missing. Therefore, in this chapter we focus on the physicochemical properties of La_2O_3-based materials in relation to the activity for the destructive adsorption of CCl_4. The goal of this chapter is to establish the link between acid-base properties of La-based solids and their destructive adsorption capacity behaviour for CCl_4. For this purpose, two distinct LaOCl materials have been prepared and characterized in detail, making use of X-ray diffraction (XRD), X-ray photoelectron spectroscopy (XPS), temperature programmed desorption (TPD) of CO_2, Raman spectroscopy, scanning electron microscopy (SEM) and IR spectroscopy (IR), while their acid-base properties were probed with CO, CO_2 and CH_3OH. As a result, it was possible to explain the difference in the reactivity of both solids in terms of difference in Lewis acid strength. This fundamental information provides guidelines for designing new catalyst materials with improved activity for the destruction of CHCs.

Experimental

Materials synthesis

Commercial samples of La_2O_3 (Acros Organics, 99.99 %, surface area of 1 m^2/g and pore volume of 0.004 mL/g) and $LaCl_3 \cdot 7H_2O$ (Acros Organics, 99.99 %, surface area of 6 m^2/g and pore volume of 0.03 mL/g) were used without additional purification. Two LaOCl materials were synthesized and are further denoted as LaOCl-S (S = solid state) and LaOCl-P (P = precipitation), with the labels indicating the preparation method.

LaOCl-S was synthesized by a solid-state reaction according to Reaction Eq. (1). An equimolar mixture of La_2O_3 (Acros Organics, 99.99 %) and $LaCl_3 \cdot 7H_2O$ (Acros Organics, 99.99 %) was exposed to a 20 mL/min flow of O_2 (Hoekloos, 99.995 %) at 700 °C.[8]

$$La_2O_3\ (s) + LaCl_3\ (s) \rightarrow 3\ LaOCl\ (s) \quad (1)$$

LaOCl-P was prepared by a precipitation process using $LaCl_3 \cdot 7H_2O$ (Acros Organics, 99.99 %) as a precursor and an aqueous NH_4OH (Acros Organics, 28-30 wt% in H_2O, p.a.) solution (Reaction Eq. (2) and (3)). The obtained gel was filtered, washed, dried at 120 °C and subsequently heated at 550 °C in pure N_2 (Hoekloos, 99.9 %) for 6 h.[9]

$$La^{3+} + 3\ Cl^- + 2\ OH^- \rightarrow La(OH)_2Cl\ (s) + 2\ Cl^- \quad (2)$$
$$La(OH)_2Cl\ (s) \rightarrow LaOCl\ (s) + H_2O\ (g) \quad (3)$$

Experimental setups

This section provides information on the IR cell combined with a vacuum system and the setup used for the activity experiments with online GC analysis. These home-built set-ups are discussed in detail because they are also used for experiments described in other chapters of this PhD thesis.

The quartz IR static vacuum cell is schematically shown in Figure 1. The lower part (Figure 1a) is built up from an oven region and the region where the IR beam passes through two KBr windows. The sample holder (Figure 1c) is placed inside the lower part of the cell, after which the upper part (Figure 1b) is connected. The sample holder, which has a piece of soft-iron incorporated, can be placed in two positions using a magnet: the sample is in the pathway of the IR beam, or the sample is hanging in the oven region. When it is in the IR beam, the sample holder is supported by the bottom of the cell. It is suspended in the oven region by using a second magnet to move a glass pin, also with soft iron incorporated, into the ring of the sample holder. In this manner, the sample can be heated, but this also enables measurement of a gas phase spectrum independent of the wafer. The oven region

can be heated to a maximum temperature of 550 °C.

The IR cell is connected to a vacuum system, which makes pre-treatment under vacuum conditions possible and is used to introduce reactants and probing compounds into the cell (Figure 2). A turbo pump enables pre-treatment of the sample at low pressure (mini-

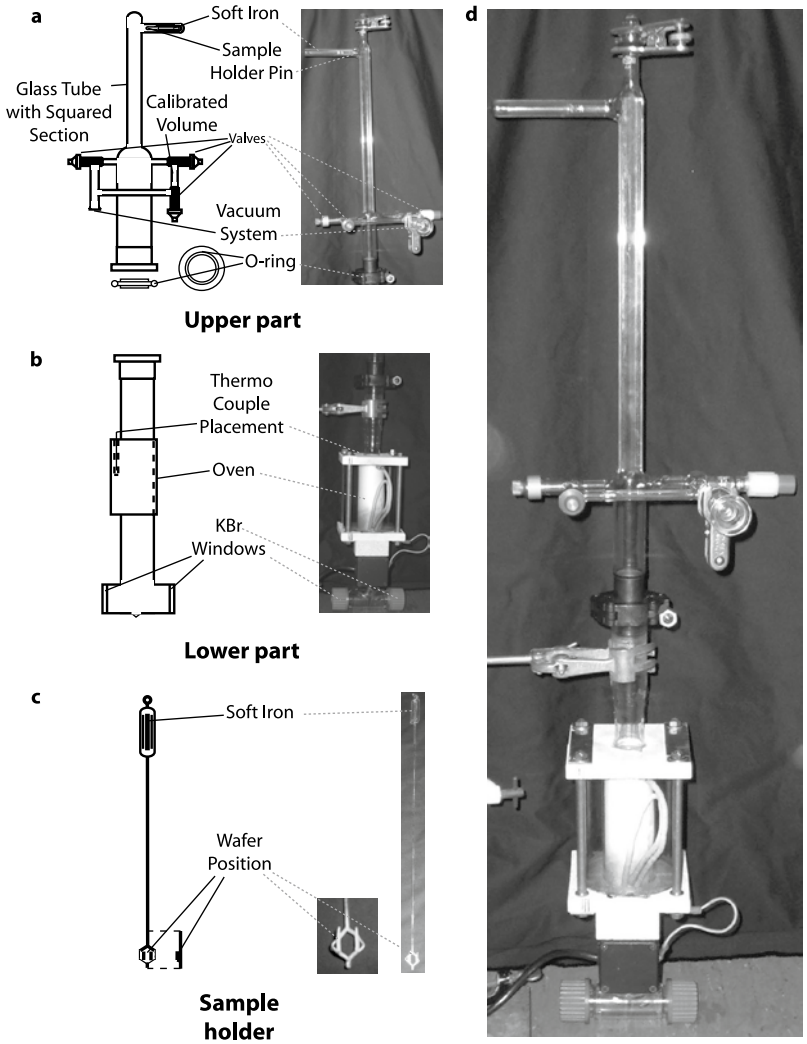

Figure 1. Schematic drawing and pictures of the parts of the quartz static vacuum IR cell used for probing experiments and in situ reactions with $CHC_{1\text{-}2}$: (a) upper part of cell, (b) lower part of cell, (c) sample holder, and (d) upper and lower part connected.

mum = 10^{-6} mbar). A membrane pump is connected to create a pre-vacuum for the turbo pump (minimum = 10^{-3} mbar) and to remove reactants and probing compounds from the cell. Liquid reactants and probing compounds are evaporated by injection via a septum into an evacuated flask under static vacuum, which was connected to the vacuum system. Gas phase reactants are led into the system by connecting gas cylinders to the vacuum systems via a pressure reducer. The system also contains two digital pressure meters to monitor the pressure of the reactants and probing compounds independently of the pressure in the vacuum cell.

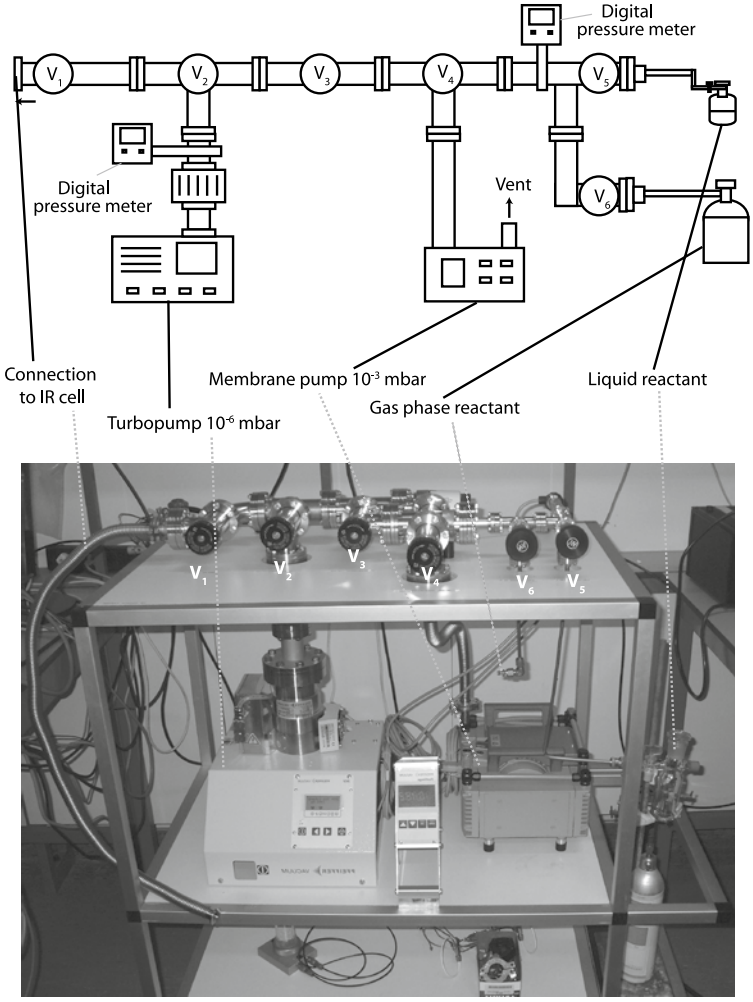

Figure 2. Schematic drawing and picture of the vacuum system connected to IR cell in Figure 1. $V_{1\text{-}6}$ indicate open/close volumes which are used to regulate pressure in the cell and the vacuum system.

The experimental setup used for the activity experiments is shown in Figure 3. The setup consists of three main parts: the automatic mass flow controller (MFC) system for the generation of the reactant feed, the oven containing the reactor and catalyst bed, and the online gas chromatograph (GC). The MFCs (Brooks 0-100 mL) and the oven are controlled by Labview and the GC is controlled by EZChrom 3.2.

The reactant flow is generated by running He through a bubbler containing a volatile liquid compound. The bubbler can be placed in an ice bath to keep the vapour pressure, and consequently the reactant concentration, constant. The concentration resulting from the He and $CHC_{1\text{-}2}$ vapour ranges between 0 and 10 vol% $CHC_{1\text{-}2}$ in He. In this manner, two flows can be generated based on volatile liquid $CHC_{1\text{-}2}$ (MFC 1 and 2). MFC 3 is a MFC which can be used for various gas phase reactants. The gas phase reactant is then diluted to the desired concentration with He provided by MFC 1 or 2 without a bubbler. The flow is led to

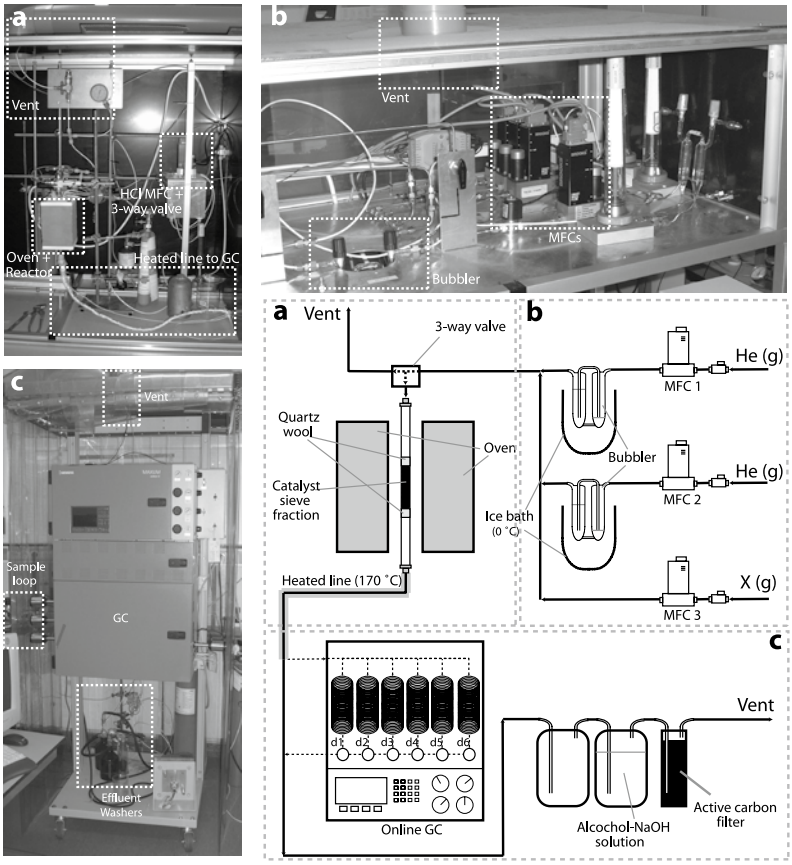

Figure 3. Schematic drawing and pictures of the setup used for catalytic activity experiments for reactions with $CHC_{1\text{-}2}$. (a) MFC system, (b) Oven and reactor, and (c) GC and effluent purification. X represents any gas different from He.

the reactor via a three-way valve, which is also connected to the vent. The three-way valve can be switched to the vent to stabilize the reactant flow concentration before contact with the catalyst and to release over-pressure. The catalyst sieve fraction is fixed between two quartz wool wads in a quartz tubular fixed bed reactor, which is positioned vertically in a tubular oven with the gas inlet at the top. The flow runs from the reactor through a heated line (170 °C) to prevent condensation of the reactants and products. This line is made of stainless steel of which the inside is fused with silica to prevent corrosion as a result of reaction products.

The composition of the reactor effluent was analyzed by a custom-built Siemens Maxum Edition 2 gas chromatograph with a sampling time of 240 s connected via a sample loop. The connectors and valves in the GC are made out of corrosion-resistant Hastelloy-C alloy. The GC contains four separate columns and detectors, which are each calibrated for a different group of compounds. All detectors are thermal conductivity detectors (TCD) using He as carrier gas. The chromatograph columns are positioned into two separate oven parts, which are kept by at 80 and 120 °C means of an air bath. The different groups of chemicals that are analyzed by each column are shown in Table 1. The gas flow finally passes through an alcohol-NaOH solution and an active carbon filter to remove acidic products and volatile organics, respectively, before it is released into the vent. The entire GC was positioned under ventilation surrounded by transparent plastic sheets to optimize the suction of the vent (Figure 3c). Both the reactor (Figure 3a) and the mass-flow controller system (Figure 3b) were positioned in closed compartments with separate connections to the ventilation.

Table 1. Siemens Maxum GC columns and the respective compounds for which each column was calibrated.

Column Name	Column T (°C)	Detected compounds
RR1 T1	80	O_2, N_2, Ar, CH_4 and CO
RR2 T2	80	CH_4, CO_2, C_2H_4 and C_2H_6
RR3 T3a	80	CH_4, CO_2, C_2H_4, C_2H_6 and HCl
RL2 T5a	120	CCl_4, $CHCl_3$, CH_2Cl_2, CH_3Cl, CH_3OH, 1,1,2-$C_2H_3Cl_3$, 1,2-$C_2H_4Cl_2$, C_2H_5Cl, 1,1-$C_2H_2Cl_2$, cis-1,2-$C_2H_2Cl_2$, trans-1,2-$C_2H_2Cl_2$, C_2H_3Cl and C_2HCl not calibrated: CH_4, H_2O, CO, CO_2 and HCl

Characterization

The phase purity of the La-based materials was checked with XRD. The XRD measurements were collected at ambient conditions with a Bruker-Nonius PDS 120 powder diffractometer system, equipped with a position-sensitive gas-filled detector of 120° 2θ, using Co $K\alpha_1$ radiation (λ = 1.78897). A Phillips XL-30 field emission gun (FEG) scanning electron

microscope was used to obtain SEM images. XPS spectra were acquired using a Perkin-Elmer (PHI) model 5500 spectrometer. All spectra were obtained using samples in the form of pressed wafers. XPS data were obtained for LaOCl-S and LaOCl-P, before and after (only for LaOCl-S) reaction with CCl_4. Raman spectra were recorded with a Holoprobe Kaiser Optical spectro-meter equipped with a holographic notch filter, CCD camera, and 532 nm laser. All spectra were measured under ambient conditions. The specific surface area and pore volume have been determined by N_2 sorption measurements with a Micromeritics accelerated surface area and porosimetry ASAP 2400 instrument. Surface areas were calculated by using the BET model with micro- and macropores described by the Horvath-Kawazoe and BJH models, respectively.

IR spectra of the probing measurements with CH_3OH and CO_2 were collected using a Nicolet 550 spectrometer with a resolution of 4 cm^{-1}. The IR quartz cell described in the previous section was used at room temperature (RT). The samples, were pressed into self-supported 2 cm^2 disks and activated in situ prior to IR measurements in vacuum (~$1 \cdot 10^{-4}$ Pa) at 550 °C. CH_3OH (Sigma-Aldrich, 99.9+ %) was initially dosed to an equilibrium pressure of 1.3 mbar. The gas was then progressively evacuated at RT and then at increasing temperatures up to 200 °C. CO_2 (Air Liquide, Inc., 99.99+ %) was dosed in steps to equilibrium pressures up to 6.5 mbar.

For CO sorption, a stainless steel IR cell was equipped with crystalline ZnSe inner windows, which, in combination with the outer KBr windows, allowed it to collect spectra in the region of 4000-500 cm^{-1}, while the temperature increased from -195 to 25 °C. The samples were pressed into self-supported 2 cm^2 wafers and activated in situ prior to IR measurements in a vacuum at 550°C for 2-3 h. Before CO introduction, the samples were cooled to the corresponding experimental temperatures (-195 °C) under a vacuum of $5 \cdot 10^{-5}$ mbar. It is important to note that the cell should be cooled below 0 °C, keeping the sample in the upper part of the cell to prevent the humidity absorbed on the cell walls to reach the sample surface. CO was dosed at -195 °C to ~6 mbar equilibrium pressure of CO and progressively desorbed in a closed cell by raising the temperature in the range from -195 to 25 °C. In this case, the pressure inside the cell rose to 10-12 mbar because of desorption and cell heating. The low temperature IR spectra were recorded using a Bruker IFS166 spectrometer with 3 cm^{-1} spectral resolution.

TPD experiments with CO_2 were performed in a tubular reactor under a He flow with the effluent analyzed by a Micromeritics Autochem II chemisorption analyzer. The heating rate was 5 °C /min. Atmospheric CO_2 was adsorbed after long-term exposure to air at ambient conditions. No pre-treatment was used for these experiments.

Activity experiments

The activity measurements for the destructive adsorption of CCl_4 were performed with the experimental setup shown in Figure 3. The catalyst bed consisted of 1.0 g of sample

pressed in a 150-500 μm sieve fraction, pretreated in a 10 mL/min He flow at 550 °C. In the case of La_2O_3, the pretreatment was under O_2 flow instead of He. To find the initial reaction temperature, the reaction was carried out from 50 to 400 °C using a 20 mL/min 6 vol % CCl_4/He flow. This flow was generated by bubbling He through a bubbler containing CCl_4 for 30 min out through a vent. Once stabilized, the flow was led over the reactor bed. The temperature of the reactor was raised from 50 to 400 °C in steps of 10 °C. The heating ramp was 3 °C/min, and after each step of 10 °C, the temperature was held constant for 5 min. In the case of LaOCl-S and LaOCl-P, the reactions were also performed at a constant temperature of 200 °C. The flow was stabilized as described above and led over the pre-treated reactor bed at 200 °C. The composition of the reaction mixture was analyzed with time by GC.

Results and Discussion

Materials synthesis and characterization

Table 2 summarizes the physicochemical properties of the La-based materials under study. The N_2 sorption results show that LaOCl-P has a relatively large surface area and pore volume. La_2O_3 possesses a lower surface area, pore volume and average pore size than LaOCl-S and LaOCl-P. LaOCl-P shows a more open structure compared to LaOCl-S and La_2O_3. More importantly, the high surface area means that there will be more reaction sites available for LaOCl-P than for LaOCl-S and La_2O_3. The XRD patterns of LaOCl-S and LaOCl-P are shown in Figure 4 and resemble those of tetragonal LaOCl.[10] As a reference, the diffractogram of La_2O_3 is included in Figure 4, and the XRD 2θ positions and intensities for LaOCl,[10] $LaCl_3$,[11] and $La_2O(CO_3)_2$[12] are summarized in Table 3.

However, both the reflection intensities and the background level clearly vary with the preparation method. Intense and sharp reflection peaks associated with a very weak back-

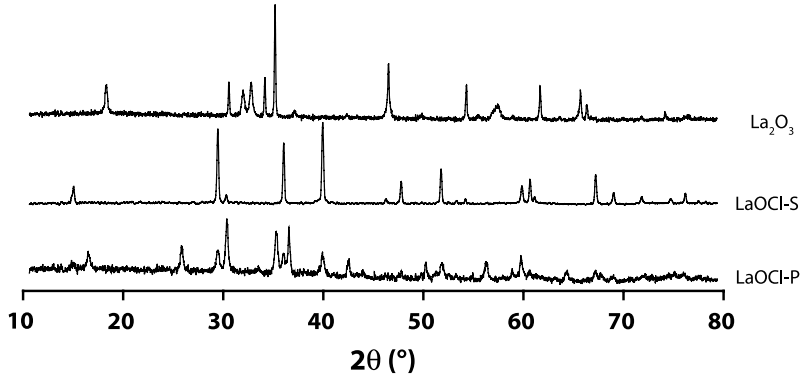

Figure 4. X-ray diffractogram of La_2O_3, LaOCl-S, and LaOCl-P materials measured under ambient conditions.

ground are observed for LaOCl-S, pointing out the high crystallinity of this sample. In contrast, the XRD patterns of LaOCl-P features broad reflections of very low intensity compared to LaOCl-S, while the background level is particularly high.

Table 2. Physicochemical properties of the La-based catalyst materials under study, together with the surface composition and phase purity as determined with XPS, XRD and Raman (na = not applicable).

Sample name	Surface area (m^2/g)	Pore volume (mL/g)	Average pore size (nm)	Surface composition as determined with XPS		Phases as determined with Raman	Phases as determined with XRD
				O/La	O/Cl		
La_2O_3	1	0.001	14.3	0.34	na	La_2O_3	La_2O_3 La carbonates
LaOCl-S	6	0.040	23.6	0.17	2.78	LaOCl	LaOCl
LaOCl-P	36	0.300	34.0	0.14	1.80	LaOCl	LaOCl $LaCl_3$ La carbonates
$LaCl_3$	6	0.030	22.4	na	na	$LaCl_3$	$LaCl_3$

This indicates that LaOCl-P contains a small number of LaOCl crystallites embedded in an amorphous phase. Also, additional peaks are present in the XRD of LaOCl-P. When compared to reference materials,[11, 12] a large amount of $La_2O(CO_3)_2$ was found to be present in LaOCl-P. The lanthanum carbonates are most likely formed with CO_2 from the water or the air during precipitation. The carbonates are very stable and remain in the material up to a temperature of 750 °C.[6] SEM photographs of LaOCl-S and LaOCl-P are presented in Figure 5. LaOCl-S shows a very homogeneous distribution of polycrystallites with lengths of ca. 4 µm and thicknesses of < 1 µm. This particular shape of grains reflects well the layered crystalline structure of LaOCl. The SEM picture of LaOCl-P sample shows polycrystallites of small size having a rodlike shape. The difference in morphology as concluded from the XRD data is therefore confirmed by these SEM images.

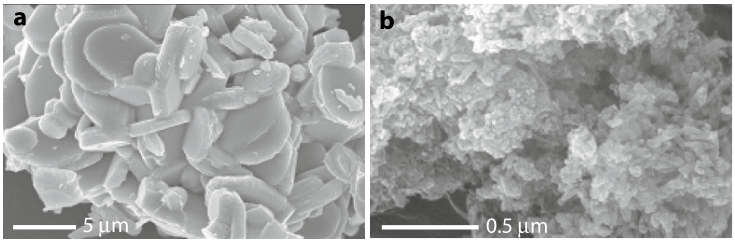

Figure 5. Scanning electron micrographs of (a) LaOCl-S and (b) LaOCl-P materials.

Destructive adsorption of CCl4 over La-based solids

The Raman spectra presented in Figure 6 both show that the main phase of LaOCl-S and LaOCl-P is LaOCl, as evidenced by the bands at 331 and 437 cm^{-1}.[13, 14] Especially, the Raman spectrum of LaOCl-P shows other bands at 413, 392, 363, 302, 243 and 224 cm^{-1}. No reference was found with respect to these bands, but they possibly result from bulk lanthanum carbonate. However, the Raman band indicative of carbonates around 1000 cm^{-1} is not observed in the spectrum, and it is presently unclear why these differences occur between

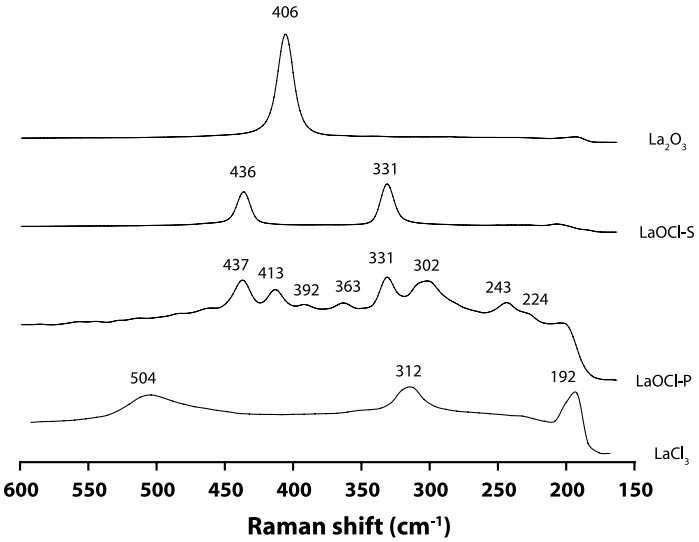

Figure 6. Raman spectra of La_2O_3, LaOCl-S, LaOCl-P and $LaCl_3$ materials measured under ambient conditions.

Table 3. XRD positions and relative intensities for $LaCl_3$, LaOCl, and $La_2O(CO_3)_2$.[10-12]

LaOCl		$LaCl_3$		$La_2O(CO_3)_2$	
20 (°)	**Relative intensity**	**20 (°)**	**Relative intensity**	**20 (°)**	**Relative intensity**
25.9	326	15.9	999	14.9	400
29.3	290	27.7	315	29.3	1000
30.0	747	28.6	520	35.8	1000
35.4	999	32.1	141	39.6	750
39.3	229	36.7	221	47.5	500
52.0	487	40.3	719	51.4	950
55.8	359	42.9	128	59.6	350
59.2	214	48.2	152	60.4	900
67.0	227	48.9	240	67.0	850
		49.4	508	75.6	750
		71.0	130	86.9	500

XRD and Raman. The bands at 413, 363, 302, 243 and 224 cm^{-1} may therefore result from the background and have become visible because of the low intensity of the LaOCl bands. XPS also provides information regarding the phase purity of LaOCl-S and LaOCl-P. According to Table 1, the O/La surface ratio for La_2O_3 is 0.34 and for $LaCl_3$ is 0. For LaOCl-S, the value of 0.17 again shows that it is a very pure LaOCl phase. LaOCl-P has a slightly lower O/La ratio and should therefore be more chlorinated.

Activity Experiments

In a first series of experiments, we have studied the destructive adsorption of CCl_4 over La_2O_3, LaOCl-S, and LaOCl-P and $LaCl_3$ as a function of the reaction temperature. Figure 7 only shows the conversion of CCl_4 to CO_2 for three materials, because no significant activity was observed for $LaCl_3$. The first CO_2 is detected at 300 °C for La_2O_3, and a sharp increase in the amount of CO_2 is observed at higher temperatures. The formation of carbonates by re-adsorption of CO_2 might delay the detection of CO_2. However, in previous TPD measurements[15] CO_2 was already released at 230 °C from La_2O_3 which contained carbonates. Since, during the experiment, CO_2 is not detected until 300 °C, the interference of carbonate formation with our experiments is not likely. The initial reaction temperature is at approximately 170 °C for both lanthanum oxychloride materials. This is at a much lower temperature than

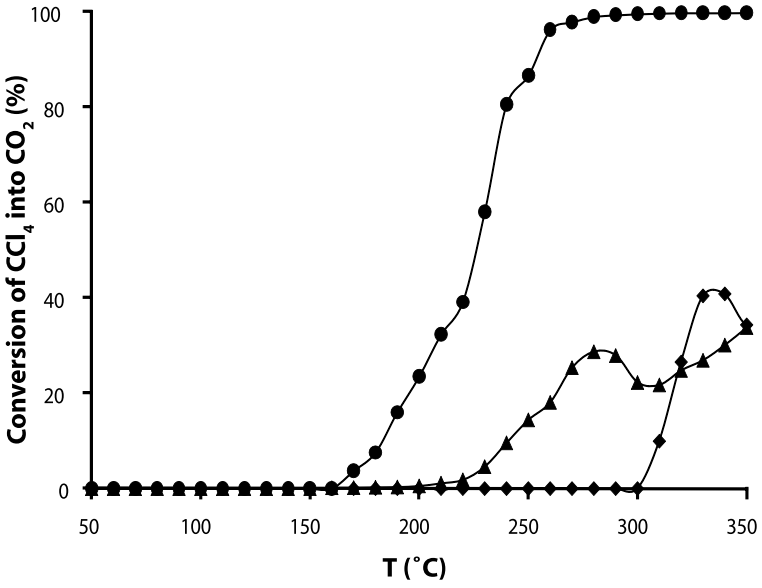

Figure 7. Conversion of CCl_4 to CO_2 measured at 200 °C for samples La_2O_3 (♦), LaOCl-S (▲) and LaOCl-P (●) as a function of temperature.

for La_2O_3, indicating that both LaOCl materials are more active than La_2O_3.

Since the samples become chlorinated during the reaction, the initial temperature of reaction is the only information available from these measurements. To be able to compare LaOCl-S and LaOCl-P, the materials were tested for the CCl_4 destruction reaction at constant temperature of 200 °C as well. The results are shown in Figure 8. In the first part of the measurement, the conversion is constant and controlled by the transformation of CCl_4 into the products. It should be noted that for LaOCl-P, the conversion is 100% in the first part of the curve and that its destruction capacity may be higher than indicated by these results. Then, as the rate of conversion decreases, bulk diffusion limitations take effect. After this, the conversion stabilizes and reaches a steady state, where the reaction is controlled by diffusion of oxygen to the surface and chlorine to the bulk. In the case of LaOCl-S, the steady-state conversion as a result of solid-state O/Cl diffusion is close to zero due to its low surface area. Eventually, the materials will become deactivated, and the conversion drops to zero.

After reaction at constant temperature, resulting in deactivation, XPS and Raman were performed on the deactivated LaOCl-S sample. LaOCl-P was not measured in this way, since it took very long to deactivate. The Raman spectra before and after reaction did not show any change in band positions or intensity. Apparently, no change in the bulk phase was observed as a result of the reaction. The XPS results tabulated in Table 4 show a relative decrease in oxygen and an increase of chlorine at the surface. Even though LaOCl-S has become deactivated, oxygen is still present at the surface. The final chlorine content increases with the reaction temperature. Higher temperatures result in a prolonged O/Cl bulk/surface diffusion and bulk diffusion decreases as the chlorine content increases. However, an increased temperature facilitates O/Cl diffusion, allowing it to continue even at higher chlorine content.

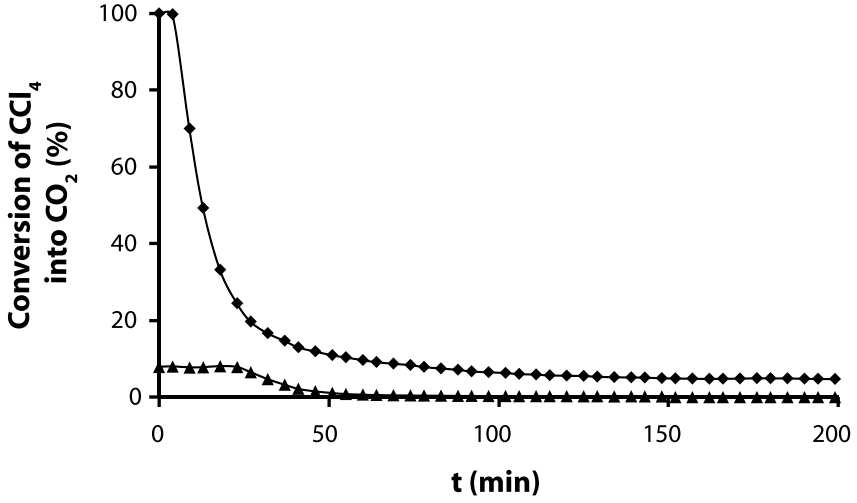

Figure 8. Conversion of CCl_4 to CO_2 measured at 200 °C for samples LaOCl-S (▲) and LaOCl-P (♦) as a function of time.

LaOCl-P has a much higher destruction activity, which was expected in view of the high surface area of LaOCl-P. Therefore, the conversion has to be normalized to enable a fair comparison between the activities of LaOCl-S and LaOCl-P. The conversion, 8% for LaOCl-S and 100% for LaOCl-P, is divided by the surface area to get the activity per square meter of material. During the reaction, the surface area that was calculated with N_2 physisorption changes as a result of the chlorination. For the first area of the curves, the change in surface area is assumed not to be significant. For LaOCl-S and LaOCl-P, respectively, the destructive capacities were $4.2 \cdot 10^{-7}$ and $8.7 \cdot 10^{-7}$ mol CO_2 formed per square meter of material per minute. However, for LaOCl-P, the obtained destructive adsorption is a lower limit. So, after normalization, LaOCl-P is over twice as active as LaOCl-S. The key factor in the activity is the strength of the acid-base couple responsible for the reaction.[16] The Lewis acid site initiates the reaction by splitting off a chlorine atom. Therefore, the trend in activity, La_2O_3 < LaOCl-S < LaOCl-P, parallels the trend in surface acidity. However, $LaCl_3$ is not active for the destructive adsorption of CCl_4, even though it is more acidic than the other materials. This is because of the absence of basic oxygen sites, which stabilize the CCl_3 fragment remaining after the initial split of a chlorine atom by the acid site. Moreover, the absence of oxygen simply implies that no stoichometric reagent is available for CO_2 formation. The difference in destructive capacity between LaOCl-S and LaOCl-P is expected to be linked to a difference in acid-base properties between them, in particular to the strength of the Lewis acid sites. Therefore, the LaOCl materials were further studied with probe molecules in combination with IR spectroscopy.

Table 4. O/Cl ratio measured by XPS of sample LaOCl-S before and after reaction with CCl_4 until deactivation at various temperatures.

Sample	O/Cl
• Before reaction	• 2.8
• Deactivated after reaction at 200 °C	• 1.7
• Deactivated after reaction at 210 °C	• 1.6
• Deactivated after reaction at 220 °C	• 1.4

Materials acid-base properties

CO_2 was adsorbed to probe the basicity of the materials under study. CO_2 can act as a Lewis acid toward either O^{2-} surface ions resulting in the formation of carbonate species, or residual basic OH surface species resulting in the formation of hydrogen carbonates. Furthermore, CO_2 can act as a Lewis base and form carboxylates. The possible compounds resulting from CO_2 coordination are described in Scheme 1.[15] For the carbonates, the principal anchoring structures are included in this scheme. The IR spectra after CO_2 adsorption for LaOCl-S and LaOCl-P are shown in Figure 9. The spectra were obtained by subtraction of the spectrum measured directly after pre-treatment. In all spectra, the spectrum of gas phase

CO_2 was subtracted in order to display only the surface species. They were also normalized for the amount of sample and the surface area.

The band around 1450 cm^{-1} in the spectrum of LaOCl-P appeared as a result of the subtraction. For LaOCl-S, three main bands were observed at 1589, 1423, and 1266 cm^{-1}. Smaller bands were present at 2349, 1523, 1326, and 1200 cm^{-1}. Bands, which are not shown here, were also detected at 1036, 845, 826, 729, 708, and 669 cm^{-1}. The latter is

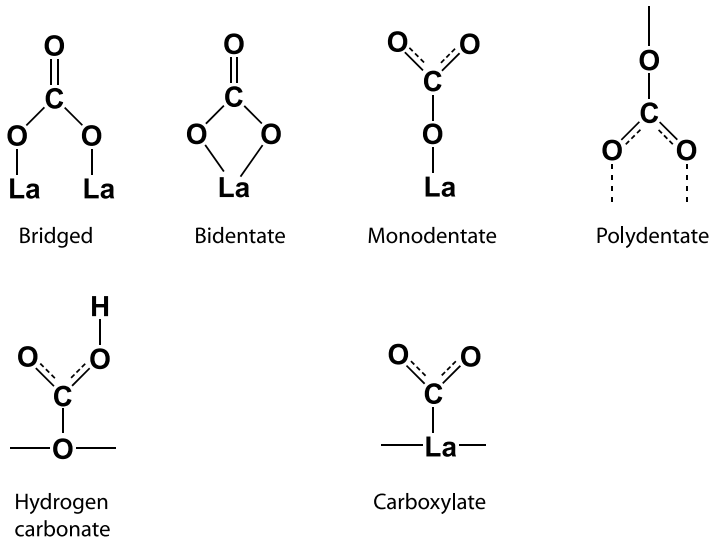

Scheme 1. Possible surface structures as a result of CO_2 adsorption on La_2O_3.

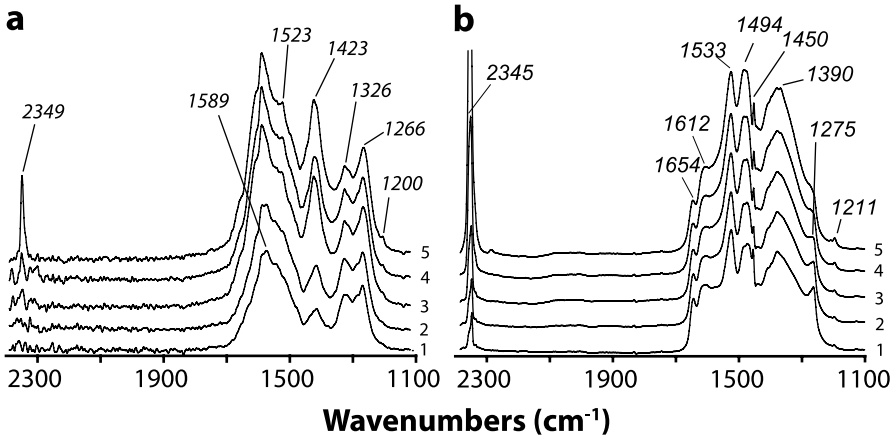

Figure 9. FTIR spectra of adsorbed CO_2 on (a) LaOCl-S and (b) LaOCl-P after 15 min of equilibration at CO_2 pressures of (1) 0.05, (2) 0.1, (3) 0.3, (4) 1.3, and (5) 6.5 mbar.

a bending mode of molecular CO_2. The band at 2349 cm^{-1} was only observed at high equilibrium pressures. This band is generated by the coordination of CO_2 on Lewis acid sites of the surface. The main band at 1423 cm^{-1} has been attributed to the doubly degenerated asymmetric ν_3 stretch of the free carbonate ion.[17] In the present case, it corresponds to a polydentate carbonate, having a strong ionic character. In the adsorbed state, the symmetry of the carbonate ion is lowered, and the species generally present two split ν(CO) bands at either side of the band at 1423 cm^{-1}.[18] This is the case for the other two main bands at 1589 and 1266 cm^{-1}, which are both at 166 cm^{-1} from this band. The bands at 1523 and 1326 cm^{-1} are also coupled with a $\Delta\nu_3$ = 100 cm^{-1}, where $\Delta\nu_3$ is the difference in frequency between the ν_3 stretch of the free carbonate ion and the split bands. It has been shown that bidentate carbonate species generally present a $\Delta\nu_3$ split between 150 and 300 cm^{-1}, and bridging carbonate species have a $\Delta\nu_3$ split above 300 cm^{-1}.[18] The bands with $\Delta\nu_3$ = 100 cm^{-1} are indicative of either monodentate or polydentate carbonates.

Using these considerations, we can unfortunately not distinguish between monodentate and polydentate carbonates, except for their thermal stability, with the former being less stable at higher temperature. The relative intensities of the bands in the spectrum of LaOCl-S would then be attributed to a low concentration of monodentate or polydentate carbonates and a high concentration of bidentate carbonate. Also, the band at 845 cm^{-1} is attributed to the $\pi(CO_3)$ of bidentate carbonate,[18] and the band at 1036 cm^{-1} has been attributed to the symmetric C-O stretching of bidentate carbonate.[17] The presence of a weak, but sharp band at 1201 cm^{-1} could be indicative of the presence of hydrogen carbonates (∂(OH) mode).[18] In such case, the corresponding stretching modes will be found at around 1600 cm^{-1} (a shoulder in the high-wavenumber tail of the bidentate carbonate band) and below the 1266 cm^{-1} peak. The corresponding ν(OH) mode could be guessed at around 3624 cm^{-1}, but that region is however very noisy. If confirmed, the presence of hydrogen carbonate species will be indicative of the basicity of hydroxyl groups.

In the spectra of LaOCl-P, the band of weakly adsorbed CO_2 is also present, but the band is present in all spectra and not just at a high equilibrium pressure. This indicates that these species are more strongly adsorbed and that the Lewis sites are more acidic. In fact, the band is also slightly shifted to lower wavenumbers. The IR spectra are very different from those of LaOCl-S in the carbonate region. A broad set of bands is present even at low equilibrium pressure. A similar spectrum was obtained for CO_2 adsorption on La_2O_3 as reported by Manoilova et al..[6] Also, the IR spectrum of $La_2(CO_3)_3$ is characterized by these absorption bands between 1650 and 1250 cm^{-1} with two peaks at 1494 and 1390 cm^{-1}.[19] The bands at 1654, 1612, and 1275 cm^{-1} were also observed by Manoilova et al. in the spectra of LaOCl and were attributed to bridged carbonate. In that case, however, these bands appeared simultaneously with another band due to bridged species on two different O adsorption sites. In the case of LaOCl-P, they are not coupled, indicating that the two O adsorption sites of these bridged species are not different. Another interpretation is that the band at 1612 cm^{-1} would be assigned to hydrogen carbonates, which are confirmed for LaOCl-P by the modes at 1211 and 3624 cm^{-1}. So, only the bands at 1654 and 1275 cm^{-1} are likely to be assigned

to a single species of bridged carbonates. Previously, the IR frequencies for monodentate, bridged, and polydentate carbonates have been calculated by DFT,[7] but the geometries for the bridged type tended to converge into the polydentate structure. This may explain the observed difference between the calculated[7] and experimentally observed frequencies.

To discriminate between the presence of either polycarbonate or monodentate carbonate on LaOCl-S, TPD with CO_2 was performed. Similar experiments were also done for LaOCl-P to verify the type of carbonates detected on the surface. The results are given in Figure 10. In Table 5, reference compounds and their respective desorption temperatures are tabu lated.[6] For LaOCl-S, the first signal on the thermal conductivity detector (TCD) is measured at 25-170 °C. At this temperature, water is desorbed from the surface. A small shoulder is also present around 160 °C, which has been assigned to physisorbed CO_2. Another peak becomes visible at 240-430 °C, which also possesses a low-intensity shoulder. The main band can be assigned to either bidentate or bridged carbonate species. However, in the case of bridged species, polydentate carbonates would be formed as a result of the CO_2 desorption. Since no signal is detected above 370 °C and polydentate carbonates desorb around 620 °C, the signal is most likely indicative of bidentate carbonates. No references were found regarding the low-intensity shoulder at 400 °C. IR spectroscopy was unable to discriminate between polydentate carbonates and monodentate carbonates before, but as stated above,

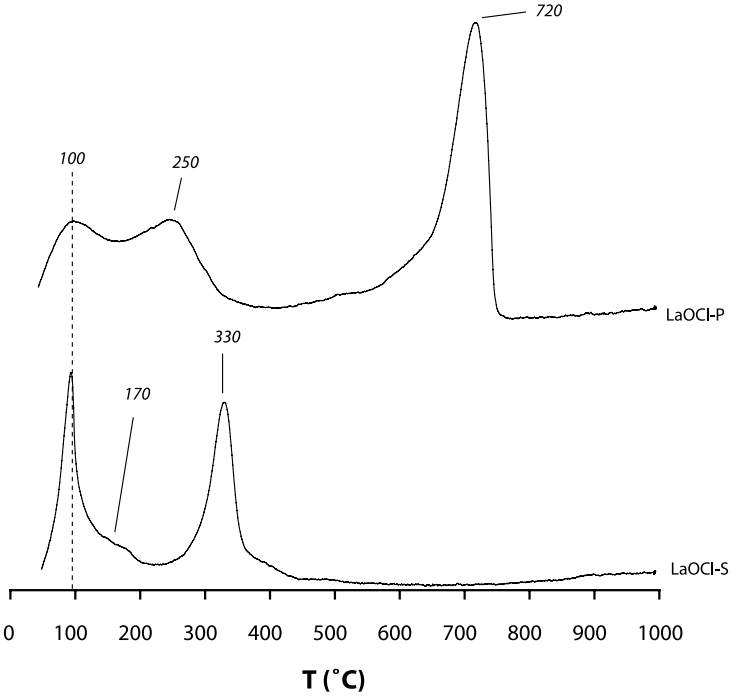

Figure 10. TPD of CO_2 adsorbed from the air under ambient conditions on LaOCl-S and LaOCl-P.

Table 5. Desorption temperatures for La-based reference compounds.[6]

Reference compound	Structure / Reaction	Desorption Temperature (°C)
La_2O_3	$La_2(CO_3)_3 \rightarrow La_2O_3 \cdot xCO_2 + (3\text{-}x)\ CO_2$ $La_2O_3 \cdot xCO_2 \rightarrow La_2O_3 + x\ CO_2$	300-400 500-730
LaOCl	physisorbed $CO_2 \rightarrow CO_2$ bridged carbonates → polydentate carbonates + CO_2 polydentate carbonates → CO_2	100 290 620
$LaCl_3$	physisorbed $CO_2 \rightarrow CO_2$	100

no polydentate carbonates were detected by TPD. The band for monodentate carbonates is usually measured around 25 °C, but is hard to distinguish since physisorbed CO_2 and water also desorb in this region. However, according to the IR results, monodentate carbonates are formed upon adsorption of CO_2 on LaOCl-S. Therefore, on LaOCl-S, a low concentration of monodentate species and a high concentration of bidentate carbonates is expected to be present after adsorption of CO_2.

For LaOCl-P, two TCD peaks are visible in the region between 25 and 380 °C. One possesses a maximum at 75 °C and the other at 230 °C. As for sample LaOCl-S, the former is assigned to water and physisorbed CO_2, while the latter is indicative of either bidentate or bridged carbonate species. Another option is the decomposition of bulk carbonates. A peak between 500 and 730 °C would then also be visible, and this is in fact the case. In the case of bridged species, formation of polydentate carbonates would be the result of CO_2 desorption. IR results indicated the presence of bridged carbonates and bulk carbonates. This is certainly a possibility, but the TPD results cannot discriminate between bridged carbonates and bulk carbonates, since they possess desorption peaks in the same temperature regions. On the basis of both the IR results and the TPD results, the formation of bridged and bulk carbonates takes place upon adsorption of CO_2 on LaOCl-P.

CO adsorption can be used to probe Lewis acidity. Absorption bands located at high wavenumbers are related to strong M-CO bonds, which is a consequence of a strong Lewis acid site. On the basis of IR spectra during adsorption and desorption of CO, a distribution of the strengths of the Lewis acid sites can be obtained. Figure 11 shows the IR spectra for sample LaOCl-S obtained after CO adsorption and consecutive desorption for increasing measurement temperature. Because of the low surface area and relatively high activation temperature, no IR bands due to hydroxyl groups could be discovered. As a consequence, we concentrate our analysis on the ν(CO) region. After CO adsorption at -195 °C, a strong band at 2165 cm^{-1} was observed with a weak shoulder at 2155 cm^{-1}, likely witnessing the presence of Brønsted acid sites. After CO desorption, the band at 2155 cm^{-1} disappears quickly, and the band at 2165 cm^{-1} decreases in intensity and shifts to 2172 cm^{-1}. The CO adsorption band and the consecutive desorption of CO show the distribution in strength of the Lewis acid sites at the surface of LaOCl-S. The strongest Lewis acid sites on LaOCl-S are

therefore represented by the band that remains after CO desorption at 2172 cm^{-1}.

In the IR spectrum of LaOCl-P presented in Figure 12, a weak band of the hydroxyl groups was observed at 3651 cm^{-1}, so confirming the presence of small amounts of Brønsted acid sites. After CO adsorption at -195 °C, the free OH band disappeared completely, and a perturbed one becomes visible at 3615 cm^{-1}. In the CO region of the IR spectra, the strong

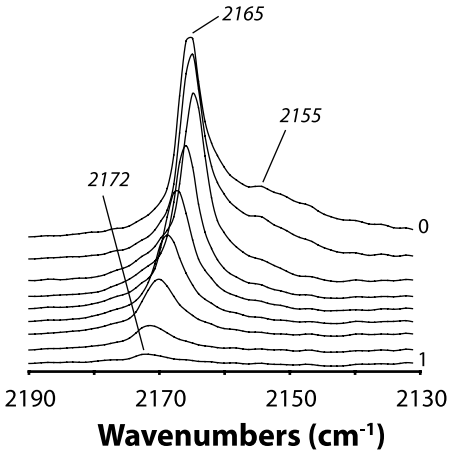

Figure 11. FTIR spectra of CO adsorbed on LaOCl-S at 6 mbar equilibrium pressure (spectrum 0) and consecutive desorption of CO, while the temperature is increased from -195 to -60 °C (spectrum 1) for the region of CO coordinated on Lewis acid sites.

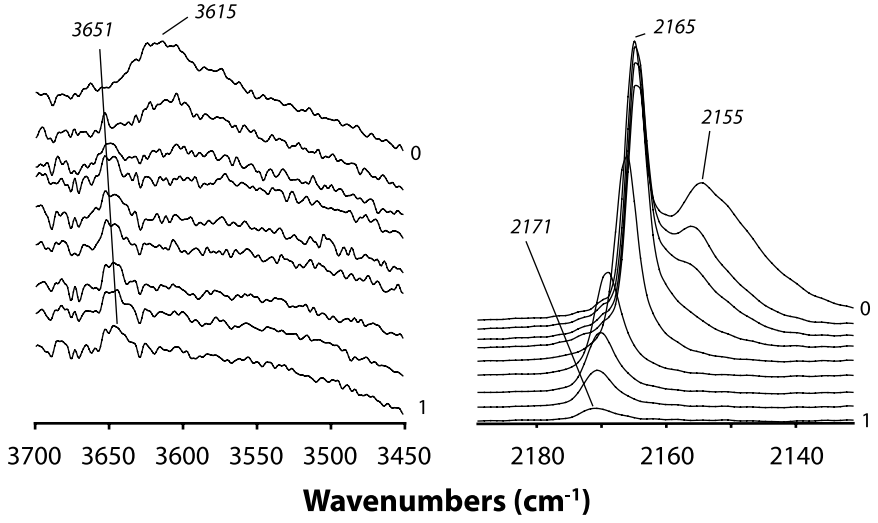

Figure 12. FTIR spectra of CO adsorbed on LaOCl-P at 6 mbar equilibrium pressure and consecutive desorption of CO, while the temperature is increased from -195 to -60 °C for (a) the region of OH vibrations and (b) the region of CO coordinated on Lewis acid sites.

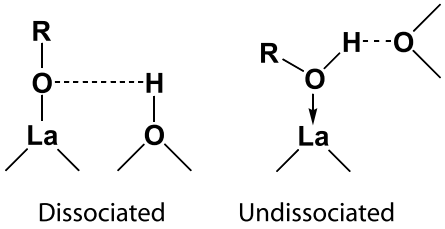

Scheme 2. Types of irreversibly adsorbed alcohols on metal oxides.

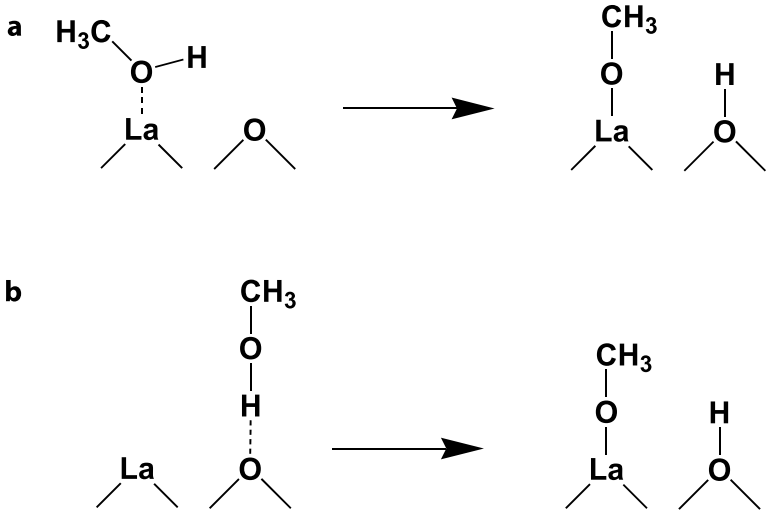

Scheme 3. Dissociation process of CH_3OH on an acid/base couple with predominant (a) Lewis acid and (b) Lewis base character.

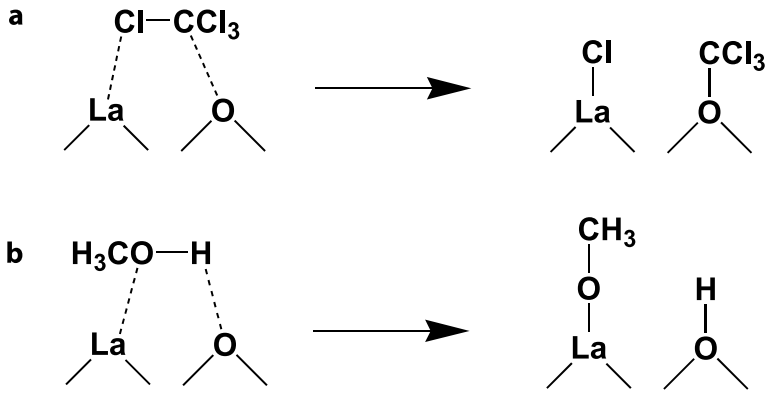

Scheme 4. Dissociation process of (a) CH_3OH and (b) CCl_4 on an acid/base couple.

band at 2165 cm^{-1} and a weak and broad one at 2155 cm^{-1} were observed. After CO desorption, the band at 2155 cm^{-1} decreases in intensity. At the same time, a free hydroxyl band reappears, and the perturbed one at 3615 cm^{-1} diminishes. In other words, the band at 2155 cm^{-1} can be assigned to H-bonded CO. After CO desorption, the band at 2165 cm^{-1} shifts toward higher wavenumber at 2171 cm^{-1}. As with LaOCl-S, the distribution of the strengths of the Lewis acid sites is reflected in the spectra upon desorption. In the case of LaOCl-P, the strongest Lewis acid site is represented by the band at 2171 cm^{-1}. So, LaOCl-S and LaOCl-P have identical Lewis acid sites and also show no large differences in the distribution of the Lewis acid sites. Thus, the type of sites available on samples LaOCl-S and LaOCl-P cannot be distinguished by CO adsorption using IR spectroscopy. To discriminate between the different sites, another more powerful probe molecule is needed. In our opinion, this is CH_3OH.

Two types of irreversibly adsorbed species (species which are not removed by a relatively short evacuation at RT) can be formed as a result of adsorption of alcohols on metal oxides: alkoxy species, resulting from dissociative chemisorption on a very weak Lewis acid site located near a very basic one, and undissociated species, coordinated on a strong Lewis acid site.[20] This is schematically represented in Scheme 2. Adsorption of CH_3OH is, however, much less specific, since it could also occur on couples having a predominantly Lewis acid character. The respective dissociation processes of an acid/base couple with predominant Lewis acid and base character can be envisaged as in Scheme 3.[4] Dissociation of CH_3OH on an acid-base couple is similar to the first reaction step for the destruction of CCl_4. DFT calculations have shown that CCl_4 is split into two fragments: $Cl^{\partial-}$, coordinated toward the Lewis acid site, and $CCl_3^{\partial+}$, stabilized on the basic oxygen.[7] CH_3OH is also split into two fragments: methoxy species coordinated toward the Lewis acid site and a hydrogen atom, which is transferred to the basic oxygen site. Since the same acid-base couple is needed for both processes, the CH_3OH adsorption results are very likely to give information on the active site for the destructive adsorption of CCl_4 over La-based materials as well. The comparison between CCl_4 and CH_3OH dissociation on a La-O acid-base couple is shown in Scheme 4. Because, compared to oxygen, the chlorine atom is more electronegative, the La-Cl bond formed during the dissociation is stronger than the La-OCH_3 bond, and the Cl is more difficult to desorb.

The IR results of the adsorption of CH_3OH on LaOCl-S and LaOCl-P are shown in Figure 13. For the spectra at 1.3 mbar of CH_3OH in equilibrium at RT, the spectrum of gas phase CH_3OH was subtracted. The spectra were also normalized for the amount of sample and the surface area. The IR spectrum of LaOCl-S at equilibrium shows a main band at 1033 cm^{-1}. This band was also visible in the gas phase spectrum of CH_3OH and is attributed to physisorbed species. A small band is present at 1104 cm^{-1}, which is attributed to an on-top coordinated methoxy species on a La^{3+} site.[21] After 15 min of evacuation at RT, the weakly adsorbed species have been removed. Also, the band of linearly adsorbed methoxy species has decreased in intensity, and two small bands have become better resolved at 1062 and 1012 cm^{-1}. These bands are attributed to doubly bridged and three-fold coordinated methoxy species, respectively.[21] Upon further evacuation, these bands also disappear, and a band

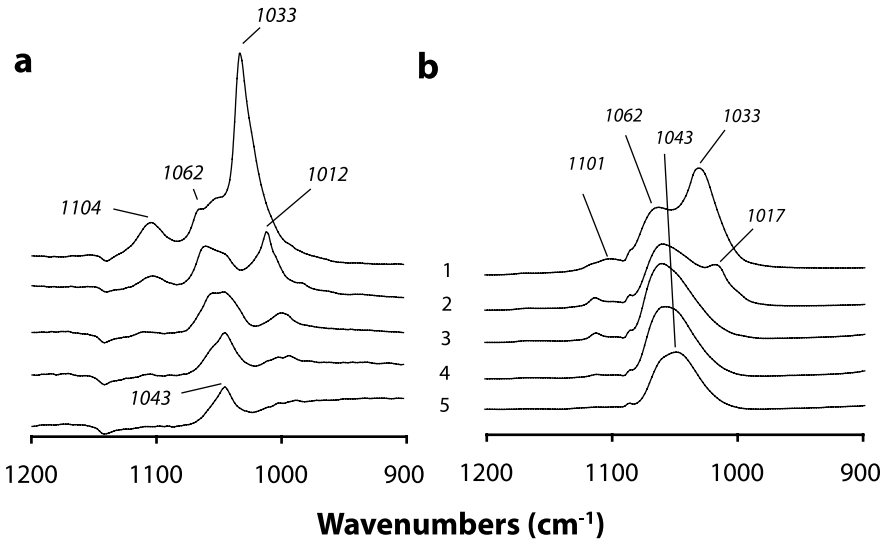

Figure 13. FTIR spectra of CH_3OH adsorbed on (a) LaOCl-S and (b) LaOCl-P at (1) 1.3 mbar equilibrium pressure and the consecutive desorption by (2) evacuation at RT, (3) evacuation at 100 °C, (4) evacuation at 150 °C, and (5) evacuation at 200 °C.

becomes visible at 1043 cm^{-1}, which is also caused by the twofold coordination of adsorbed methoxy species.[21] It has been proposed that the two bridging species are differing from the coordinative unsaturation of the cations constituting the site.[21] The possible coordinated methoxy species can be envisaged as in Scheme 5.

As with LaOCl-S, a strong band resulting from a weakly adsorbed species is visible on LaOCl-P at 1033 cm^{-1}, which is removed by evacuation at RT. Again, bands become visible after evacuation at RT at 1017, 1062, and 1101 cm^{-1}, attributed to three-fold coordinated, doubly bridged, and linearly adsorbed methoxy species, respectively. The bands of three-fold coordinated and linearly adsorbed methoxy species have disappeared after evacuation at 100 °C. After evacuation at 150 and 200 °C, the broad bands of the doubly bridged species show a different behaviour for its two components, with the doubly bridged species in the presence of defects (those at lower wavenumber) being less susceptible to evacuation. It seems that at higher loading the methoxy species prefer a doubly bridged coordination, where at lower loading three-fold coordination is preferred. Also, the methoxy species remain adsorbed at much higher temperatures than on LaOCl-S, which indicates the presence of relatively more acidic Lewis sites on LaOCl-P.

To verify this hypothesis, we have integrated the area under the adsorption bands for the adsorbed methoxy groups. The results are summarized in Table 6. It is clear that the integrated area is larger for LaOCl-S for spectra 1, 2 and 3. These spectra are, however, dominated by the physisorbed CH_3OH and the weakly adsorbed methoxy species, such as the three-fold and linearly adsorbed species. The bridged methoxy species are adsorbed more strongly and remain on the surface the longest. In spectra 4 and 5, the bridged methoxy

species are the only species remaining on the surface of LaOCl-S and LaOCl-P. In these spectra, however, LaOCl-P has a larger integrated area than LaOCl-S. This indicates that LaOCl-S might contain more Lewis acid sites, but LaOCl-P possesses the strongest Lewis acid sites. The main difference between LaOCl-S and LaOCl-P was the amount of chlorine present at the surface, as was determined by XPS. Apparently, the higher amount of chlorine is not reflected in the strength of the Lewis acid sites, but in the number of specific sites that are present. For LaOCl-P, the sites to which the methoxy species were most strongly adsorbed, namely, the sites forming bridged methoxy species, are more abundant than for LaOCl-S.

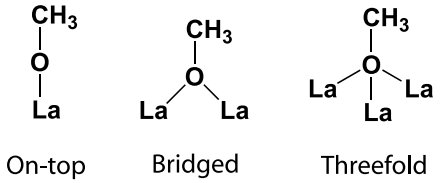

Scheme 5. Possible coordinated methoxy species to La-based materials.

Table 6. Relative integrated areas (error margin = ± 0.1)) under spectra of Figure 8 at different stages of CH_3OH adsorption/desorption on samples LaOCl-S and LaOCl-P.

Conditions	**Species present**	**LaOCl-S**	**LaOCl-P**
CH_3OH at equilibrium pressure of 1.3 mbar	Physisorbed CH_3OH Linear, bridged and three-fold methoxy species	17.2	6.0
Evacuation at RT	Linear, bridged and three-fold methoxy species	7.6	4.1
Evacuation at 100 °C	Bridged and three-fold methoxy species	4.3	3.6
Evacuation at 150 °C	Bridged and three-fold methoxy species	2.8	3.1
Evacuation at 200 °C	Bridged methoxy species	1.8	2.5

Conclusions

It was found that the synthesis method of the LaOCl materials has a dramatic influence on the bulk as well as on the surface properties. LaOCl-S, prepared via a solid-state reaction, is highly crystalline and a pure LaOCl phase. The high crystallinity is also reflected by its low surface area and pore volume. LaOCl-P, prepared via a sol-gel reaction, is characterized by a relatively high surface area and pore volume. LaOCl-P mainly consists of LaOCl crystallites

embedded in an amorphous phase. Moreover, LaOCl-P contains bulk lanthanum carbonate.

Furthermore, IR spectroscopy, in combination with probe molecules such as CO_2, CO, and CH_3OH, is a powerful method to assess the acid-base properties of LaOCl materials. Lewis acidity has been probed with CO and CH_3OH. The CO adsorption experiments have shown that LaOCl-S and LaOCl-P do possess similar Lewis acid sites. On the other hand, CH_3OH probing shows that LaOCl-P contains a larger number of strong adsorption sites than LaOCl-S, more specifically sites that are likely used for the destructive adsorption of CCl_4. The larger amount of chlorine at the surface that was observed with XPS appears to increase the number of active Lewis acid sites at the surface of LaOCl-P. Basicity has been assessed via CO_2 adsorption, and these experiments show that the type of carbonate formed on LaOCl-S and LaOCl-P differs.In the case of LaOCl-S, a high amount of bidentate carbonates and a low amount of monodentate carbonates are observed. For LaOCl-P, bulk carbonates are formed together with some bridged carbonates.

Finally, La-based materials are active in the destructive adsorption of CCl_4, and the following activity trend was observed: $LaCl_3 << La_2O_3 < LaOCl\text{-}S < LaOCl\text{-}P$. The difference in Lewis acidity between La_2O_3 and LaOCl is reflected by the lower initial reaction temperature of LaOCl. The higher activity of LaOCl-P is caused by its higher density of strong Lewis acid sites in comparison with LaOCl-S. These conclusions are in line with the observation of XPS that the surface of LaOCl-S and contains more chlorine than that of LaOCl-P. Because chlorine is more electronegative than oxygen, more strong Lewis acid sites are available on LaOCl-P. However, these differences in strength cannot be revealed by CO IR adsorption measurements. Nevertheless, we believe that the strength of the Lewis acid sites remains a key factor for activity and that stronger Lewis acid sites result in a higher intrinsic activity for CCl_4 destruction. However, basic oxygen sites remain necessary to enable the conversion of CCl_4 to CO_2. In other words, the appropriate acid-base pair should be available at the catalyst surface to have an active material. These observations also suggest that novel catalyst materials can be synthesized by modifying the surface composition of basic oxides. In this context, addition / removal of chlorine can be used as a way to tune the acid-base pair in a basic oxide.

Acknowledgements

Virginie Bellière (Utrecht University) is thanked for her contribution to the discussion and interpretation of the data. L. Espinosa Alonso (Utrecht University) is acknowledged for performing the activity experiments. Marco Daturi (University of Caen, France) is thanked for discussion and help with the interpretation of the IR results. We are also grateful to Olga Manoilova (Utrecht University) for measuring the CO adsorption/desorption IR spectra. Phillipe Bazin (University of Caen, France) is thanked for his help with the CO_2 and CH_3OH probing experiments. Ad Mens (Utrecht University) is acknowledged for building the setup used for the activity experiments, and for performing XPS and N_2 physisorption. Vincent Koot

(Utrecht University) is thanked for doing the TPD experiments. The Dow Chemical Company is acknowledged for providing the GC instrument for the flow-gas setup. Stacey Beyer (Dow Chemical Company, USA) is thanked for her help with the calibration and installation of the GC. This work was supported by the National Research School Combination Catalysis (NRSC-C) and the Dutch Science Foundation (VICI/NWO-CW and Van Gogh grants).

References

1. P. van der Avert, *Catalytic destruction of chlorinated hydrocarbons over lanthanide oxides*, Katholieke Universiteit Leuven: Leuven, 2003.
2. P. van der Avert, B. M. Weckhuysen, *Angew. Chem. Int. Ed.* **2002**, 41, 4730.
3. P. van der Avert, B. M. Weckhuysen, *Phys. Chem. Chem. Phys.* **2004**, 6, 5256.
4. P. van der Avert, S. G. Podkolzin, O. V. Manoilova, H. de Winne, B. M. Weckhuysen, *Chem. Eur. J.* **2004**, 10, 1637.
5. J. L. Tallon, B.-E. Mellander, *Science* **1992**, 258, 781.
6. O. V. Manoilova, S. G. Podkolzin, B. Tope, J. Lercher, E. E. Stangland, J. M. Goupil, B. M. Weckhuysen, *J. Phys. Chem. B* **2004**, 108, 15770.
7. S. G. Podkolzin, O. V. Manoilova, B. M. Weckhuysen, *J. Phys. Chem. B* **2005**, 109, 11634.
8. C. T. Au, H. He, S. Lai, C. F. Ng, *Appl. Catal. A* **1997**, 159, 133.
9. A. E. Schweizer, M. E. Jones, D. A. Hickman, US 6452058, 2002.
10. L. H. Brixner, E. P. Moore, *Acta Crystallogr.* **1983**, C39, 1316.
11. B. Morosin, *J. Chem. Phys.* **1968**, 49, 3007.
12. J. P. Attfield, G. Ferey, *J. Solid State Chem.* **1989**, 82, 132.
13. H. Haeuseler, *J. Raman Spectrosc.* **1984**, 15, 120.
14. Y. Hase, L. Dunstan, M. L. A. Temperini, *Spectrochim. Acta* **1981**, 37, 597.
15. C. Binet, M. Daturi, J. C. Lavalley, *Catal. Today* **1999**, 50, 207.
16. K. J. Klabunde, A. Khaleel, D. Park, *High. Temp. Mater. Sci.* **1995**, 33, 99.
17. M. W. Urban, *Vibrational Spectroscopy of Molecules and Macromolecules on Surfaces*, John Wiley and Sons, Ltd: Chichester, 1994.
18. J. C. Lavalley, *Catal. Today* **1996**, 27, 377.
19. Y. S. Skylarenko, I. S. Skylarenko, T. M. Chubukova, *Zh. Anal. Khim.* **1961**, 16, 417.
20. A. Badri, C. Binet, J. C. Lavalley, *J. Chem. Soc. Faraday Trans.* **1997**, 93, 2121.
21. C. Binet, M. Daturi, *Catal. Today* **2001**, 70, 155.

3

Intermediates in the Destruction of Chlorinated C_1 Hydrocarbons on La-based Materials: Mechanistic Implications

The reaction steps for the destructive adsorption of $CHCl_3$, CH_2Cl_2 and CH_3Cl over a LaOCl-P catalyst material were investigated to gain more insight into the reaction network of the destructive adsorption of chlorinated C_1 (CHC_1). The activity and selectivity for the destructive adsorption of the CHC_1 series was tested over LaOCl-P in flow-gas experiments. Surface intermediates on LaOCl-P and related gas phase products were studied using in situ infrared spectroscopy (IR). The IR results show that during reaction, LaOCl-P is covered with carbonate, formate and methoxy groups. The relative amount of each of these surface intermediates depends on the Cl/H ratio of the reactant. The decomposition of the surface species leads to the formation of the reaction products. This is influenced by the temperature and the relative amount of Cl present on the surface. Effluent analysis results show that the activity for the destructive adsorption of H-containing CHC_1 decreases with increasing hydrogen content of the reactant. The influence of the chlorination degree of the material on selectivity and activity could be used to tune the catalyst for optimal conversion of a specific mixture: the chlorination degree of the material largely determines what type of surface groups are formed and into which gas phase products they dissociate.

Introduction

The destructive adsorption and catalytic destruction of CCl_4 over La_2O_3-based materials has been studied extensively and the reactivity of C-Cl bonds towards these catalysts is well-understood.[1-6] However, the light ends mixtures formed during the production of C_2H_3Cl also contain H-containing CHC_1, namely $CHCl_3$, CH_2Cl_2 and CH_3Cl. Preliminary research on the catalytic destruction of H-containing chlorinated C_1 (CHC_1) over supported and unsupported La_2O_3 catalysts indicates that all CHC_1 follow a similar reaction path.[2, 5] However, as opposed to the case of CCl_4, CO was found to be the main product in the catalytic destruction of $CHCl_3$ and CH_2Cl_2.

The reactant molecule is thought to first exchange two chlorine atoms with one lattice oxygen atom from the catalyst, as illustrated by Reaction Eq. (1), similarly to the reaction of CCl_4. The resulting reaction intermediate consecutively dissociates into CO and HCl/H_2. However, since HCl was already present as a result of the dechlorination reaction with water, the presence of either H_2 or HCl could not be confirmed.[2, 5] Therefore, further studies on the reaction mechanism is needed to gain understanding of the role and behaviour of the C-H bond in the destructive adsorption of CHC_1. Also, the influence of the acid-base properties of the catalyst with respect to activity and selectivity should be investigated to achieve control of the reaction towards re-usable products.

$$CH_xCl_{4-x}\ (g) + \text{La-O-La}\ (s) \rightarrow COH_xCl_{2-x}\ (g) + 2\ \text{La-Cl}\ (s) \qquad (1)$$

In this chapter, we report on a general reaction scheme for the destructive adsorption of CHC_1 and the relationship between the composition of the catalyst and the observed activity and selectivity. In situ infrared (IR) spectroscopy and gas chromatography (GC) analysis were used to monitor the reaction of $CHCl_3$, CH_2Cl_2 and CH_3Cl over the LaOCl-P catalyst material. As a result, fundamental insight is obtained into the intermediates of destructive adsorption when applying La-based materials to convert mixtures of CHC_1. This is of high relevance when destroying the light ends in industrial waste streams. Moreover, the results demonstrate that several products, formed during the reactions described in this chapter, are potentially re-usable as fuel or feed-stock.

Experimental

Materials

For this chapter, the LaOCl-P sample was used for the activity and in situ IR experiments. The preparation method and physicochemical properties of this sample have been described in detail in Chapter 2.

In Situ IR Temperature-Programmed Reaction

Due to interference of the bands of bulk carbonates on La_2O_3 with the adsorbed species, only LaOCl-P was used for the IR measurements. For these IR measurements, the quartz cell was used, which was discussed in Chapter 2. All IR spectra were measured using a Perkin Elmer 2000 spectrometer with a resolution of 4 cm^{-1}. LaOCl-P was pressed into self-supporting wafers (2 cm^2), and activated in situ prior to the IR measurements in dynamic vacuum at 550 °C for 30 min. After pre-treatment, the reactant (50 mbar) was introduced to the cell after which the cell was closed. The reactant was equilibrated with the sample at room temperature and, subsequently, spectra of the solid and the gas phase were measured. The temperature of the sample was raised to 300 °C in steps of 50 °C. After each step, spectra were recorded. Spectra were measured for the adsorption of 50 mbar of HCOOH (Acros Organics, 98+ %) and CH_3OH (Acros Organics, 99.8 %) on LaOCl-P to use as a reference for the assignment of formate and methoxy groups, respectively.

Flow-Gas Activity Experiments

The activity measurements for the destructive adsorption of CCl_4 (Acros Organics, 99.8 %), $CHCl_3$ (Acros Organics, 99.9 %), CH_2Cl_2 (Acros Organics, 99.9 %) and CH_3Cl (Fluka, ≥ 99.8 %) were performed in a tubular fixed bed quartz reactor. The catalyst bed consisted of LaOCl-P (1.0 g) pressed in a sieve fraction (150-500 µm), pre-treated in a He (Hoekloos, ≥99.996 %) flow (10 ml/min) at 550 °C. The reactions were performed at constant temperature of 400 °C. The total flow rate of the reactant feed was 20 ml/min 4-6 vol% CHC_1 in He (Hoekloos, ≥99.996 %). Details of the setup can be found in Chapter 2.

Results and Discussion

IR Spectroscopic Studies

When CHC_1 adsorb on La_2O_3-based materials, C-Cl bonds are broken and C-O bonds are formed resulting in chemisorption of the CHC_1. Both bonds are related to IR active vibrations and therefore IR enables characterization of the surface species and chemisorbed reaction intermediates. IR spectra of the gas phase and catalyst wafer were measured separately during the reaction of LaOCl-P with $CHCl_3$, CH_2Cl_2 and CH_3Cl and are shown in Figure 1 and 2. Unfortunately, small fluctuations in the concentration of ambient CO_2 and H_2O prevented the accurate detection of these species as reaction products. Consequently, CO_2 and H_2O are not included in the spectra and in the discussion of the IR results.

For the reactions with $CHCl_3$, several bands are observed in the gas phase spectra at

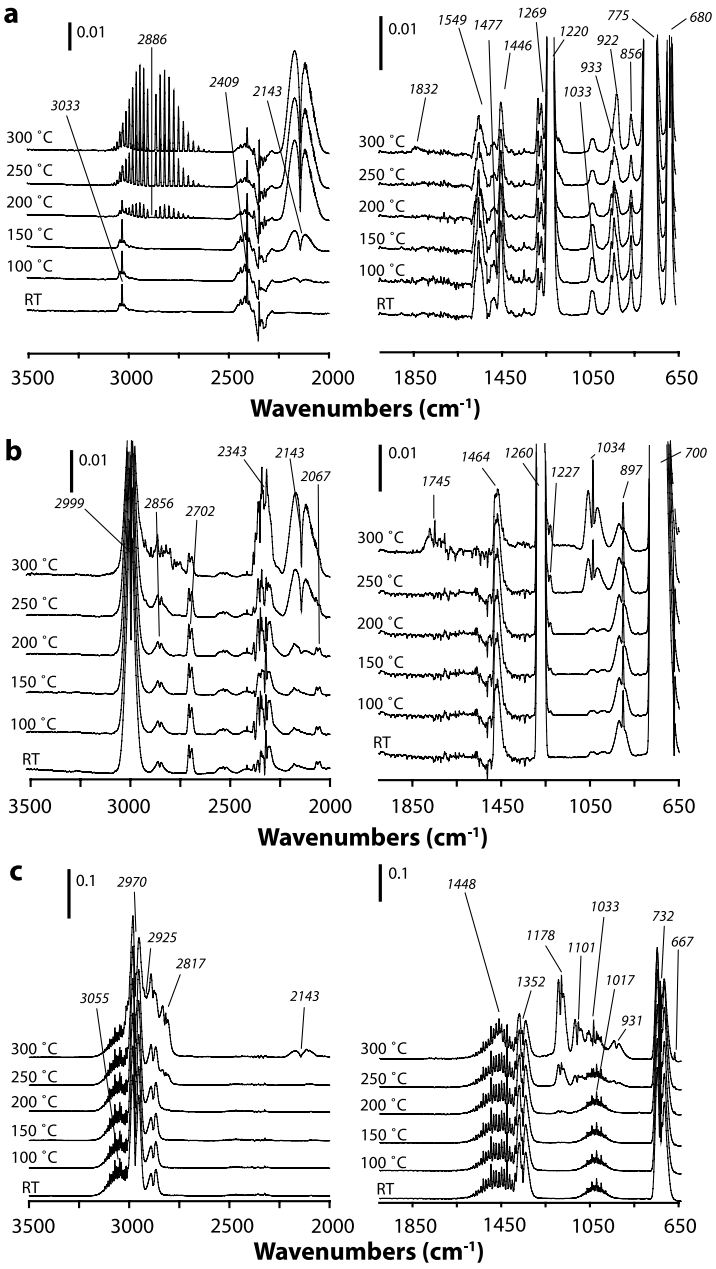

Figure 1. Gas phase IR spectra measured during the destructive adsorption of $CHCl_3$ (a), CH_2Cl_2 (b) and CH_3Cl (c) on LaOCl-P at RT, 100, 150, 200, 250 and 300 °C. For comparison, a relative intensity scale is included for each spectrum.

RT, shown in Figure 1a. The band at 1269 cm^{-1} is indicative of CH_2Cl_2 that was present as a contaminant in the reactant.[7] The remainder of the bands is assigned to $CHCl_3$.[7] At 150 °C a band arises at 2143 cm^{-1}, which is characteristic for CO.[7] The intensity of the CO band increases with increasing reaction temperature. At 200 °C, the rotation-vibration pattern of HCl is observed at 2886 cm^{-1}.[7] As the temperature increases, the intensity of the HCl band increases also. A low intensity band at 1832 cm^{-1} is visible at 300 °C and is accompanied by a broadening of the band at 856 cm^{-1}. The bands are due to the formation of $COCl_2$ and regarding the relatively low intensity, a small amount is formed.[7] In addition, a band arises at 922 cm^{-1}, which is assigned to C_2Cl_4.[7]

To elucidate the surface reaction steps of the conversion of $CHCl_3$, spectra of the wafer were also measured. In Figure 2a, each spectrum is shown after subtraction of the corresponding gas phase spectrum and the spectrum of the wafer prior to reaction. The bands at 3020 and 1223 cm^{-1} are assigned to physisorbed $CHCl_3$. In addition, immediately after introduction of $CHCl_3$, a broad band at 3579 cm^{-1} is visible, characteristic of surface hydroxyl groups. Simultaneously with the OH bands at RT, bands appear at 1402, 1496 and 1597 cm^{-1}. These bands are also visible in the spectrum of LaOCl-P under ambient conditions and are attributed to the presence of bulk carbonate (1402 and 1496 cm^{-1}) and bidentate carbonate (1597 cm^{-1}). As a result of the high basicity of La_2O_3-based materials, carbonates and hydroxyl groups are formed readily at RT by reaction with CO_2 and H_2O from air.

In a blank experiment, LaOCl-P was kept under static vacuum in the reaction cell to verify whether the observed bands are a result of the presence of air, or of destructive adsorption of $CHCl_3$. The intensity of the carbonate bands in the blank experiment was of the same order of magnitude as observed in the spectrum at RT for the experiment with $CHCl_3$. The carbonate bands at RT in Figure 2a are therefore a result of residual air in the reaction cell. During the blank experiment surface hydroxyl groups were also formed, but after 4 h the intensity of the ν(OH) band was still significantly lower in comparison with the band observed after 15 min at RT with $CHCl_3$ in the cell. This implies that the hydroxyl groups are formed as a result of the interaction of $CHCl_3$ with the LaOCl-P surface.

Table 1. Measured vibrational frequencies and mode assignment of methoxy and formate groups after adsorption of CH_3OH and HCOOH, respectively, on LaOCl-P at RT after evacuation.

CH_3OH on LaOCl-P (cm^{-1})	**Methoxy Mode**	**HCOOH on LaOCl-P (cm^{-1})**	**Formate Mode**
1017	ν(CO) 3-fold	1261	$\nu(OCO)_s$ Monodentate
1043	ν(CO) bridged	1348	$\nu(OCO)_s$ Bidentate
1062	ν(CO) bridged	1375	$\nu(OCO)_s$ Bidentate
1101	ν(CO) on-top	1400	∂(CH)
1460	$\partial(CH_3)$	1556	$\nu(OCO)_{as}$ Bidentate
2794	$\nu_s(CH_3)$	1607	$\nu(OCO)_{as}$ Bidentate
2852	$\nu_s(CH_3)$ 3-fold	1689	$\nu(OCO)_{as}$ Monoden-
2873	$\nu_s(CH_3)$	2859	tate
2926	$\nu_{as}(CH_3)$		ν(CH)
2953	$\nu_{as}(CH_3)$ 3-fold		

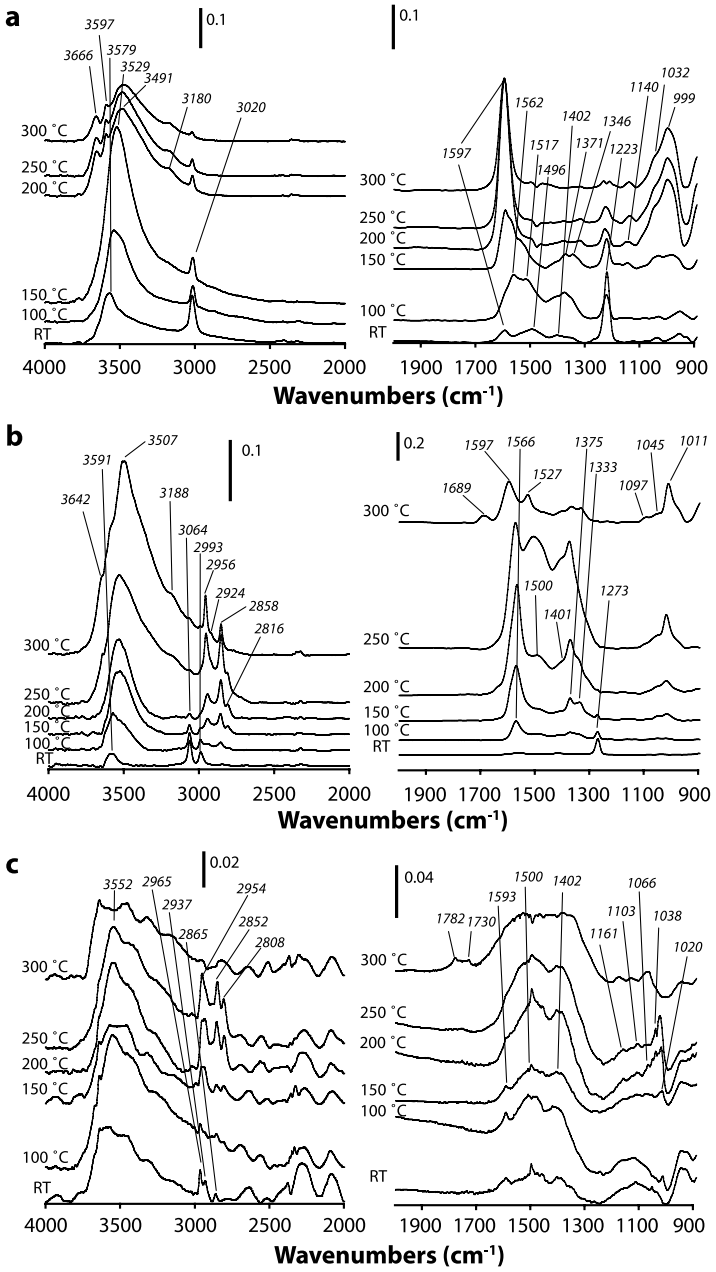

Figure 2. IR spectra of the LaOCl-P wafer measured during the destructive adsorption of $CHCl_3$ (a), CH_2Cl_2 (b) and CH_3Cl (c) at RT, 100, 150, 200, 250 and 300 °C. For comparison, a relative intensity scale is included for each spectrum.

Intermediates in the destruction of chlorinated C_1 on La-based Materials

The abstraction of the proton from $CHCl_3$ by strong basic O sites initiates the reaction, which was also proposed by Koper et al. from experiments on the destructive adsorption of $CHCl_3$ on CaO (Scheme 1, Species 1b to 2b).[8] This proton abstraction is expected to be accompanied by the removal of a chlorine atom from the reactant resulting in the formation of a carbene-like intermediate. The formation of dichlorocarbene (CCl_2) on a metal oxide surface has been proven by adsorption of CCl_4 on Fe_3O_4 studied using Scanning Tunnelling Microscopy (STM).[9] Moreover, it was found that the CCl_2 fragment is mobile on the surface at RT. Koper et al. found from pulse experiments that $CHCl_3$ is initially converted on CaO into CO exclusively, whereas addition of larger amounts resulted in the formation of $COCl_2$ and C_2Cl_4.[8] Hydration of CaO already led to formation of $COCl_2$ and C_2Cl_4 after introduction of lower amounts of $CHCl_3$. Since both chlorination and hydration of the surface result in the decrease of O availability, the formation of $COCl_2$ and C_2Cl_4 is indicative of O deficiency. The formation of C_2Cl_4 and $COCl_2$ is confirmed in the gas phase IR spectrum for destructive adsorption of $CHCl_3$ at 300 °C (Figure 1a).

At 100 °C, bands are visible at 1346, 1371 and 1562 cm^{-1}, which are characteristic for chemisorbed formate groups (Table 1). The intensity of the formate bands has decreased in the spectrum measured at 150 °C, and simultaneously CO is formed (Figure 1a). The formation of formate groups is the result of a Cl abstraction rather than proton abstraction as the initial reaction step. Initially, COHCl, an intermediate similar to $COCl_2$, is formed after exchange of two Cl atoms for an O atom (Scheme 1, Species 1a to 2a). This intermediate is known to thermally dissociate into CO and HCl (Scheme 1, Species 3a to 3a`). However, when COHCl is formed at the surface, rapid re-adsorption is possible, resulting in the formation of formate groups (Scheme 1, Species 4a to 5a). During the increase of temperature

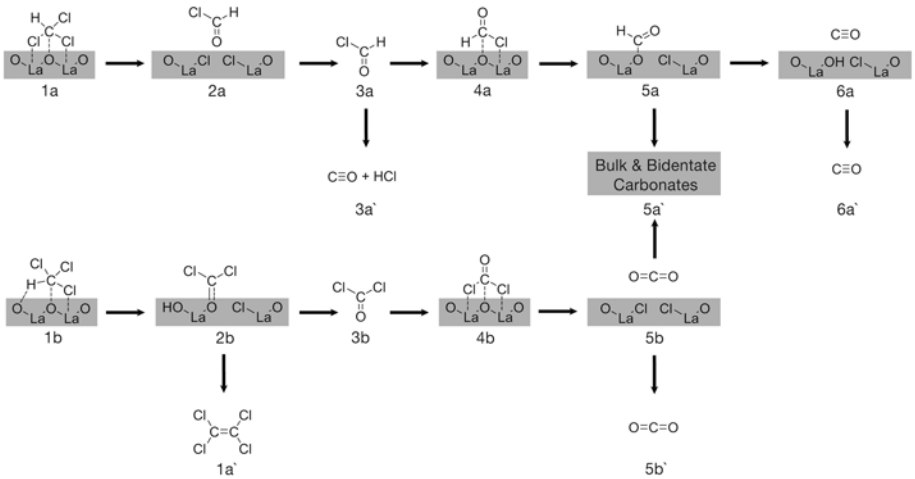

Scheme 1. Proposed reaction scheme for the destructive adsorption of $CHCl_3$ on LaOCl-P. To illustrate the difference between adsorbed species and gas phase species, the catalyst surface is highlighted grey.

from RT to 150 °C, the OH-band at 3579 cm^{-1} also increases in intensity and shifts to 3529 cm^{-1}. The broadening and perturbation of the OH-band can be explained by the interaction between OH groups and $CHCl_3$.[10]

At 200 °C, the formate bands have disappeared and the intensity of the OH-bands has decreased. Moreover, three distinct maxima are visible in the ν(OH) region and a low-intensity band appears at 3180 cm^{-1}, which may be the result of hydrogen bonding between chloroform and surface hydroxyl groups. The three OH bands have previously been linked to the occurrence of different phases in La_2O_3 powders based on XRD.[11] The bands at 3491, 3597 and 3666 cm^{-1} are assigned to LaOOH, $La(OH)_3$ and isolated La-OH, respectively.[11] The different bands are related to the degree of hydration of the sample. Initially, through proton abstraction the surface becomes saturated with OH groups and at higher chlorination degree, the OH groups react with Cl to form HCl and regenerate basic O sites. The thermal dissociation of COHCl (Scheme 1, Species 3a to 3a`) may be more favourable at 200 °C than the re-adsorption and consecutive formation of formate groups, since bands related to formate groups are not found in the spectrum. An alternative interpretation is that the formate groups are formed, which immediately dissociate to CO and surface hydroxyl groups (Scheme 1, Species 6a to 6a`). The decrease of the formate bands parallels the increase of the carbonate band at 1597 $cm^{-1}$. This implies that the formate groups convert into bidentate carbonates (Scheme 1, Species 5a to 5a`).[12] Above 200 °C, the intensity of the carbonate band at 1597 cm^{-1} decreases, which leads to CO_2 formation. As previously mentioned, however, CO_2 could not be detected due to experimental limitations. The bands at 999 and 1032 cm^{-1} are assigned to La-O vibrations. The broadness of the bands is most likely due to the rearrangement of the LaOCl-P structure as a result of chlorination of the catalytic surface. The band at 1140 cm^{-1} appears simultaneously with bidentate carbonate, however, no reference was found with respect to this band.

Bands, which are all assigned to CH_2Cl_2, are observed at RT in the gas phase spectra (Figure 1b) during the destructive adsorption of CH_2Cl_2 over LaOCl-P.[7] At 150 °C, a small shoulder arises at 1227 cm^{-1}, which can be assigned to $CHCl_3$.[7] At 200 °C, CO is formed and the intensity of the CO band increases as the temperature increases. At 300 °C, several bands arise at 1034 and 1745 cm^{-1}. In addition, bands are visible between 2700 and 3000 cm^{-1}. The bands at 1034 and 1745 cm^{-1} are characteristic for CH_3OH and CH_2O, respectively.[7] The pattern of bands in the 2700-3000 cm^{-1} region confirms the formation of CH_2O and CH_3OH.[7] The bands may in addition be indicative of HCl formation.[7]

The spectra of the catalyst, measured during the destructive adsorption of CH_2Cl_2, are shown in Figure 2b. At RT, bands are observed at 3064, 2993 and 1273 cm^{-1}, assigned to physisorbed CH_2Cl_2. Also, a low intensity hydroxyl band is observed at 3591 cm^{-1}, indicating proton abstraction similar to the destructive adsorption of $CHCl_3$ (Scheme 2, Species 1b to 2b). The recombination of CHCl to $C_2H_2Cl_2$ is not observed at high temperature, however. Apparently, the surface reaction involving CHCl is limited to lattice O extraction resulting in the formation of COHCl. As the temperature increases, the hydroxyl band broadens and at 300 °C, three maxima are visible at 3507, 3591 and 3642 cm^{-1}. This is similar to the hydroxyl

bands observed during the experiment $CHCl_3$ (Figure 2a). Even though no products are observed in the gas phase below 250 °C, the wafer spectra show bands at 1566, 1375, 1336 and 2858 cm^{-1} at 100 °C, indicating formation of formate groups. This can be explained by the previously discussed consecutive re-adsorption and formation of formate groups from COHCl (Scheme 2, Species 4b to 5b).

At 200 °C, a broad set of bands is present at 1600-1300 cm^{-1}, which increases in intensity at 250 °C. The broad bands between the two maxima at 1566 and 1375 cm^{-1} are assigned to bulk carbonates. At 150 °C and higher temperatures, bands are also present around 1011 cm^{-1} and 2800-3100 cm^{-1} as a result of methoxy group formation. In previous IR experiments of CH_3OH probing on LaOCl-P, different types of methoxy species have been identified based on the vibrational frequencies in the low wavenumber region (Table 1). These experiments were discussed in Chapter 2.3.2. The bands observed at 1097, 1045 and 1011 cm^{-1} have been assigned to on-top, bridged and three-fold methoxy species, respectively. The methoxy species are predominantly in the three-fold adsorbed state and are stable up to 300 °C. The intensity of the bands at 2956 and 2858 cm^{-1} in the ν(CH) region parallels the intensity of the ν(CO) band of three-fold adsorbed methoxy. The decrease in intensity at 300 °C of the band at 2858 cm^{-1} is caused by the overlap between the ν(CH) bands of formate and methoxy groups, since the formate species dissociate at 300 °C. In addition to three-fold methoxy species, a relatively low concentration of bridged and on-top adsorbed methoxy species is formed at the surface. Similar to the reaction with $CHCl_3$, a reaction pathway initiated by Cl abstraction may explain the formation of methoxy species. Analogous to $CHCl_3$, CH_2Cl_2 produces CH_2O after Cl removal (Scheme 2, Species 1a to 2a).

CH_2O is known to form dioxymethylene (O_2CH_2) and polyoxymethylene species on the surface of ionic solids, which can convert further into formate and methoxy groups.[12] However, the bands characteristic for dioxymethylene and polyoxymethylene are not observed in the spectra. Moreover, the formation of dioxymethylene requires reduction of a metal site,

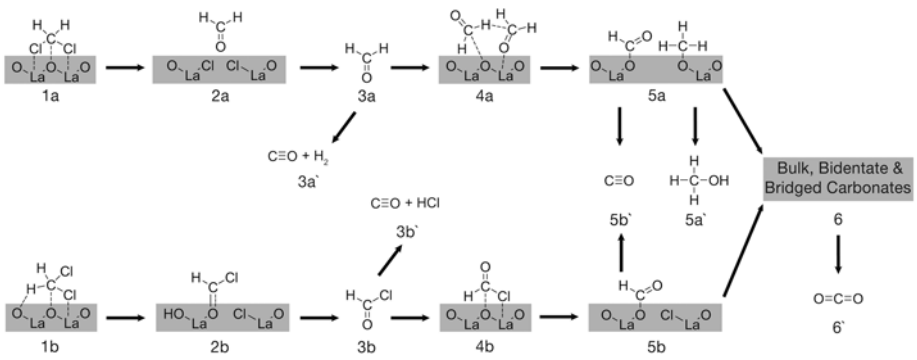

Scheme 2. Proposed reaction scheme for the destructive adsorption of CH_2Cl_2 on LaOCl-P. To illustrate the difference between adsorbed species and gas phase species, the catalyst surface is highlighted grey.

which is highly unlikely in the case of lanthanum.[13] On the other hand, it has been shown recently that even though La^{3+} is unable to change oxidation state, oxidation of OCl is possible.[14, 15] A more likely explanation, however, is that CH_2O reacts via a Cannizzaro-like reaction to form a methoxy and formate group (Scheme 2, species 4a to 5a)). At 250 °C, CH_3OH is formed in the gas phase. The formation of CH_3OH is linked to the increased concentration of methoxy species and hydroxyl groups at the surface. As a result, basic O sites are regenerated by CH_3OH desorption (Scheme 2). The fact that CH_2O is observed in the gas phase spectrum at 300 °C indicates that re-adsorption is becoming less favourable, or that more CH_2O is formed at the surface (Scheme 2).

At 300 °C, bands are visible at 1689, 1597, 1527 and 1333 cm^{-1}. The band at 1689 cm^{-1} is ascribed to monodentate formate (Table 1), which means that compared to the $CHCl_3$ experiment, the formate groups remain on the surface up to higher temperatures. Therefore, temperature is not the only factor influencing dissociation. Chlorination of the catalytic surface is likely to be an additional parameter. The bands at 1597, 1523 and 1333 cm^{-1} are assigned to carbonates remaining on the surface after dissociation of bulk carbonates. The bands at 1523 and 1333 cm^{-1} have previously been assigned to polycarbonates (Chapter 2.3.2).

For CH_3Cl on LaOCl-P at RT, the observed bands are all assigned to gas phase CH_3Cl (Figure 1c). At 250 °C, a strong band arises at 1178 cm^{-1} assigned to $(CH_3)_2O$. At 300 °C, other bands indicative of $(CH_3)_2O$ arise at 931, 1101, 2817 and 2925 cm^{-1}. A band is also observed at 1033 cm^{-1} as a result of CH_3OH formation. Moreover, gas phase C≡O at 2143 cm^{-1} is visible in the spectrum at 300 °C.

During the experiment with CH_3Cl on LaOCl-P, bands assigned to physisorbed CH_3Cl are observed at 2965, 2937 and 2865 cm^{-1} (Figure 2c). The intensity of the surface species bands is significantly lower than for the experiments with $CHCl_3$ and CH_2Cl_2, making the spectra rather noisy after subtraction. At room temperature, the ν(OH) band is visible at 3552 cm^{-1}. The intensity of this band is relatively constant throughout the experiment. This indicates that hydrogen abstraction is not favourable in the case of CH_3Cl (Scheme 3, Species 1b to 2b). At 150 °C, the previously assigned bands of methoxy groups are observed at 2954, 2852 and 2808 cm^{-1}. Broad bands are also observed in the low wavenumber region, confirming the presence of methoxy species. The position of the band at 1020 cm^{-1} is indicative of three-fold adsorbed methoxy species (Table 1). The bands at 1038, 1066 and 1103 cm^{-1} show that a relatively small amount of two-fold and on-top adsorbed methoxy groups is also present at the surface. The formation of methoxy groups is accompanied by gas phase $(CH_3)_2O$.

Two possible pathways can lead to the formation of $(CH_3)_2O$; 1) recombination of two surface methoxy species, resulting in the regeneration of an O site. However, due to the low intensity of the methoxy bands compared to the experiment with CH_2Cl_2 on LaOCl-P, it appears unlikely that $(CH_3)_2O$ is not formed for CH_2Cl_2. 2) a more probable pathway is the exchange of two Cl atoms from two CH_3Cl molecules for one O atom (Scheme 3, Species 1a to 1a`). The CH_3Cl molecule is relatively small compared to the molecules containing more

Intermediates in the destruction of chlorinated C_1 on La-based Materials

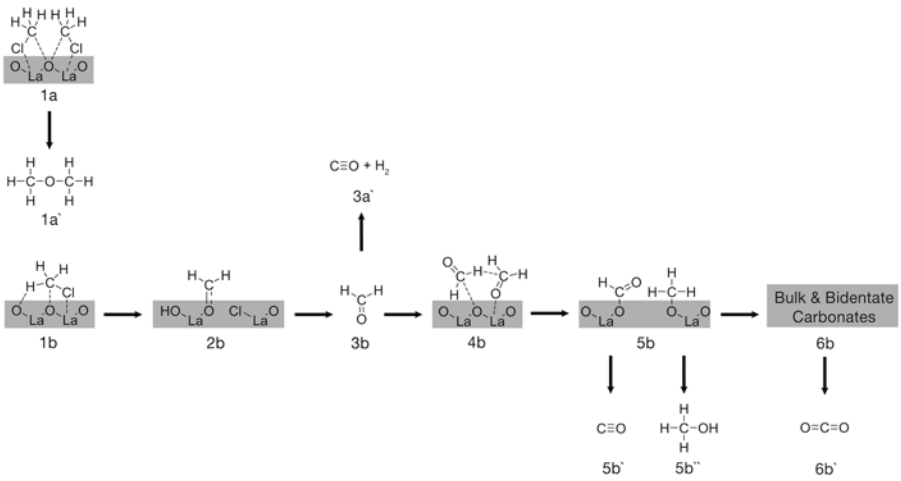

Scheme 3. Proposed reaction scheme for the destructive adsorption of CH_3Cl on LaOCl-P. To illustrate the difference between adsorbed species and gas phase species, the catalyst surface is highlighted grey.

of the large Cl atoms. Therefore, the conversion of CH_3Cl into $(CH_3)_2O$ is able to occur without the formation of large amounts of surface species.

At 300 °C, the methoxy groups have dissociated simultaneously with the formation of CH_3OH as was observed for the destructive adsorption of CH_2Cl_2. In addition to methoxy species, broad bands are visible at 1700-1200 cm^{-1}. These bands are similar in position and intensity for the carbonate bands that are observed for the experiments at RT with $CHCl_3$ and CH_2Cl_2 (Figure 2a and 2b). These bands were ascribed to residual air in the vacuum cell and, consequently, the formation of carbonates. The intensity of the carbonates is relatively constant in all spectra. However, at 300 °C the carbonate band is broader and two low intensity bands arise at 1782 and 1730 cm^{-1}. No reference has been found for the assignment of these bands. The broadening of the carbonate bands at 300 °C may indicate the formation of formate groups. The dissociation of formate groups would consequently explain the gaseous CO that is observed at 300 °C (Figure 1c).

GC Activity Experiments

To evaluate activity and selectivity, flow gas experiments were performed. The region in the chromatogram where $COCl_2$ is observed contains other peaks and $COCl_2$ is therefore difficult to detect. As a result, both the assignment and the quantification of $COCl_2$ may be susceptible to a rather large error. Therefore, $COCl_2$ has been omitted from the GC results, since it is generally formed together with CO_2. Another point of discussion is the fact that CH_3Cl and CH_3OH are co-eluting. Fortunately, the IR results complement the GC results. In the IR experiments, the formation of CH_3OH was observed, whereas CH_3Cl

formation was not observed. The product formed during the GC experiments is therefore assigned to CH_3OH. This also means that the formation of CH_3OH could not be confirmed during the GC experiments with CH_3Cl. $(CH_3)_2O$ was also not detected by GC and consequently the conversion of this reaction is actually higher than experimentally determined.

To enable comparison of selectivity, the reactions were performed on LaOCl-P at 400 °C. The overall conversion is shown in Figure 3. It is defined as the sum of flow concentrations of the C-containing products, divided by the sum of the flow concentrations of the reactant and the C-containing products, multiplied by 100 %. The overall conversion at 400 °C shows the following trend: the conversion of destructive adsorption of CH_xCl_{4-x} decreases as x increases. A trend is observed in the conversion as a function of time. Initially, the conversion is relatively high. This may not seem the case for CH_3Cl; nevertheless, because of the co-elution of CH_3Cl and CH_3OH, the conversion is likely to be significantly higher than measured by the GC analysis. After some time a sharp decrease in conversion is observed. The decrease in activity is caused by the complete chlorination of the catalyst surface. Once the surface is fully chlorinated, the reaction becomes controlled by the diffusion of lattice O to the surface and lattice Cl to the bulk.

In Figure 4, the conversion of the products is shown for the destructive adsorption of $CHCl_3$, CH_2Cl_2 and CH_3Cl on LaOCl-P at 400 °C as a function of time. The conversion was defined as the flow concentration of a product, divided by the sum of the flow concentrations of the reactant and the products, multiplied by 100 %. As the reaction time increases, the surface becomes more chlorinated. Therefore, the timescale can be translated into a chemical parameter, namely surface chlorination. The conversion curves have similar shapes;

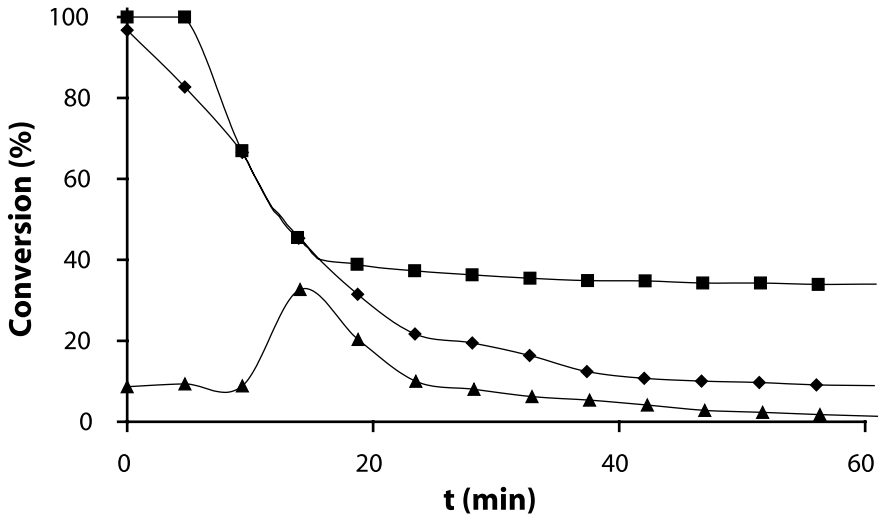

Figure 3. Overall conversion for the destructive adsorption of 6-7 vol% of $CHCl_3$ (■), CH_2Cl_2 (♦) and CH_3Cl (▲) in He on LaOCl-P at 400 °C as a function of time.

Intermediates in the destruction of chlorinated C_1 on La-based Materials

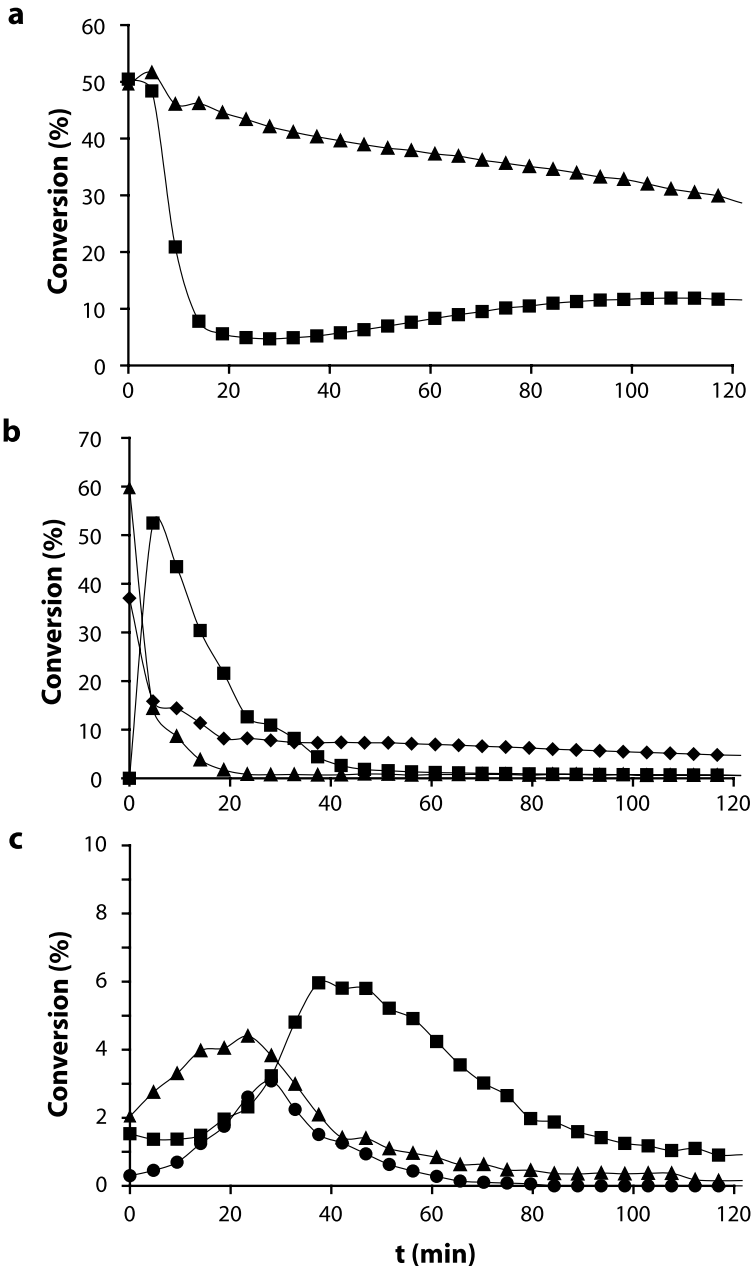

Figure 4. Conversion to each product for the destructive adsorption of $CHCl_3$ (a), CH_2Cl_2 (b) and CH_3Cl (c) on LaOCl-P as a function of time at 400 °C. The symbols in the graphs refer to the products: CO (▲), CO_2 (■), CH_3OH (♦) and CH_4 (●).

an increase, followed by a maximum value, ending in a decrease. The maximum conversion indicates that a certain degree of chlorination increases conversion. This is in agreement with the experiments mentioned in Chapter 2 for CCl_4 on LaOCl-P, where higher intrinsic activity was observed for a more chlorinated surface. An increase in chlorination leads to stronger Lewis acid sites, which are important for the initial reaction step. Once a C-Cl bond has been broken, basic O sites are needed to stabilize the remaining fragment and to convert it into O-containing products. Therefore, an optimum combination of strong Lewis acid sites with sufficient basic O sites exists, which is controlled by the surface chlorination degree. In the experiments on LaOCl-P, a maximum was not observed in some cases. The chlorination degree of the surface has probably exceeded the optimum value. Therefore, the measurements only show the decrease in conversion following the maximum. In all experiments, the formation of CO_2 follows the formation of other products, such as CO, CH_3OH and CH_4. Also, the maximum conversion of CO_2 is observed later in the reaction as the H-content of the reactant increases. This indicates that the chlorination of the surface results in the formation of CO_2. Either it promotes the formation of CO_2 as a reaction product, or carbonates are formed in an earlier stage of the reaction and desorb as CO_2 as a result of surface chlorination. The latter is regarded the most likely scenario.

General Discussion

The results of the IR analysis are summarized in Table 2. Even though different products are formed for each reaction, the reaction pathways described in Schemes 1-3 can be summarized by a general reaction scheme (Scheme 4). Two initial pathways are proposed for the destructive adsorption of the CHC_1 series, i.e. CCl_4, $CHCl_3$, CH_2Cl_2 and CH_3Cl. The first reaction pathway is known from the destructive adsorption of CCl_4 and is similar for the other CHC_1. Two Cl atoms of the reactant are exchanged for a lattice O atom, which leads to the formation of a gas phase intermediate, namely COH_xCl_{2-x}. In the case of CH_3Cl, another reaction may occur which resembles this pathway, since this molecule possesses only one Cl atom. Two CH_3Cl molecules both donate one Cl atom and an O atom is exchanged in return. As a result, $(CH_3)_2O$ is formed as a gas phase product. For the destructive adsorption of CCl_4, it was found in Chapter 2 that an optimum combination of Lewis acidity/basicity exists for the active sites. The C-Cl bond becomes elongated when the Cl-atom is attracted by a La^{3+} Lewis acid site resulting in the breaking of the C-Cl bond and the formation of a La-Cl bond. The basic O sites are necessary to stabilize the remaining CCl_3 fragment and enable the conversion of CCl_4 into CO_2. The strength of the Lewis acid site therefore is a key factor for activity and this is also applicable to the other CHC_1.

The second pathway results in the formation of an adsorbed $CH_{x-1}Cl_{3-x}$ fragment after removal of an H and Cl atom from the reactant (Scheme 4). Obviously, CCl_4 is unable to react via this reaction pathway due to the absence of H atoms. However, for the other CHC_1 the O site is able to abstract a H atom. A hydroxyl group is formed as a result of the

removal of the H atom and the Cl atom forms a bond with the La atom. Based on these results, it is not possible to determine whether the formation of the hydroxyl group precedes or follows the formation of the La-Cl bond. Nevertheless, the strength of the basic O atom directly influences the initial step of the reaction pathway. The $CH_{x-1}Cl_{3-x}$ fragment is able to migrate across the surface and remove a lattice O atom to form the gas phase intermediate $COH_{x-1}Cl_{3-x}$. The removed O atom is not replaced by another anion and this would result in an overall positive charge on the catalyst material. However, La_2O_3-based materials are able to incorporate additional O atoms and reconstruct the catalytic surface.[16] Moreover, carbonates which are on the catalyst surface can change coordination to compensate for the loss of O. This means that removal of H/Cl from the CHC_1 is dependent on the number of additional O atoms that is incorporated into the material and the amount and type of carbonates present on the catalytic surface.

Two initial pathways result in the formation of two similar intermediate products (Scheme 4). The rapid re-adsorption of the two intermediates, COH_xCl_{2-x} and $COH_{x-1}Cl_{3-x}$, results in the formation of hydroxyls, formates, carbonates or methoxy groups. The formed surface species can further interconvert or dissociate into gas phase products, depending on the chlorination degree of the surface and the reaction temperature. $COCl_2$ is converted into

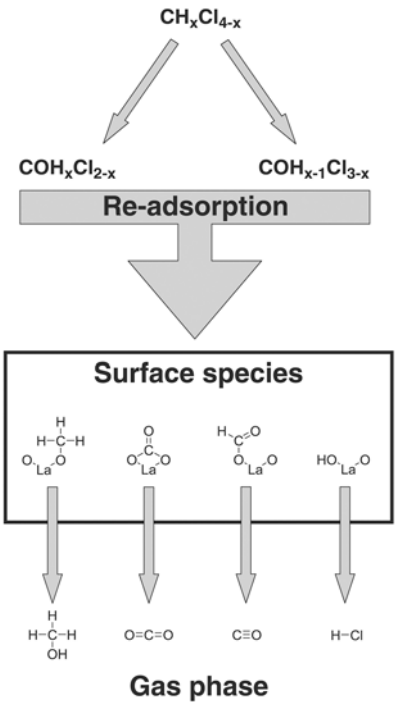

Scheme 4. Proposed general reaction scheme for the destructive adsorption of CH_xCl_{4-x} on LaOCl-P.

CO_2 after re-adsorption, which may re-adsorb again resulting in carbonate formation. In the case of COHCl, a formate group is formed when re-adsorption occurs. Via a Cannizzaro-like reaction COH_2 is re-adsorbed leading to the formation of a methoxy and formate group.[13] In some cases, the intermediates are observed in the gas phase spectra, i.e. CH_2O and $COCl_2$ for CH_2Cl_2 and $CHCl_3$, respectively.

The constant temperature experiments show that the conversion of H-containing CHC_1 decreases as the H-content of the reactant increases. This trend can be explained by the change in polarization in the bonds of the CH_xCl_{4-x} molecule. The polarization of the reactant molecule is linked to the electronegativities (EN) of the atoms.[17] The difference in EN between the C atom and the Cl atom results in a polarization between the central atom and the substituents. Since the EN of the H atom is relatively the same as for the C atom, a C-H bond is less polarized than the C-Cl bond. Even though the direction of the polarization of the C-H is opposite to that of the C-Cl bond, the influence of the C-H bond on the polarization of the molecule is negligible. According to the proposed reaction scheme, the initial steps involve the lengthening and consecutive breaking of the C-H bond and/or C-Cl bond. Loss of polarization as a result of decreasing Cl content stabilizes the reactant molecule, and hence reduces the susceptibility to H or Cl abstraction, resulting in lower activity. In addition to the reactant, the chlorination of the catalyst is also found to be of influence on the conversion. After a certain reaction time, a maximum conversion is reached. This shows that a specific chlorination degree represents the optimum combination of Lewis acidity and basicity.

Table 2. Overview of gas phase and surface species detected on LaOCl-P with IR for the destructive adsorption of $CHCl_3$, CH_2Cl_2 and CH_3Cl at RT, 100, 150, 200, 250 and 300 °C (diss. = dissociation, form. = formation).

	$CHCl_3$		**CH_2Cl_2**		**CH_3Cl**	
T (°C)	**Surface species**	**Gas phase**	**Surface species**	**Gas phase**	**Surface species**	**Gas phase**
RT	Hydroxyl form.	-	Hydroxyl form.	-	-	-
100	Formate form.	CO	Formate form.	-	-	-
150	Carbonate form. Formate diss.	CO	Methoxy form.	-	Methoxy form.	-
200	Hydroxyl diss.	CO HCl	Carbonate form. Formate diss.	CO	-	-
250	Carbonate diss.	CO HCl	-	CO CH_3OH	-	$(CH_3)_2O$
300	-	CO HCl $COCl_2$ C_2Cl_4	Carbonate diss.	CO CH_3OH CH_2O	Formate form. Methoxy diss.	$(CH_3)_2O$ CH_3OH CO

Intermediates in the destruction of chlorinated C_1 on La-based Materials

The IR studies on the destructive adsorption of the H-containing CHC_1 series revealed different products and surface species. In general, higher H-content of the reactant results in more hydrogenated reaction products. The surface species follow the same trend. The GC experiments at constant temperature show that CO_2 is formed after an initial period of chlorination. The conversion into CO_2 parallels the trend in activity for the reactants; the time of maximum conversion to CO_2 is longer as the reactant becomes more hydrogenated. The IR experiments have shown that carbonates are formed in all reactions discussed here. Therefore, it is concluded that carbonates are retained on the surface of the catalyst as long as sufficient O is available. As the surface becomes chlorinated, CO_2 is released from the surface. The exclusive formation of CH_3OH from CH_2Cl_2 was observed on LaOCl-P after an induction period. This illustrates how the chlorination degree of the surface influences the selectivity. The two proposed reaction pathways based on the IR results yield different products for each reactant. A sharp decrease in the conversion into CO_2 and CO is observed for $CHCl_3$ and CH_2Cl_2, respectively. These are products resulting from the proposed pathway proceeding via H/Cl abstraction. Since the surface is O-rich at the beginning of the experiment, the abstraction by the Lewis basic site is favourable. As the catalyst surface becomes more chlorinated, the material is becoming less basic. This results in a decreased conversion of CO_2 and CO for the experiment with $CHCl_3$ and CH_2Cl_2, respectively. The second pathway is also dependent on the availability of O atoms to enable the exchange of two Cl atoms for one O atom between the reactant and the catalytic material. However, the strength of the basic O site is not of direct influence as it is in the H/Cl abstraction pathway. This explains why a more gradual decrease in conversion is observed for the formation of CO and CH_3OH in the experiments with $CHCl_3$ and CH_2Cl_2, respectively.

Conclusions

For the destructive adsorption of $CHCl_3$, CH_2Cl_2 and CH_3Cl on La_2O_3-based materials, two reaction pathways are established that lead to the formation of gas phase intermediates (Scheme 4). It was found that a basic O site is able to abstract a H atom from the gas phase molecule, which is a new aspect for the destructive adsorption in comparison to the previous experiments with CCl_4. The intermediates can rapidly re-adsorb on the catalyst surface and form surface species. The surface species can interconvert and/or dissociate into gas phase products. The dissociation of the surface species is dependent on the reaction temperature and the degree of surface chlorination.

With respect to activity, the same result is found as for the catalytic destruction of the same compounds found in the PhD thesis of Van der Avert.[2, 5] As the number of hydrogen atoms in the molecule increases, the initial temperature of reaction increases. Conversion of the CHC_1 at constant temperature decreases with an increasing number of hydrogen atoms. This trend is believed to be a result of the decrea-sing polarization of the bonds in the CHC_1 molecule as a consequence of more hydrogen atoms. The H and Cl abstraction that initiates

the reaction is therefore less favourable with increasing H-content. A second factor which influences conversion is the chlorination degree of the LaOCl surface. An optimum degree of surface chlorination exists, which translates to an optimal combination of Lewis acidic and basic surface sites. Therefore, control of the chlorination degree of the surface is important when steam is added to the system to make the reaction catalytic.

The selectivity for the destructive adsorption of H-containing CHC_1 largely depends on the reactant. It implies that the relative concentrations of the reactant will directly influence the product distribution when mixtures of CHC_1 are converted. In order to use the catalytic conversion of CHC_1 for the production of re-usable chemicals, the selectivity has to be directed towards products containing C-H bonds, such as CH_3OH, $(CH_3)_2O$ and CH_2O. Also, the formation of CO, $COCl_2$, CO_2 and C_2Cl_4 needs to be minimized. A way to tune the reaction towards more desirable products may be the combination of waste streams with a hydrogen and carbon rich source. The surface chlorination is, in view of the proposed reaction scheme, of direct influence on the selectivity. A catalyst with ample O promotes the reaction pathway involving H/Cl removal. The removal of H results in less hydrogenated, and hence less desirable, surface intermediates and gas phase products. The surface chlorination also inhibits the formation of carbonates, which reduces the formation of CO_2. Therefore, a chlorinated catalyst is more selective than, for example, pure La_2O_3. This is important when applying steam to make the reaction catalytic, because the chlorination degree of the steady state catalyst can be tuned for optimal conversion.

Acknowledgements

Maria Garcia Ramos (Utrecht University) is thanked for performing the GC activity experiments. Marco Daturi (University of Caen, France) and Ad Mens (Utrecht University) are thanked for their contribution to the design of the IR vacuum setup used in these experiments. We also thank Tom Visser (Utrecht University) for his input regarding the IR results. This work was supported by the National Research School Combination Catalysis (NRSC-C) and the Dutch Science Foundation (VICI/NWO-CW grant).

References

1. P. van der Avert, B. M. Weckhuysen, *Angew. Chem. Int. Ed.* **2002**, 41, 4730.
2. P. van der Avert. *Catalytic destruction of chlorinated hydrocarbons over lanthanide oxides,* Katholieke Universiteit Leuven: Leuven, 2003.
3. O. V. Manoilova, S. G. Podkolzin, B. Tope, J. A. Lercher, E. E. Stangland, J. M. Goupil, B. M. Weckhuysen, *J. Phys. Chem. B* **2004**, 108, 15770.
4. P. van der Avert, S. G. Podkolzin, O. V. Manoilova, H. de Winne, B. M. Weckhuysen, *Chem. Eur. J.* **2004**, 10, 1637.

5. P. Van der Avert, B. M. Weckhuysen, *Phys. Chem. Chem. Phys.* **2004**, 6, 5256.
6. S. G. Podkolzin, O. V. Manoilova, B. M. Weckhuysen, *J. Phys. Chem. B* **2005**, 109, 11634.
7. C. J. Pouchet, *Aldrich Library of FT-IR Spectra: Vapor Phase,* Aldrich Chemical Co.: Milwaukee, 1989; Vol. 3.
8. O. Koper, Y.-X. Li, K. J. Klabunde, *Chem. Mater.* **1993**, 5, 500.
9. R. S. Cutting, C. A. Muryn, G. Thornton, D. J. Vaughan, *Geochim. Cosmochim. Acta* **2006**, 70, 3593.
10. H. Viqué, P. Quintard, T. Merle-Mejean, V. Lorenzelli, *J. Eur. Ceram. Soc.* **1998**, 18, 305.
11. B. Klingenberg, M. Albert Vannice, *Chem. Mater.* **1996**, 8, 2755.
12. G. Busca, G. Lamotte, J.-C. Lavalley, V. Lorenzelli, *J. Am. Chem. Soc.* **1987**, 109, 5197.
13. C. Li, K. Domen, K. Maruya, T. Onishi, *J. Catal.* **1990**, 125, 445.
14. E. Peringer, S. G. Podkolzin, M. E. Jones, R. Olindo, J. A. Lercher, *Top. Catal.* **2006**, 38, 211.
15. S. G. Podkolzin, E. E. Stangland, M. E. Jones, E. Peringer, J. A. Lercher, *J. Am. Chem. Soc.* **2007**, 129, 2569.
16. M. Alfredsson, C. R. A. Catlow, A. Paulidou, R. M. Nix, *Chem. Commun.* **2002**, 38, 2128.
17. M. V. Putz, N. Russo, E. Sicilia, *Theor. Chem. Acc.* **2005**, 114, 38.

4

Dehydrochlorination of Intermediates in the Production of Vinyl Chloride over La_2O_3-Based Catalysts

Light ends waste mixtures contain both chlorinated C_1 (CHC_1) and C_2 (CHC_2). In this chapter, the dehydrochlorination of CHC_2 over La_2O_3 and LaOCl catalyst materials is studied. This reaction is important for the conversion of the CHC_2 in the light ends mixtures into more desirable chlorinated ethenes, such as 1,1-$C_2H_2Cl_2$ and C_2H_3Cl. Moreover, the dehydrochlorination of 1,2-$C_2H_4Cl_2$ into C_2H_3Cl is a key step in the production of polyvinyl chloride (PVC), which is performed uncatalyzed in industry. Therefore, the conversion of chlorinated ethanes over La_2O_3-based catalysts is not only interesting from a waste conversion point of view, but also as a potential process in the production of PVC. It was found both La_2O_3 and LaOCl are active for the elimination of HCl under formation of chlorinated ethenes. When a catalytic surface is oxygen-rich, side-reactions occur resulting in chlorination of the catalyst material and the formation of oxygenated products, such as CO and CO_2. Instead, when a catalytic surface is chlorine-rich, a stable product distribution and surface composition is achieved with 100 % selectivity towards the formation of chlorinated ethenes.

Introduction

1,1-$C_2H_2Cl_2$, which is the monomer for the production of polyvinylidene chloride (PVDC), is prepared from the dehydrochlorination of 1,1,2-$C_2H_3Cl_3$ using alkaline solutions.[1] Actually, in most cases 1,1,2-$C_2H_3Cl_3$ is used to produce 1,1-$C_2H_2Cl_2$, since sufficient quantities are formed during the production of C_2H_3Cl. Also, the cracking of 1,2-$C_2H_4Cl_2$ to C_2H_3Cl is a non-catalytic dehydrochlorination reaction. Not many heterogeneous catalysts are known for the dehydrochlorination of chlorinated ethanes, mainly because of low selectivity and chlorine poisoning. In fact, alumina is active for this reaction and has been studied because dehydrochlorination is an undesirable side-reaction in the oxychlorination of ethene into 1,2-$C_2H_4Cl_2$, which is catalyzed by $CuCl_2/\gamma$-Al_2O_3.[2, 3] Therefore, dehydrochlorination of chlorinated ethanes is not only interesting from a waste conversion point of view as an active dehydrochlorination catalyst could be used in the preparation steps towards C_2H_3Cl as well.

The goal of this Chapter is to investigate the relation between the La_2O_3-based catalyst composition and its activity and selectivity in the dehydrochlorination of chlorinated ethanes. C_2H_5Cl and 1,1,2-$C_2H_3Cl_3$ were chosen as reactants because they are the main C_2 byproducts found in the light ends mixtures, as was shown in Chapter 1. 1,2-$C_2H_4Cl_2$ was selected to test the catalyst for the conversion of into C_2H_3Cl, which is a commercially important reaction. Flow-gas experiments over LaOCl as a function of temperature were performed with C_2H_5Cl, 1,2-$C_2H_4Cl_2$, 1,1,2-$C_2H_3Cl_3$, C_2H_3Cl and C_2HCl_3 with online gas chromatography (GC) analysis. The latter two reactants were chosen to evaluate the catalyst activity towards unsaturated chlorinated C_2. Also, the conversion of 1,1,2-$C_2H_3Cl_3$ as a function of temperature was monitored in a static vacuum cell using gas phase infrared spectroscopy (IR) to complement the GC results. The stability and selectivity of La_2O_3 and LaOCl were evaluated in a flow-gas experiment at constant temperature with 1,1,2-$C_2H_3Cl_3$ as reactant. In addition, the catalyst composition before and after this experiment was characterized with X-ray photoelectron spectroscopy (XPS) and X-ray diffraction (XRD).

Experimental

Materials and Characterization

For this chapter, the LaOCl-P sample was used for the temperature-programmed and constant temperature activity experiments. The method of preparation and physicochemical properties of this sample have been described in detail in Chapter 2. The experiments with 1,1,2-$C_2H_3Cl_3$ were repeated with La_2O_3 (Acros Organics, 99.99 %). The phase composition of La_2O_3 and LaOCl-P after reaction as a function of time with 1,1,2-$C_2H_3Cl_3$ was determined using XRD and XPS. XRD measurements were performed at ambient conditions with a Bruker-AXS D8 diffractometer equipped with a $Co_{K\alpha 1,2}$ source. The XPS spectra were acquired

using a Perkin-Elmer (PHI) model 5500 spectrometer. All XPS spectra were obtained using samples in the form of pressed wafers.

Flow Gas Experiments

The activity experiments for the dehydrochlorination of C_2H_5Cl (Aldrich, ≥99.7 %), 1,2-$C_2H_4Cl_2$ (Acros Organics, 98+ %) and 1,1,2-$C_2H_3Cl_3$ (Acros Organics, 98 %) were performed in a tubular fixed-bed quartz reactor. The catalyst bed consisted of 0.5 g LaOCl-P or La_2O_3 pressed in a 200-500 µm sieve fraction, pretreated in 10 mL/min He (Hoekloos, ≥99.996 %) at 550 °C. To find the initial reaction temperature, the reaction was carried out from 50 to 400 °C using a 25 mL/min 3-4 vol% reactant/He flow. In the case of 1,1,2-$C_2H_3Cl_3$, the reactions were also performed at 400 °C over La_2O_3 and LaOCl-P. Details of the setup can be found in Chapter 2.

IR Experiments

During the flow gas experiments with 1,1,2-trichloethane over La_2O_3, several products were detected which could not be assigned by GC. To complement the GC data, the reaction of 1,1,2-trichloethane on La_2O_3 was monitored in situ by IR. For these IR measurements, the quartz cell was used, which was discussed in Chapter 2. All IR spectra were recorded using a Perkin Elmer 2000 spectrometer with a resolution of 4 cm^{-1}. La_2O_3 (Acros Organics, 99.99 %) was pressed into a self-supporting wafer (2 cm^2), and activated in situ prior to the IR measurements in dynamic vacuum at 550 °C overnight. After pretreatment, 1,1,2-$C_2H_3Cl_3$ (Acros Organics, 98 %) (30 mbar) was introduced into the cell and the wafer was placed in the oven position of the cell, enabling the measurement of gas phase IR spectra. The temperature was raised from 100 to 400 °C in steps of 50 °C. After each step the temperature was held constant during which gas phase spectra were recorded.

Results and Discussion

Temperature Programmed Reaction Experiments

The effluent composition of the temperature programmed dehydrochlorination reactions over LaOCl is shown in Figure 1. In the case of C_2H_5Cl and 1,2-$C_2H_4Cl_2$, 100 % selectivity is observed towards C_2H_4 and C_2H_3Cl, respectively (Reaction Eqs. (1) and (2)). 1,1,2-$C_2H_3Cl_3$ is converted into several products. A significantly lower initial reaction temperature is observed for chloroethane compared to 1,2-$C_2H_4Cl_2$ and 1,1,2-$C_2H_3Cl_3$. It has been established that the

cleavage of the C-Cl bond typically precedes the removal of a H atom.[4, 5] Furthermore, it has been shown that the initial reaction rate for the dehydrochlorination of chlorinated ethanes increases with an increasing number of chlorine atoms.[6] It should be noted, however, that this trend was established based on mono-, di- and tri-substituted chloroethanes with all chlorine atoms on the same carbon atom. With more C-Cl bonds on the same carbon atom in a chlorinated ethane mo-lecule, the C-Cl bonds become more polarized. As a result, the C-Cl bonds are more susceptible to cleavage. Instead, C-Cl bonds on both carbon atoms may stabilize the polarization of the C-Cl bonds, which explains the higher initial temperature of reaction of 1,2-$C_2H_4Cl_2$ and 1,1,2-$C_2H_3Cl_3$ with respect to C_2H_5Cl.

The main product for the dehydrochlorination of 1,1,2-$C_2H_3Cl_3$ is 1,1-$C_2H_2Cl_2$ and in addition C_2H_3Cl and cis-1,2-$C_2H_2Cl_2$ are formed. The formation of C_2H_3Cl implies that Cl_2 elimination occurs. This reaction is, however, energetically highly unfavourable and is not expected to proceed. A possible explanation would be that a different product is co-eluting with C_2H_3Cl. Therefore, the product assigned by the GC as C_2H_3Cl has been labelled as X in Figure 1 and 2. Chlorine and hydrogen atoms can be removed from the reactant molecule via two pathways of HCl elimination, shown in Reaction Scheme 1. The formation of 1,1-$C_2H_2Cl_2$ (Scheme 1, Reaction a) is favoured over the reaction towards 1,2-$C_2H_2Cl_2$ (Scheme 1, Reaction b). In addition, no formation of trans-1,2-$C_2H_2Cl_2$ (Scheme 1, Reaction c) was detected. At 400 °C, trace amounts of CO and CO_2 were detected. Blank experiments were also performed and no significant product formation was observed, which rules out non-catalytic gas phase reactions. Based on these results, it is concluded that LaOCl is an active catalyst for the dehydrochlorination of chlorinated ethanes.

$$CH_2Cl\text{-}CH_3 \rightarrow CH_2{=}CH_2 + HCl \quad (1)$$
$$CH_2Cl\text{-}CH_2Cl \rightarrow CH_2{=}CHCl + HCl \quad (2)$$

The dehydrochlorination of chlorinated ethanes over heterogeneous catalysts is catalyzed by three types of active sites: acidic, basic or dual sites.[7] It has been shown that for the dehydrochlorination of 1,1,2-trichloroethane, the selectivity towards the 1,1- and 1,2-product are influenced by the acid-base properties of the catalyst.[7] Control of the chlorination degree of the catalyst is crucial to tune the acid-base properties and optimize the performance of the catalyst when converting mixtures of chlorinated C_1 and C_2. In Chapters 2 and 3, it was shown that the acid-base properties of La_2O_3-based catalysts are a key factor for the activation of C-Cl and C-H bonds in chlorinated C_1. Hence, the degree of chlorination may also be of influence on the selectivity of the dehydrochlorination of chlorinated C_2. Therefore, the reaction with 1,1,2-$C_2H_3Cl_3$ was repeated with La_2O_3, which contains weaker La^{3+} Lewis acid sites. The reactor effluent composition was analyzed throughout the experiment, as shown in Figure 2. In addition to the products observed over LaOCl, trans-1,2-$C_2H_2Cl_2$ is detected. However, as the temperature increases the selectivity towards 1,1-$C_2H_2Cl_2$ increases, while it decreases towards the other products. Low concentrations of CO and CO_2 were detected as in the case of LaOCl. Also, small amounts of two products were detected

Dehydrochlorination of chlorinated ethanes over La_2O_3-Based materials

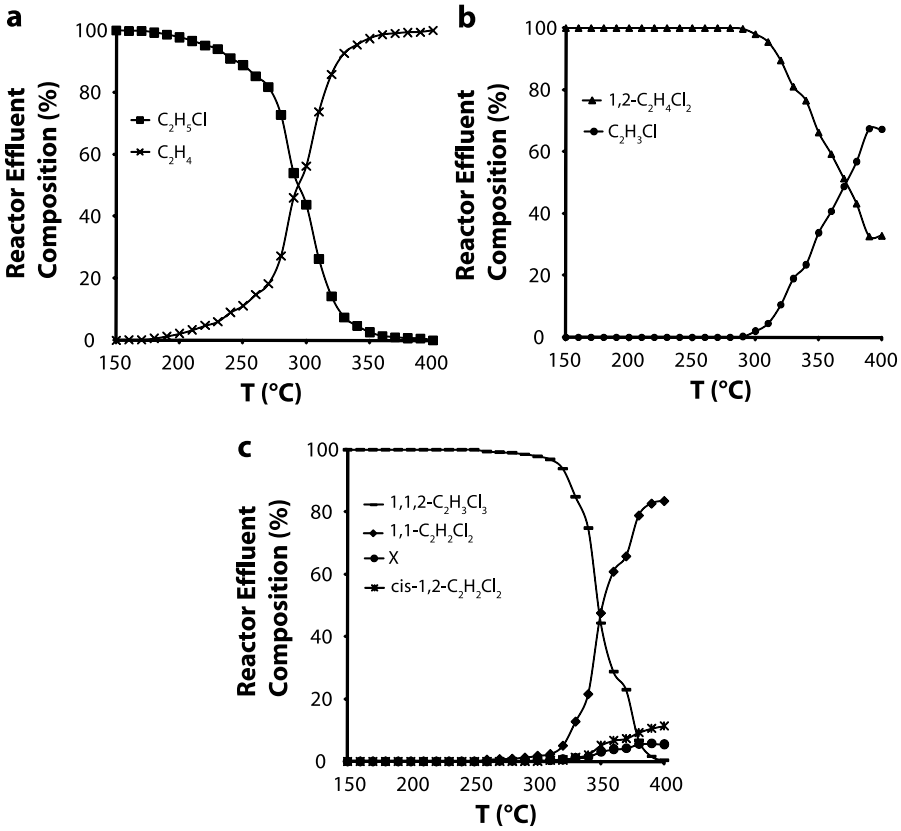

Figure 1. Effluent composition for the dehydrochlorination of (a) C_2H_5Cl, (b) 1,2-$C_2H_4Cl_2$ and (c) 1,1,2- $C_2H_3Cl_3$ over LaOCl as a function of temperature (GHSV = 2000 h^{-1}, inlet concentration: [C_2H_5Cl] = 3.7 vol%, [1,2-$C_2H_4Cl_2$] = 3.4 vol% and [1,1,2-$C_2H_3Cl_3$] = 3.2 vol%, X = product unassigned based on GC).

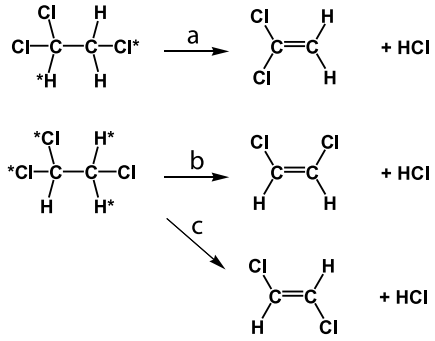

Scheme 1. Reaction pathways for the dehydrochlorination of 1,1,2-$C_2H_3Cl_3$ into (a) 1,1-$C_2H_2Cl_2$, (b) cis-1,2-$C_2H_2Cl_2$ and (c) trans-1,2-$C_2H_2Cl_2$ (* indicates the positions of the atoms which are eliminated as HCl).

which could not be assigned based on the GC results. Even though these products could not be identified, the retention times indicate that these compounds are chlorinated hydrocarbons (CHCs). Therefore, the same response factor as for the other CHCs is assumed to be valid for these unknown products.

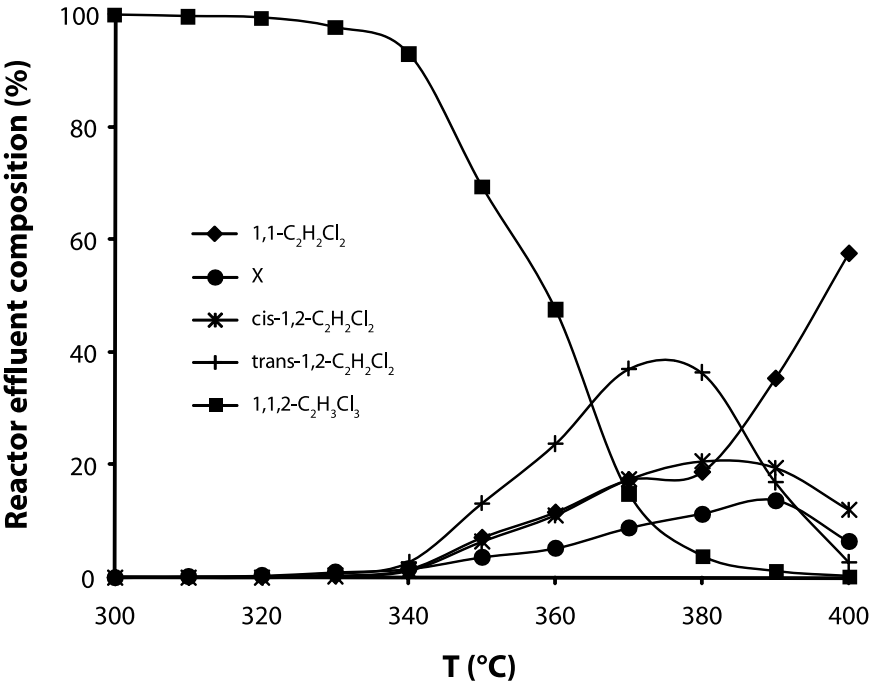

Figure 2. Effluent composition for the dehydrochlorination of 1,1,2-$C_2H_3Cl_3$ over La_2O_3 as a function of temperature (GHSV = 2000 h^{-1}, inlet concentration: [1,1,2-$C_2H_3Cl_3$] = 3.2 vol%, X = product unassigned based on GC).

In Situ IR Reaction Experiments

The flow-gas experiments indicate that La_2O_3 and LaOCl catalyze the dehydrochlorination of chlorinated ethanes and that the acid-base properties of the catalyst directly influence the selectivity. However, the assignment of the products is difficult with gas chromatography only. Therefore, the gas phase composition of the temperature programmed reaction on La_2O_3 in a vacuum cell was monitored using IR spectroscopy to complement the GC results. The recorded spectra are shown in Figure 3. In the spectral regions 2250-2400 and 1350-1900 cm^{-1}, the strong bands of ambient CO_2 and H_2O, respectively, were removed by spectroscopic software. Figure 3a illustrates the increase and decrease of the bands in the gas phase spectra as a function of temperature during the experiment. In Figure 3b, the spectrum of the reactant at room temperature (RT) is shown together with that of Spectrum

Dehydrochlorination of chlorinated ethanes over La_2O_3-Based materials

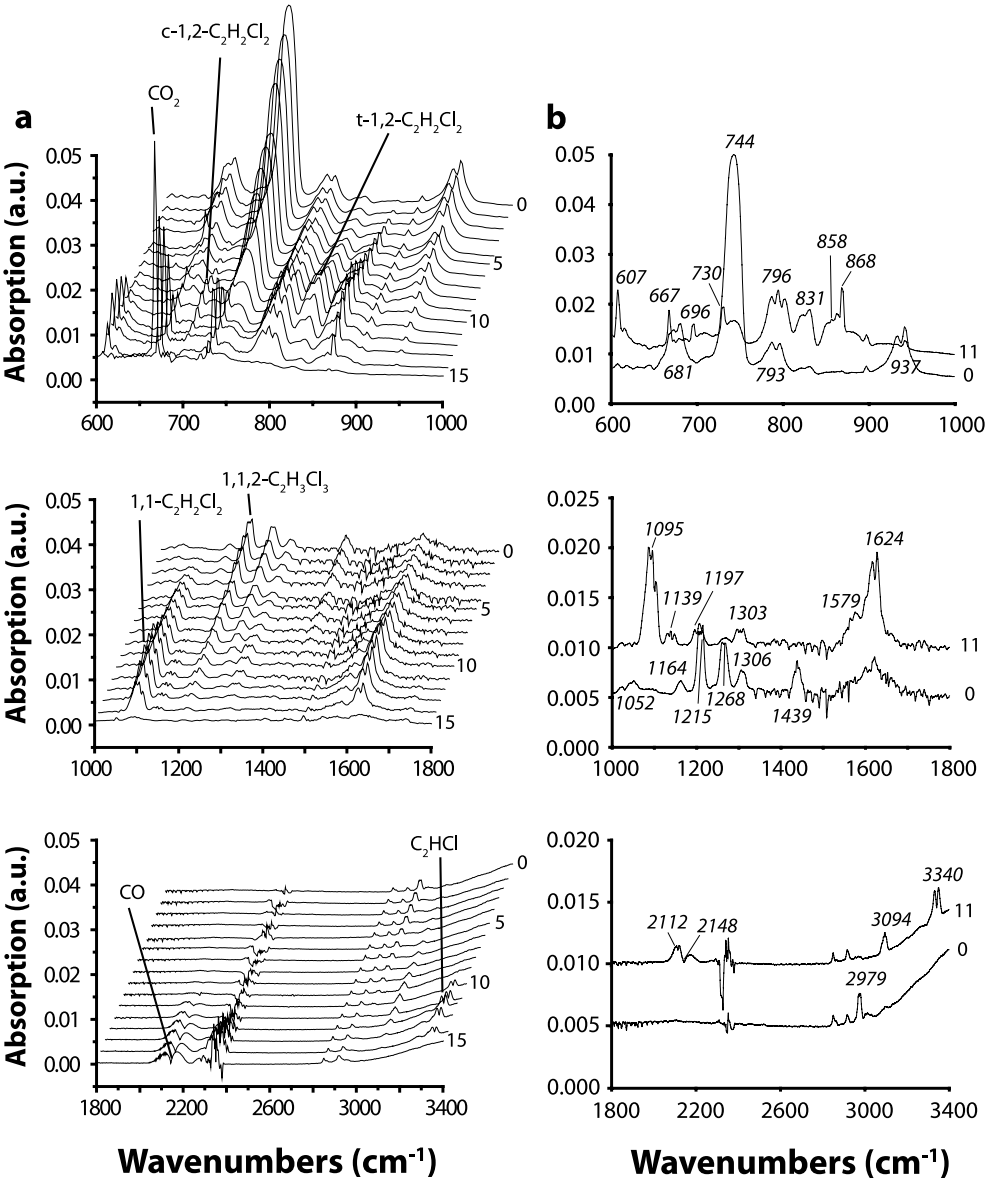

Figure 3. (a) Gas phase IR spectra recorded during the dehydrochlorination of 1,1,2-$C_2H_3Cl_3$ over La_2O_3 as a function of temperature: (0) reactant at RT, (1) 5 min at 100 °C, (2) 5 min at 150 °C, (3) 5 min at 200 °C, (4-6) 5, 10 and 25 min at 250 °C, (7-9) 5, 10 and 25 min at 300 °C, (10-12) 5, 10 and 25 min at 350 °C, (13-15) 5, 10 and 75 min at 400 °C. (b) Spectrum (0) and (11) used for band assignment of products.

11 from Figure 3a. Spectrum 11 was chosen for the assignment of the bands of the products, because all the bands which are observed during the experiment are present in this spectrum.

The assignment of the bands based on reference spectra is shown in Table 1.[8] The products that are formed throughout the experiment are 1,1-$C_2H_2Cl_2$, cis-1,2-$C_2H_2Cl_2$, trans-1,2-$C_2H_2Cl_2$, C_2HCl, CO and CO_2. Specific bands were chosen, which possesses high intensity and minimal overlap with other bands, to derive the relative ratios of the products as a function of temperature as shown in Figure 3a. The spectra show that $C_2H_2Cl_2$ derivatives are formed simultaneously at 200 °C (Figure 3a, spectrum 4).

Table 1. Assignment of the gas phase IR bands in spectrum recorded after 10 min of conversion of 1,1,2-trichloethane over La_2O_3 at 350 °C shown in Figure 3b (vs =strong, s =strong).

Spectrum 11	**1,1-$C_2H_2Cl_2$**	**c-1,2-$C_2H_2Cl_2$**	**t-1,2-$C_2H_2Cl_2$**	**C_2HCl**	**CO_2**	**CO**
607	603 (s)					
667					667 (s)	
696		697 (vs)				
796	800 (vs)					
831			828 (vs)			
858		857 (vs)				
868	875 (vs)					
1095	1095 (vs)					
1139	1139 (s)					
1197			1200 (s)			
1303		1303 (s)				
1579		1574 (s)				
1624	1627 (vs)					
2112				2110 (s)		
2148						2144
3094			3090 (s)			(vs)
3340				3340 (vs)		

As the temperature increases (Figure 3a, spectrum 5-9), the intensity of the chlorinated ethene bands increases with maximum intensity at 250 °C (Figure 3a, spectrum 9). Further increase of the temperature results in a decrease in intensity of the bands assigned to cis/trans-1,2-$C_2H_2Cl_2$. The intensity of the 1,1-$C_2H_2Cl_2$ band, however, remains constant. The decrease in intensity of the bands of the 1,2-derivatives is accompanied by the formation of CO, CO_2 and C_2HCl (Figure 3a, spectrum 10). The formation of C_2HCl indicates that a second dehydrochlorination reaction may occur resulting in the formation of a C≡C bond. At 350 °C, a band becomes visible at 730 cm^{-1}, for which a reference could not be found. Strong

absorption at this position is characteristic for C-Cl stretch vibrations. When the temperature reaches 400 °C, the bands of C_2HCl and 1,1-$C_2H_2Cl_2$ also decrease and a strong increase in intensity of the CO_2 band is observed. The formation of CO and CO_2 is characteristic for destructive adsorption of CHCs. After more than 1 h of reaction, only CO and CO_2 are detected. These results show that high temperatures should be avoided to prevent undesirable secondary reactions.

No bands indicative of C_2H_3Cl were observed in the spectra. The other products which were detected during the temperature programmed flow-gas experiment over La_2O_3 (Figure 2), namely 1,1-$C_2H_2Cl_2$ and cis/trans-1,2-$C_2H_2Cl_2$, were also observed in the in situ IR experiment. Therefore, based on these spectra it is proposed that the product which co-elutes with C_2H_3Cl is C_2HCl. The dehydrochlorination of 1,1,2-$C_2H_3Cl_3$ proceeds at relatively low temperature. At higher temperature, two secondary reactions of the chlorinated ethenes are favorable; a second elimination of HCl or destructive adsorption. The former results in the formation of C_2HCl. The latter leads to the breaking of the C-C bond and formation of CO and CO_2 via exchange of oxygen and chlorine atoms. The 1,2-$C_2H_2Cl_2$ derivatives are more susceptible to the secondary reactions than 1,1-$C_2H_2Cl_2$. It should be noted that no significant amounts of CO and CO_2 were detected during the flow-gas experiments. A possible reason for this may be the different nature of the experiments; the IR experiments are in a closed cell as opposed to the flow-gas experiment in which the reactant has a limited residence time.

Catalyst Behaviour

The temperature programmed flow-gas experiment over La_2O_3 suggests there is an induction period during which the selectivity changes. This is supported by the in situ IR experiments. Moreover, no bands indicative of HCl were found in the gas phase spectra. It is known that La_2O_3 and LaOCl can be chlorinated into a pure $LaCl_3$ phase using HCl. The HCl reacts with the basic oxygen sites according to Reaction Eq. (3). During the dehydrochlorination of chlorinated ethanes, HCl may either be re-adsorbed or the H and Cl atom are abstracted directly by the La-O couple and remain on the surface. Either way, the catalytic surface will change which may affect the activity and selectivity. The stability of LaOCl and La_2O_3 materials for the dehydrochlorination of 1,1,2-$C_2H_3Cl_3$ was tested in a flow-gas experiment at 400 °C. The reactor effluent composition as a function of time is shown in Figure 4. The experiment over La_2O_3 was stopped prematurely because the reactor became plugged.

$$\text{La-O-La (s)} + \text{HCl (g)} \rightarrow \text{La-OH (s)} + \text{Cl-La (s)} \qquad (3)$$

The experiments show that over La_2O_3, an induction period precedes a stable conversion and product distribution. The same products which were detected during the temperature programmed reactions are formed. The two unknown products, labelled x1 and x2, are

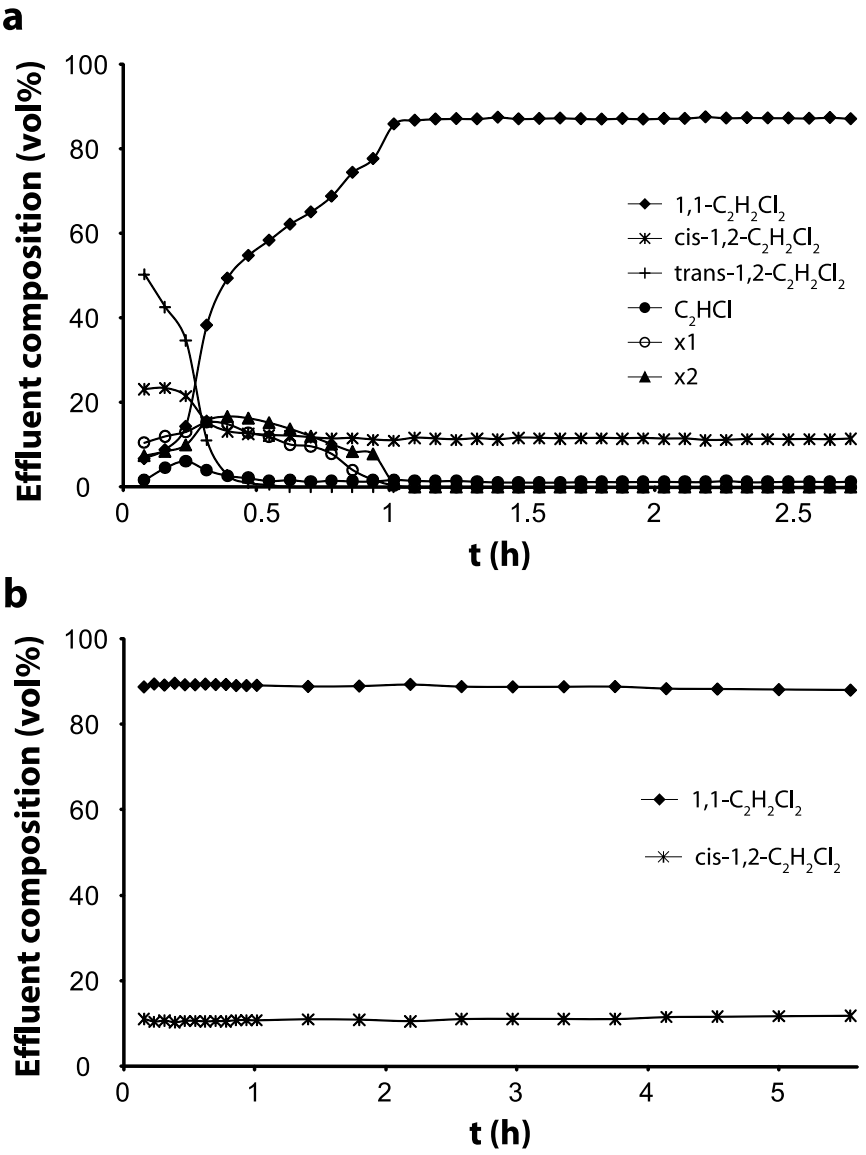

Figure 4. Effluent composition for the dehydrochlorination of 1,1,2-$C_2H_3Cl_3$ over (a) La_2O_3 and (b) LaOCl at 400 °C as a function of time (GHSV = 2000 h^{-1}, inlet concentration: [1,1,2-$C_2H_3Cl_3$] = 3.2 vol%, x_n = product unassigned based on GC and IR).

formed at higher concentrations than during the temperature programmed experiments and are therefore included in Figure 4. In the case of LaOCl, the induction period is not observed. After the induction period, the product distribution in the constant temperature experiments is similar for both LaOCl and La_2O_3. Although coke formation was observed, no significant loss of activity occurs in the experiments. LaOCl has proven to be a more stable catalyst with high selectivity towards chlorinated ethenes.

Even though the GC is not calibrated for HCl and H_2O, these products are visible in the chromatogram at low retention times. The intensities of the peaks assigned to HCl and H_2O are shown in Figure 5 as a function of time. The hydroxyl groups formed after HCl elimination can react into both HCl and H_2O. Initially, H_2O is eliminated from the oxygen-rich catalytic surface according to Reaction Equation (4). As the reaction proceeds, less hydroxyl groups are available and more chlorine is present on the surface. As a result, elimination of HCl from the surface becomes more favourable. The reaction time at which HCl formation becomes more dominant than H_2O formation, is also when the product distribution becomes stable. Therefore, it is proposed that a specific degree of chlorination of the catalyst material results in steady-state conversion of chlorinated ethanes. It should be noted that a small amount of H_2O is probably still formed together with HCl once the product distribution has stabilized, but due to overlap of the H_2O and HCl peak, the intensity of the H_2O peak is considered zero.

$$2\ \text{La-OH (s)} \rightarrow \text{H}_2\text{O (g)} + \text{La-O-La (s)} \qquad (4)$$

If a specific chlorination degree is needed for steady-state conversion, the catalyst materials used in the constant temperature experiments should possess similar surface compositions. To verify this, the LaOCl and La_2O_3 catalyst were characterized before and after reaction with 1,1,2-trichloethane using XPS and XRD. The XRD results, as shown in Figure 6, provide information on the bulk phase composition of the catalyst materials. Before reaction, the characteristic diffraction patterns of LaOCl and La_2O_3 are observed (Figure

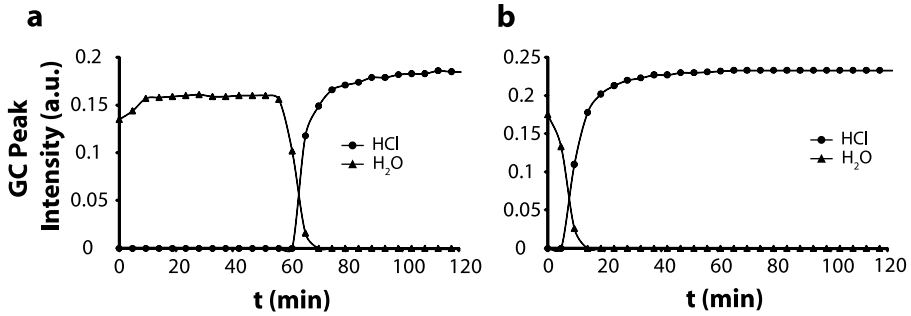

Figure 5. Intensity of H_2O and HCl peak in the chromatograms for the dehydrochlorination of 1,1,2-$C_2H_3Cl_3$ over (a) La_2O_3 and (b) LaOCl at 400 °C as a function of time as shown in Figure 4 (GHSV = 2000 h^{-1}, inlet concentration: [1,1,2-$C_2H_3Cl_3$] = 3.2 vol%, x_n = product unassigned based on GC and IR).

6a and 6c, respectively). The diffractogram of La_2O_3 after approximately 3 h of reaction at 400 °C is shown in Figure 6b. The peaks observed after reaction show that during reaction the crystalline La_2O_3 phase has been converted into a pure crystalline LaOCl phase. Even though the peaks are much broader in the amorphous LaOCl catalyst material, the similarity is straightforward. The dehydrochlorination of 1,1,2-trichloethane at 400 °C over LaOCl was performed for ca. 6 h, which is over two times as long as in the case of La_2O_3. The pattern of the LaOCl phase is partially preserved after reaction. However, a second phase is present, which was assigned as $LaCl_3.3H_2O$. The peaks at 2θ = 17.3, 29.2, 38.5, 42.5 and 46.9 ° and their relative intensities are characteristic of $LaCl_3.3H_2O$. It is uncertain whether LaOCl is converted into $LaCl_3.3H_2O$ directly or into $LaCl_3$, which becomes hydrated when it is exposed to air prior to the XRD measurement. Either way, the bulk phase of both La_2O_3 and LaOCl has become chlorinated during the constant temperature reactions. Chlorination of the bulk phase is also observed during the destructive adsorption and catalytic destruction of chlorinated C_1. This is caused by the solid-state diffusion of oxygen and chlorine atoms between the catalytic surface and the bulk. As the surface becomes chlorinated, the chlorine atoms diffuse into the bulk and surface oxygen is regenerated. It is therefore viable to assume that the same process occurs when the surface becomes chlorinated as a result of the dehydrochlorination reaction.

The surface composition of LaOCl and La_2O_3 before and after reaction was determined with XPS. All spectra were normalized to the La3d bands. Because La_2O_3-based materials strongly adsorb CO_2 and H_2O, the exposure to air may influence the characterization of O atoms. The intensity of the Cl2p band was therefore chosen as a measure of surface chlo-

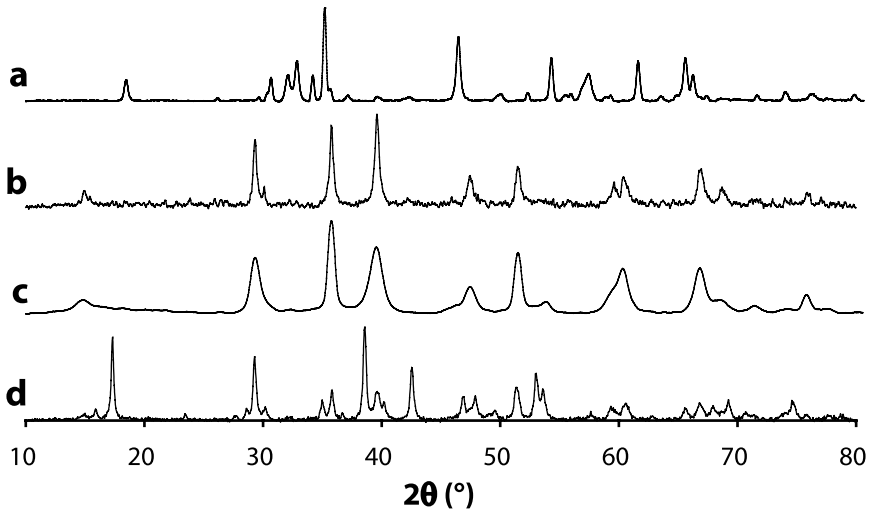

Figure 6. X-ray diffractograms of La_2O_3 and LaOCl before (a and c, respectively) and after (b and d, respectively) the dehydrochlorination of 1,1,2-$C_2H_3Cl_3$ at 400 °C, as shown in Figure 4.

rination. Figure 7 shows the Cl2p band for LaOCl and La_2O_3 before and after reaction. The Cl2p band is obviously not observed in the spectrum of La_2O_3 before reaction (Figure 7a). However, the La4p band is observed in the same region at 197 eV. Both these XPS bands are known to possess a shoulder at higher energy than the maximum, which is also observed here. The La4p band appears as a shoulder of the Cl2p band in the spectra of the materials containing chlorine. The Cl2p band positioned at 200 eV is observed in Figure 7b-d. The spectra show that the surface chlorination of the materials after reaction is approximately the same and in both cases higher than before reaction. This result confirms the hypothesis that a specific degree of chlorination is required to reach steady-state conversion.

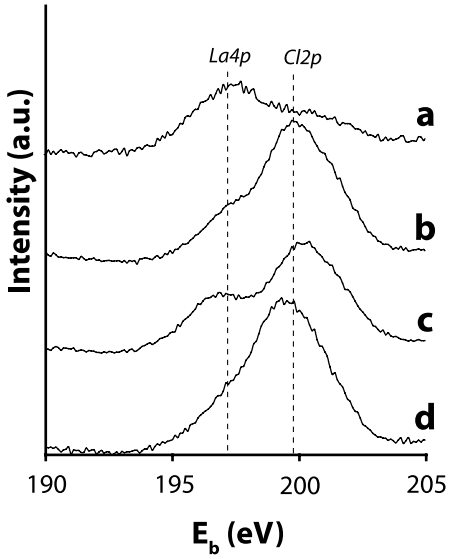

Figure 7. X-ray photoelectron spectra of La_2O_3 and LaOCl before (a and c, respectively) and after (b and d, respectively) the dehydrochlorination of 1,1,2-$C_2H_3Cl_3$ at 400 °C, as shown in Figure 4.

Conclusions

La_2O_3-based materials are active catalysts for the dehydrochlorination of chlorinated ethanes. The reaction scheme for the dehydrochlorination of chlorinated ethanes over La_2O_3-based catalyst materials is schematically shown in Scheme 2. A hydrogen and chlorine atom is abstracted from the chlorinated ethane, resulting in the formation of a hydroxyl group and a lattice chloride (Reaction b). In the case of an O-rich surface, such as La_2O_3, the hydroxyl groups will react with other hydroxyl groups under formation of H_2O (Reaction c). However, when a specific degree of chlorination of the catalytic surface is reached, the elimination of H_2O becomes less pronounced and HCl is formed (Reaction a). After the induction period

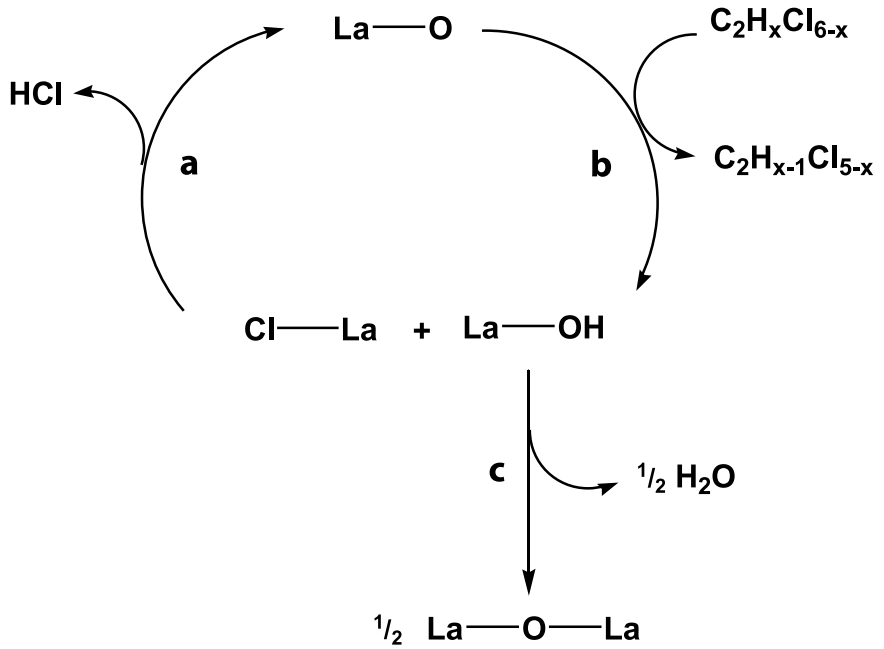

Scheme 2. Catalytic cycle for the dehydrochlorination of chlorinated ethanes over La_2O_3-based materials: (a) desorption of HCl from the catalyst material, (b) H + Cl abstraction by catalytic surface and (c) desorption of H_2O from the catalyst material

characterized by the formation of H_2O, the product distribution and conversion become stable and the chlorination degree of the catalyst surface also remains constant.

The in situ IR experiment has shown that at relatively high temperature, secondary reactions may occur, such as a second dehydrochlorination step resulting in the formation of an ethyne, or destructive adsorption leading to the formation of CO and CO_2. This indicates that the reaction temperature and chlorination degree are key factors to achieve optimal selectivity towards the formation of ethenes. Because the chlorination degree of the catalyst is of influence on both activity and selectivity for the conversion of chlorinated C_1 and C_2, it may be used to tune the catalytic properties of the La_2O_3-based catalyst.

Acknowledgements

René Bogerd (Utrecht University) is thanked for performing the flow gas experiments. Ad Mens (Utrecht University) is thanked for performing the XPS measurements. This work was supported by the National Research School Combination Catalysis (NRSC-C) and the Dutch Science Foundation (VICI/NWO-CW grant).

References

1. E. Milchert, W. Pazdzioch, J. Myszkowski, *Ind. Eng. Chem. Res.* **1995**, 34, 2138.
2. D. Carmello, E. Finocchio, A. Marsella, B. Cremaschi, G. Leofanti, M. Padovan, G. Busca., *J. Catal.* **2000**, 191, 354.
3. B. Mile, T. A. Ryan, T. D. Tribbeck, M. A. Zammitt, G. A. Hughes, *Top. Catal.* **1994**, 1, 153.
4. J. Bozzelli, Y. Chen, *Chem. Eng. Comm.* **1992**, 115, 1.
5. J. R. Anderson, B. H. McConkey, *J. Catal.* **1968**, 11, 54.
6. K. A. Frankel, B. W.-L. Jang, G. W. Roberts, J. J. Spivey, *Appl. Catal. A,* **2001**, 209, 401.
7. I. Mochida, A. Uchino, H. Fujitsu, K. Takeshita, *J. Catal.* **1976**, 43, 264.
8. C. J. Pouchet, *Aldrich Library of FT-IR spectra: Vapor Phase, Vol. 3,* Aldrich Chemical Co.: Milwaukee, 1989.

5

Hydrogen-Chlorine Exchange between Chlorinated Waste Compounds over $LaCl_3$-based Catalysts under Oxygen-Free Conditions

CCl_4 has been banned from commercial uses and is currently only produced in chemical industries as a by-product. The combination of its low economic value and environmental regulation makes this compound undesirable and its conversion into more valuable products advantageous. In this chapter, the H-Cl exchange reaction of CCl_4 with other chlorinated hydrocarbons (CHCs), specifically CH_2Cl_2, over unsupported and carbon nanofiber (CNF)-supported $LaCl_3$ catalysts is studied. The chapter starts with an introduction on the potential of $LaCl_3$ as a catalyst material for the H-Cl exchange reaction. Next, thermodynamic calculations, the synthesis of the $LaCl_3$ materials, density functional theory (DFT) calculations and activity experiments are discussed. It will be shown that $LaCl_3$ is an active catalyst for the H-Cl exchange reaction between CCl_4 and CH_2Cl_2 with 100 % selectivity towards $CHCl_3$ and 45 % conversion per g $LaCl_3$ at 450 °C. Unsupported $LaCl_3$ catalysts show low conversion due to their low surface area. In contrast, CNF-supported $LaCl_3$ catalysts are found to be significantly more active than the unsupported catalysts based on both weight and volume. DFT calculations indicate that weakly adsorbed hydride and chloride species are present on the catalytic surface and are exchanged with H and Cl atoms from the gas phase reactant. To the best of our knowledge, this is the first catalyst for the exchange of H and Cl between gas phase reactants without the presence of either lattice or gas phase oxygen atoms.

Introduction

CCl_4 is one of the most hazardous chlorinated compounds and has been banned from commercial use in many countries. As a result, the production of CCl_4 has been decreasing and will continue to phase out.[1] Hence, the economic value of this chemical is low and it is considered a waste product. However, CCl_4 is still produced in chemical industries as a by-product. Therefore, both the production and disposal of CCl_4 are heavily regulated.[1, 2] H-Cl exchange with other chlorinated hydrocarbons (CHCs) would be advan-tageous to make more valuable CHCs, which could be recycled in the production process.

Reaction thermodynamics are favorable for using CCl_4 as a Cl source with CH_4 or another chloromethane. The best known way for running these reactions is thermal gas phase radical chemistry.[3] The disadvantage of radical chemistry is its low selectivity due to the formation of various chlorinated C_1 (CHC_1) and C_1 (CHC_2) coupling products.[3] In addition, coke formation at the temperatures that are required for radical generation is severely hampering the process. As a result, commercial application of this reaction is currently not feasible and incineration is commonly used as a route for the destruction of CCl_4.

La_2O_3-based catalysts are known to be active for the catalytic conversion of CHC_1 [4-9] as well as the activation of hydrocarbons, such as CH_4 and C_2H_6.[10-12] In other words, these catalyst materials are able to activate both C-H and C-Cl bonds. Here, we report for the first time that $LaCl_3$ can be used as a highly active and stable catalyst for the H-Cl exchange between CHC_1; i.e. a mixture of CH_2Cl_2 and CCl_4. Catalytic H-Cl exchange of CCl_4 with CH_4 has been studied before, focusing on supported Pt/Mn systems in combination with O_2. This catalytic system is, however, markedly different from the materials described here. So far, all catalytic systems involving the exchange of H and Cl between gas phase reactants require the presence of O atoms, either as lattice oxygen or in gas phase molecules, such as O_2 and H_2O. In this case, the La-based catalysts were synthesized by chlorination of a precursor to $LaCl_3$ to exclude the presence of lattice oxygen in the catalyst. This is necessary to prevent the destructive adsorption processes of the reactant molecules. A catalyst for this type of reaction without O atoms is novel and offers new possibilities for the conversion of CHCs, in particular CCl_4.

Experimental

Calculations with HSC Chemistry 4.1

The equilibrium composition of an equimolar mixture of CCl_4 and CH_2Cl_2 was calculated as a function of temperature. Three sets of input data were used for the calculations and are summarized in Table 1. Data set 1 consists of all $CHC_{1\text{-}2}$, HCl, Cl_2 and C. In data set 2, C was omitted to exclude dissociation of the reactants into coke. Data set 3 only consists of

the CHC_{1-2} to prevent HCl elimination reactions. The temperature range was 0 to 600 °C at ambient pressure and 101 data points were calculated. In addition, the free Gibbs energy change was calculated for several reactions that resulted from data sets 1-3 as a function of temperature.

Table 1. Input data sets for HSC calculations for equilibrium composition of an equimolar mixture (1 mol) of CCl_4 and CH_2Cl_2.

	Data set 1	**Data set 2**	**Data set 3**
Reactant	CCl_4 CH_2Cl_2	CCl_4 CH_2Cl_2	CCl_4 CH_2Cl_2
Allowed products	$CHCl_3$ (g) CH_3Cl (g) CH_4 (g) C_2Cl_6 (g) C_2HCl_5 (g) 1,1,1,2-$C_2H_2Cl_4$ (g) 1,1,2,2-$C_2H_2Cl_4$ (g) 1,1,1-$C_2H_3Cl_3$ (g) 1,1,2-$C_2H_3Cl_3$ (g) 1,1-$C_2H_4Cl_2$ (g) 1,2-$C_2H_4Cl_2$ (g) C_2H_5Cl (g) C_2H_6 (g) C_2Cl_4 (g) C_2HCl_3 (g) 1,1-$C_2H_2Cl_2$ (g) cis-1,2-$C_2H_2Cl_2$ (g) trans-1,2-$C_2H_2Cl_2$ (g) C_2H_3Cl (g) C_2H_4 (g) HCl (g) Cl_2 (g) C (s)	$CHCl_3$ (g) CH_3Cl (g) CH_4 (g) C_2Cl_6 (g) C_2HCl_5 (g) 1,1,1,2-$C_2H_2Cl_4$ (g) 1,1,2,2-$C_2H_2Cl_4$ (g) 1,1,1-$C_2H_3Cl_3$ (g) 1,1,2-$C_2H_3Cl_3$ (g) 1,1-$C_2H_4Cl_2$ (g) 1,2-$C_2H_4Cl_2$ (g) C_2H_5Cl (g) C_2H_6 (g) C_2Cl_4 (g) C_2HCl_3 (g) 1,1-$C_2H_2Cl_2$ (g) cis-1,2-$C_2H_2Cl_2$ (g) trans-1,2-$C_2H_2Cl_2$ (g) C_2H_3Cl (g) C_2H_4 (g) HCl (g) Cl_2 (g)	$CHCl_3$ (g) CH_3Cl (g) CH_4 (g) C_2Cl_6 (g) C_2HCl_5 (g) 1,1,1,2-$C_2H_2Cl_4$ (g) 1,1,2,2-$C_2H_2Cl_4$ (g) 1,1,1-$C_2H_3Cl_3$ (g) 1,1,2-$C_2H_3Cl_3$ (g) 1,1-$C_2H_4Cl_2$ (g) 1,2-$C_2H_4Cl_2$ (g) C_2H_5Cl (g) C_2H_6 (g) C_2Cl_4 (g) C_2HCl_3 (g) 1,1-$C_2H_2Cl_2$ (g) cis-1,2-$C_2H_2Cl_2$ (g) trans-1,2-$C_2H_2Cl_2$ (g) C_2H_3Cl (g) C_2H_4 (g)

Catalyst Preparation

Three $LaCl_3$-based catalyst materials were investigated; two bulk catalysts and one supported on CNF. The precursors used for the bulk materials were synthesized LaOCl and commercial $LaCl_3 \bullet 7H_2O$. The preparation of LaOCl-P has been described in Chapter 2. $LaCl_3 \bullet 7H_2O$

was dried at 60 °C overnight, which resulted in dehydration into $LaCl_3 \bullet 3H_2O$ as determined by X-ray diffraction (XRD) (not shown). The carbon-supported catalyst was synthesized by the incipient wetness impregnation method making use of an aqueous $LaCl_3$ solution on synthesized carbon nanofibers (CNF). In this manner, 20 wt% $LaCl_3$ was loaded on the CNF material. CNF were grown as described by Toebes et al.[13] Supported Ni/SiO_2 catalyst with a metal loading of 5 wt% was used to grow low density CNF (140 m^2/g), prepared by homogeneous deposition precipitation.[14] After impregnation the catalyst was dried at 60 °C overnight. Before chlorination, sieve fractions of the pre-treated precursors were heated at 500 °C in He for 6 h. Next, the precursors were chlorinated in situ using the setup described in Chapter 2.2.2. $LaCl_3 \bullet 3H_2O$ was chlorinated with 6 vol% CCl_4/He for 30 h at 460 °C, and was labelled $LaCl_3$-H. LaOCl-P and the CNF-supported catalyst were chlorinated with 10 vol% HCl/He at 460 °C for 20 and 4 h, respectively. They were labelled $LaCl_3$-P and $LaCl_3$-C, respectively. In Table 2, an overview of the catalysts and preparation methods is provided.

Table 2. Overview of preparation and nomenclature of $LaCl_3$ catalyst materials.

Name	**Precursor**	**Precursor pre-treatment**	**Method of chlorination**	**Precursor BET surface area (m^2/g)**
$LaCl_3$-H	$LaCl_3 \bullet 3H_2O$	Dried in air at 60 °C Heated in He at 500 °C	6 vol% CCl_4/He at 460 °C	1
$LaCl_3$-P	LaOCl-P	Heated in He at 500 °C	10 vol% HCl at 460 °C	20-30
$LaCl_3$-C	$LaCl_3 \bullet 7H_2O$ CNF	CNF impregnated with 20 wt% $LaCl_3 \bullet 7H_2O$ Dried in air at 60 °C Heated in He at 500 °C	10 vol% HCl at 460 °C	120

Activity Experiments

The catalytic experiments were performed in the setup described in Chapter 2.2.2. Equimolar mixtures of either CH_2Cl_2 with CCl_4 of 4-6 vol% each in He were led over the catalyst with a flow rate of 5 ml/min (GHSV = 400 h^{-1}). As the catalysts materials were synthesized by in situ synthesis, the amount of LaOCl and $LaCl_3 \bullet 7H_2O$ was pre-calculated for 1 g of $LaCl_3$. In the case of the carbon supported catalyst, the reactor was filled with approximately the same volume as in the case of the bulk catalyst. For the bulk materials, blank experiments were performed with quartz pellets. For the supported catalyst, CNF were used for a blank experiment. During the temperature programmed experiments, the reactor temperature was raised from 300 to 460 °C in steps of 20 °C, and the effluent was continuously analyzed by GC. In addition, the H-Cl exchange of CCl_4/CH_2Cl_2 was performed over the CNF supported catalyst at 400 °C for 36 h.

Density Functional Theory (DFT) Calculations

Gradient-corrected spin-polarized periodic DFT calculations using DMol3 code in Materials Studio 3.2 by Accelrys were performed with a $LaCl_3$(100) model surface based on a 2x2 periodic unit cell with 16 layers (total of 64 atoms), similarly to calculations reported previously.[6, 9, 11] The 6 bottom layers were constrained during the calculations to simulate bulk properties, and the remaining top layers were optimized with an adsorbate. A vacuum spacing of 1.5 nm was used in all surface models. The calculations used the double numerical with polarization (DNP) basis set and the generalized gradient-corrected Perdew-Wang (GGA PW91) functional. Tightly bound core electrons for La were represented with semi-core pseudopotentials. Reciprocal-space integration over the Brillouin zone was approximated through k-point sampling with a separation of 0.5 nm^{-1} using the Monkhorst-Pack grid (1x2x1). Convergence with respect to the number of k-points was tested by decreasing the k-point separation distance to 0.4 nm^{-1} for representative structures. An orbital cutoff distance of 0.5 nm was used for all atoms. All adsorption and surface reaction energies were calculated at 0 K without zero-energy corrections.

Results and Discussion

Thermodynamic Calculations

The calculations were performed by creating several datasets. The software consists of a database with the thermodynamic properties of chemicals. The reactant input amounts were chosen as 0.5 mol of CCl_4 and 0.5 mol of CH_2Cl_2. The computer program calculates equilibrium compositions based on these input amounts as a function of temperature. Apart from the reactants, the data set also consists of the products which are permitted. When a product is not included in the dataset, the program will not allow it as a product. It should be noted that these equilibria are based on thermodynamics and do not provide information on the kinetics. The equilibrium mixtures found for each data set are shown in Figure 1.

In data set 1, all likely products are included, namely CH_xCl_{4-x}, $C_2H_xCl_{6-x}$, $C_2H_xCl_{4-x}$, HCl, Cl_2 and C. Figure 1a shows that in the whole temperature range, CH_2Cl_2 is not present in the equilibrium mixture. Up to 200 °C, no reaction of CCl_4 occurs and CH_2Cl_2 fully dissociates according to Reaction Eq. (1) At higher temperatures, CCl_4 dissociates into C and Cl_2 (Reaction Eq. (2)). Based on this result, dissociation of CH_2Cl_2 into carbon and HCl is expected to be more favourable than in the case of CCl_4. Overall, this means that catalyst coking may occur during reaction.

$$CH_2Cl_2\ (g) \rightarrow C\ (s) + 2\ HCl\ (g) \quad (1)$$

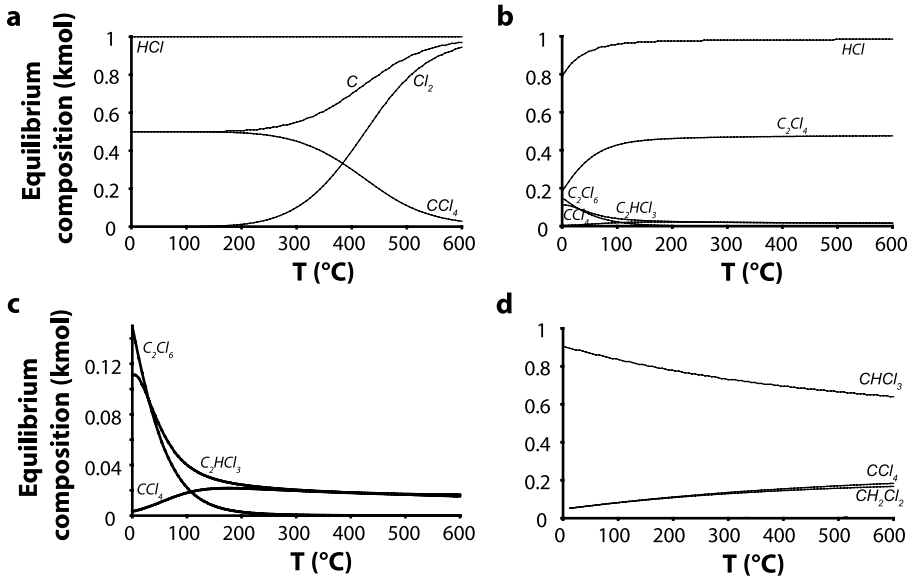

Figure 1. Equilibrium composition calculations of an equimolar mixture of CCl_4 and CH_2Cl_2 as a function of temperature using Data set 1 (a), Data set 2 (b, c) and Data set 3 (d).

$$CCl_4\ (g) \rightarrow C\ (s) + 2\ Cl_2\ (g) \quad (2)$$

In Data set 2, carbon was omitted from the products. In other words, the formation of coke was excluded from the equilibrium calculations. This translates into formation of CHC_2 via elimination of HCl. The main product in the equilibrium mixture is expected to be C_2Cl_4 and HCl (Reaction Eq. (3)). The formation of C_2Cl_4 has been observed experimentally, indicating that the reaction is also kinetically favourable.[3] At low temperature, C_2Cl_6 and C_2HCl_3 are formed.

$$CCl_4\ (g) + CH_2Cl_2\ (g) \rightarrow C_2Cl_4\ (g) + 2\ HCl\ (g) \quad (3)$$

In the third data set, the formation of HCl and Cl_2 was excluded in addition to carbon. This set was used to evaluate the reactions yielding $CHC_{1\text{-}2}$ only. It is found that CCl_4 and CH_2Cl_2 are equilibrated with $CHCl_3$ by H-Cl exchange (Reaction Eq. (4)). The calculations show that the reaction mixture cannot be fully converted into $CHCl_3$ in this temperature range.

$$CCl_4\ (g) + CH_2Cl_2\ (g) \rightarrow 2\ CHCl_3\ (g) \quad (4)$$

The free Gibbs energy change for the main reactions found in the equilibrium composition calculations were determined (Figure 2), namely: 1) the dissociation of CCl_4, 2) the dissociation of CH_2Cl_2, 3) the formation of C_2Cl_4 via HCl elimation and 4) formation of $CHCl_3$ via

H-Cl exchange (Reaction Eqs. (1), (2), (3) and (6), respectively). Based on thermodynamics, the following trend was observed going from most favourable to least favourable: dissociation of CH_2Cl_2 > the formation of C_2Cl_4 via HCl elimation > formation of $CHCl_3$ via H-Cl exchange > the dissociation of CCl_4. In gas phase experiments at relatively high temperatures (>500 °C), three reactions were observed: the formation of coke, C_2Cl_4 and $CHCl_3$. Both the formation of C_2Cl_4 and coke are undesirable reactions. Therefore, a catalyst for the selective exchange of H and Cl atoms, such as for CCl_4 and CH_2Cl_2, would be advantageous.

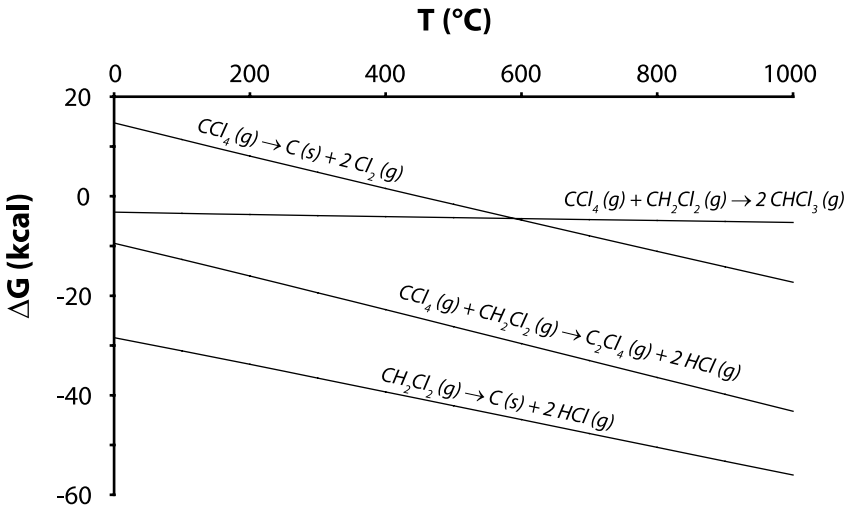

Figure 2. Free Gibbs energy change for reactions involving CCl_4 and CH_2Cl_2 as a function of temperature.

Catalyst Activity and Stability

The reaction between CH_2Cl_2 and CCl_4 over $LaCl_3$ yielded $CHCl_3$ exclusively according to Reaction Eq. (4). Unfortunately, coke formation was observed and may hamper the long-term application of the catalyst material. Figure 1a shows that $LaCl_3$-H has a low, but appreciable activity. Although determination of the catalyst surface area is impracticable due to the hygroscopic nature of $LaCl_3$, the low conversion is most likely a result of the low surface area of the $LaCl_3.7H_2O$ percursor. Therefore, LaOCl-P with a relatively high surface area (Table 2) was used as a precursor and was chlorinated with HCl. This resulted only in a slight increase in catalytic conversion as shown in Figure 3a. The higher surface area of the LaOCl-P precursor is most likely lost by the chlorination pre-treatment with HCl. To efficiently increase the catalyst surface area, $LaCl_3$ was impregnated onto CNF. This support was selected because of its relative inertness to the chlorination of the precursor with HCl and the absence of lattice oxygen, which may lead to destructive adsorption of the reactants.

In addition, the deposition of non-metals on carbon supports has been proven successful.[15] Figure 3a clearly shows that this catalyst exhibits the highest conversion on a weight basis. Also on a volume basis, $LaCl_3$-C is almost two factors more active compared to the unsupported materials (Figure 3b).

To evaluate the stability of $LaCl_3$-C, the reaction was run for 36 h at 400 °C. The results are shown in Figure 4 and indicate the presence of an induction period in the first hour of reaction. In that period a significant amount of coke is formed together with HCl and Cl_2 (Reaction Eqs. (1) and (2)). The conversion into coke was calculated based on the difference be-

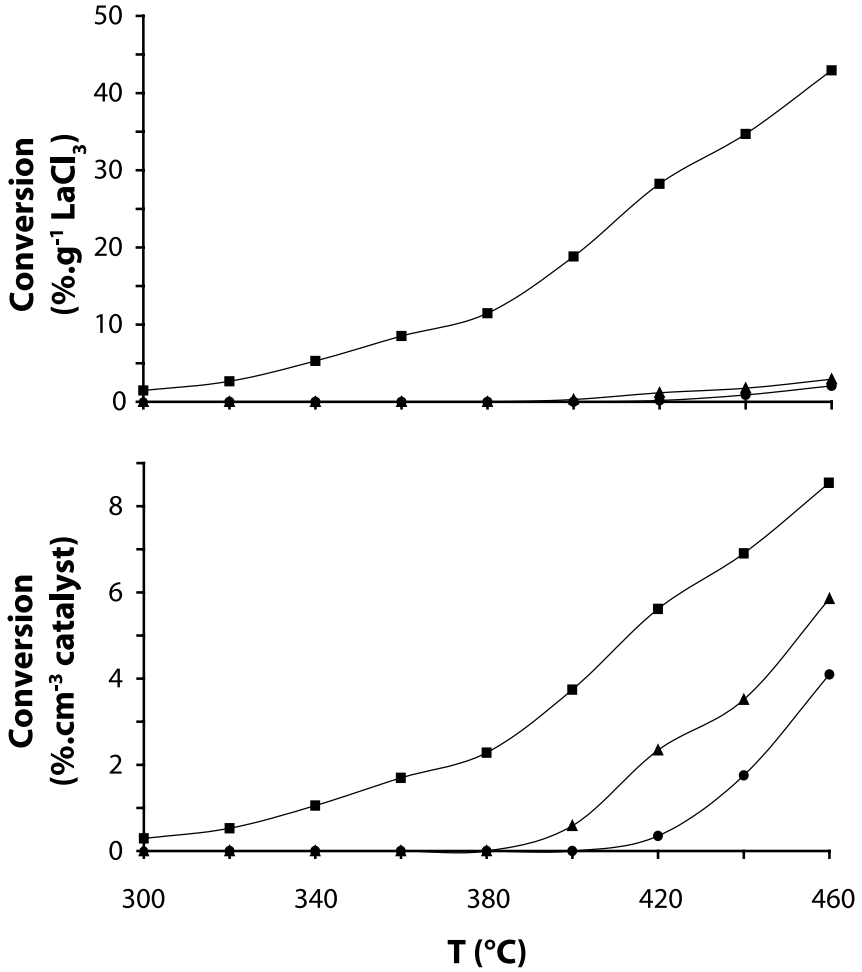

Figure 3. Conversion of a mixture of CH_2Cl_2 and CCl_4 into $CHCl_3$ based on weight (a) and volume (b) of the catalyst material over $LaCl_3$-H (●), $LaCl_3$-P (▲) and $LaCl_3$-C (■). (GHSV = 400 h^{-1}, inlet concentration CCl_4 = CH_2Cl_2 = 4.7 vol% in He)

tween the reactant concentration and the product concentrations. The carbon deficit in the reactor effluent was assumed to be a result of coke formation. It should be noted that the H-Cl exchange reaction also proceeds at relatively low conversion in the gas phase. Therefore, the product formation of the blank experiment has been subtracted in Figures 3 and 4. Despite the coke formation, the selectivity to $CHCl_3$ remains constant. A possible explanation for the induction period is that Ni remaining from the CNF growth catalyzes the conversion of CCl_4 into coke. CNF are grown on a Ni/SiO_2 catalyst. After CNF have been grown, Ni and SiO_2 are removed by washing steps. However, a trace amount of Ni is encapsulated in the CNF and can therefore not be removed by washing. During the H-Cl exchange experiments it may become accessible as a result of thermal expansion and the severe chlorination treatment needed for the synthesis of $LaCl_3$. In that case, the induction period is a result of the Ni catalyzed dissociation of the reactants. Especially CCl_4 is dissociating during this period as shown in Figure 2. Another explanation could be that CHC_2 species are formed and are not detected by GC. This would account for the carbon deficit in the reactor effluent and is supported by the thermodynamics and previous experiments, when C_2Cl_4 was detected in the gas phase reaction.[3]

The H-Cl exchange reaction proceeds via net exchange of a H and Cl atom between CCl_4 and CH_2Cl_2 (Reaction Eq. (4)). The catalytic reaction can be envisaged as two separate H/Cl exchange reactions between the catalyst surface and a gas phase reactant (Reaction Eqs. (5) and (6)).

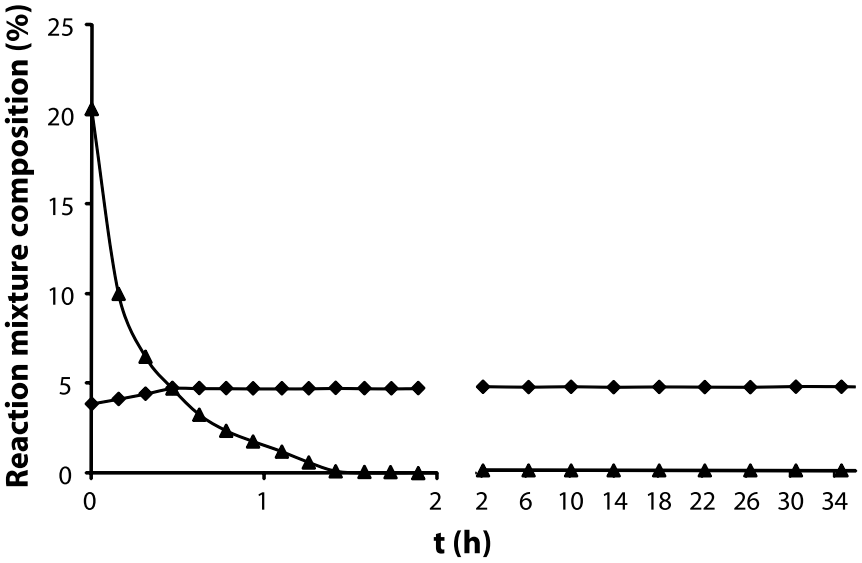

Figure 4. Reaction mixture composition for the H-Cl exchange between CCl_4 and CH_2Cl_2 at 400 °C over $LaCl_3$-C as a function of time. Only C-containing products are shown, namely $CHCl_3$ (♦) and C (▲). The formation of carbon was calculated based on the concentration of the gas phase products. (GHSV = 400 h^{-1}, inlet concentration CCl_4 = CH_2Cl_2 = 4.7 vol% in He)

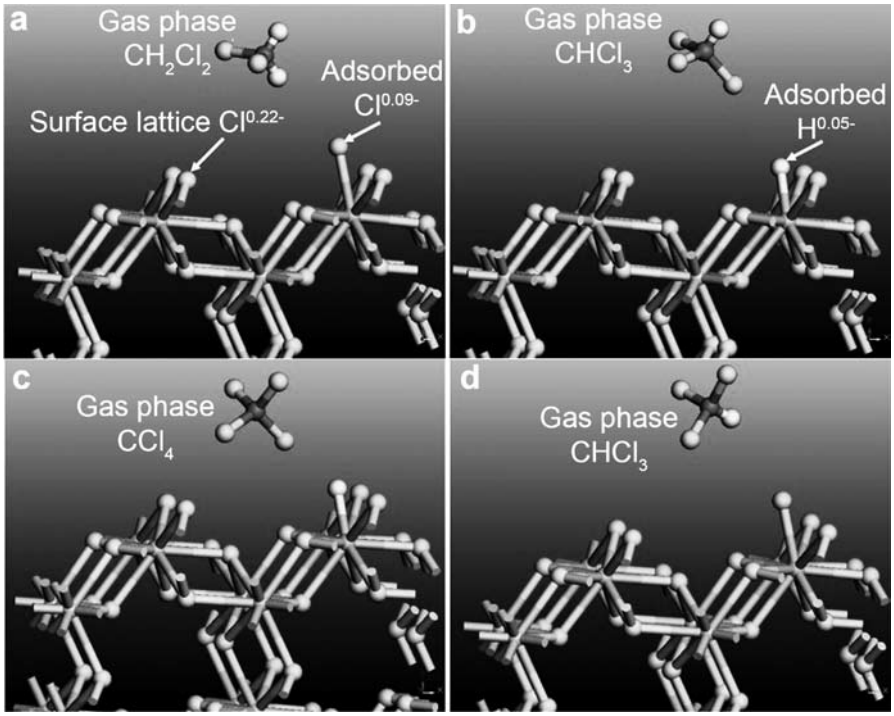

Figure 5. Proposed reaction mechanism for H-Cl exchange between CCl_4 and CH_2Cl_2 over $LaCl_3$ catalyst based on DFT calculations: a) gas phase CH_2Cl_2 above $LaCl_3$ catalyst, b) gas phase $CHCl_3$ formed after Cl for H exchange with the surface, c) gas phase CCl_4 above $LaCl_3$ catalyst and d) gas phase $CHCl_3$ formed after H for Cl exchange with the surface. Atomic charges were calculated with the Hirshfeld method.

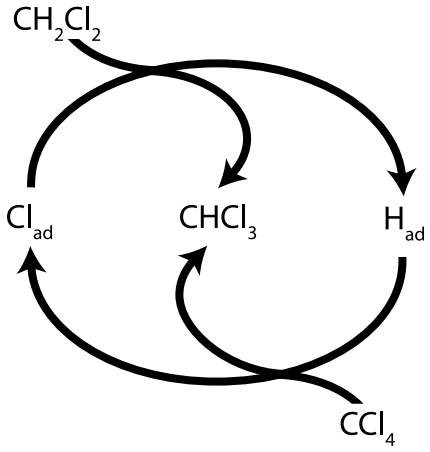

Figure 6. Schematic representation of the H-Cl exchange reaction between CCl_4 and CH_2Cl_2 over $LaCl_3$-based catalysts.

$$CH_2Cl_2\ (g) + Cl^{\delta-}\ (s) \rightarrow CHCl_3\ (g) + H^{\delta-}\ (s) \quad (5)$$
$$CCl_4\ (g) + H^{\delta-}\ (s) \rightarrow CHCl_3\ (g) + Cl^{\delta-}\ (s) \quad (6)$$

To verify whether this mechanism is viable, DFT calculations were performed on the H-Cl exchange between CCl_4 and CH_2Cl_2. It was found that regardless of the position of the exchanged lattice Cl anions and presence of any neighbouring defects, the H/Cl exchange reaction is estimated to be highly endothermic at 310-324 kJ/mol. The calculations, therefore, suggest that gas phase moieties, such as CH_2Cl_2, are unlikely to exchange their H with Cl anions from the $LaCl_3$ lattice. However, the calculations also suggest that adsorbed Cl atoms can be stabilized on the surface of $LaCl_3$. These atoms can be characterized as adsorbed surface species, as opposed to lattice Cl anions, because they are held weakly by the surface and are calculated to have a significantly smaller atomic partial charge of -0.09, compared to the calculated charge of about -0.22 for surface lattice Cl anions (Figure 5a). This can be viewed as a build-up of an additional Cl layer for the bulk structure, so that the coordination of surface La atoms increases from 8 to 9, the same as for the bulk La atoms. A gas phase chloromethane, such as CH_2Cl_2, can exchange one of its H atoms for an adsorbed surface Cl atom. The products are gas-phase $CHCl_3$ and a surface hydride (Figure 5b). Similarly to the surface Cl, surface H is weakly held by the surface, and it has only a small atomic charge of -0.05. The calculated energy change for this reaction is 210 kJ/mol. With gas phase CCl_4 as a reactant (Figure 5c), the reaction regenerates the catalytic surface site and produces gas-phase $CHCl_3$ as a product, as shown in Figure 5d. This second reaction is predicted to be exothermic at -225 kJ/mol.

Conclusions

It has been shown for the first time that $LaCl_3$ is able to catalyze the H-Cl exchange reaction of CCl_4 with CH_2Cl_2 as illustrated in Figure 6. To achieve high conversion both on weight and volume basis, the $LaCl_3$ was supported on CNF, thereby greatly increasing the surface area in comparison to bulk $LaCl_3$ catalysts. As a support material, carbon has two main advantages for the H-Cl exchange reaction: 1) the support material is able to withstand the harsh pre-treatment with HCl, and 2) it contains no oxygen, which excludes the destructive adsorption of the reactants. DFT calculations have shown that weakly adsorbed H and Cl atoms exist on the catalytic surface as intermediates. The reaction is suited for the efficient conversion of CCl_4, which is a highly stable and toxic compound with low economic value. More importantly, this is the first time that no O atoms are involved in the exchange of H and Cl atoms between gas phase CHCs. This means that no O-containing products are formed during reaction. Moreover, the selectivity of the H-Cl exchange reaction over $LaCl_3$ is high as opposed to the systems using a source of O atoms.

Acknowledgements

The H-Cl exchange reaction between CCl_4 and CH_2Cl_2 was discovered by Mark E. Jones at the Dow Chemical Company in Midland, USA. Simon G. Podkolzin (Dow Chemical Company, USA) is thanked for performing the DFT calculations and the discussions. Johannes H. Bitter (Utrecht University) is thanked for valuable discussions, especially with respect to the CNF materials. Arjan J. Plomp (Utrecht University) is thanked for the CNF synthesis. This work was supported by the National Research School Combination Catalysis (NRSC-C) and the Dutch Science Foundation (VICI/NWO-CW grant).

References

1. United Nations Environment Programme, International Labour Organisation, World Health Organization, *Carbon Tetrachloride Health and Safety Guide,* International Programme on Chemical Safety: Geneva, 1998.
2. Ozone Secretariat of the United Nations Environment Programme, *Handbook for the Montreal Protocol on Substances that Deplete the Ozone Layer,* Secretariat of The Vienna Convention for the Protection of the Ozone Layer &The Montreal Protocol on Substances that Deplete the Ozone Layer: Nairobi, 2006.
3. V. N. Antonov, V. I. Rozhkov, A. A. Zalikin, *Zh. Prikl. Khim.* **1987**, 60, 1347.
4. P. van der Avert, B. M. Weckhuysen, *Angew. Chem. Int. Ed.* **2002**, 41, 4730.
5. P. van der Avert, *Catalytic destruction of chlorinated hydrocarbons over lanthanide oxides,* Katholieke Universiteit Leuven: Leuven, 2003.
6. O. V. Manoilova, S. G. Podkolzin, B. Tope, J. A. Lercher, E. E. Stangland, J. M. Goupil, B. M. Weckhuysen, *J. Phys. Chem. B* **2004**, 108, 15770.
7. P. van der Avert, S. G. Podkolzin, O. V. Manoilova, H. de Winne, B. M. Weckhuysen, *Chem. Eur. J.* **2004**, 10, 1637.
8. P. van der Avert, B. M. Weckhuysen, *Phys. Chem. Chem. Phys.* **2004**, 6, 5256.
9. S. G. Podkolzin, O. V. Manoilova, B. M. Weckhuysen, *J. Phys. Chem. B* **2005**, 109, 11634.
10. E. Peringer, S. G. Podkolzin, M. E. Jones, R. Olindo, J. A. Lercher, *Top. Catal.* **2006**, 38, 211.
11. S. G. Podkolzin, E. E. Stangland, M. E. Jones, E. Peringer, J. A. Lercher, *J. Am. Chem. Soc.* **2007**, 129, 2569.
12. M. E. Jones, M. M. Olken, D. A. Hickman, US 6909024. 2005.
13. M. L. Toebes, J. M. P. van Heeswijk, J. H. Bitter, A. J. van Dillen, K. P. de Jong, *Carbon* **2004**, 42, 307.
14. M. K. van der Lee, A. J. van Dillen, J. W. Geus, K. P. de Jong, J. H. Bitter, *Carbon* **2006**, 44, 629.
15. F. Winter, A. J. van Dillen, K. P. de Jong, *Chem. Commun.* **2005**, 3977.

6

Exploration of the Catalytic Potential of La-based Materials for the Conversion of Chlorinated Waste Compounds

La-based materials have proven to be versatile catalysts in the conversion of chlorinated hydrocarbons (CHCs). The reactions of CHCs over La-based materials may be used for the destruction of these compounds at relatively low temperature or the conversion into more desirable products, such as chemical intermediates or transportation fuels. In this chapter, the potential of these catalyst materials is explored by the following experiments: 1) a mixture of chlorinated C_1 and C_2 ($CHC_{1\text{-}2}$) is converted over La_2O_3-based materials, 2) the destructive adsorption of CCl_4 is combined into a catalytic cycle with the activation of CH_4 over $LaCl_3$ using O_2, and 3) La_2O_3 is combined with a special silicoaluminophosphate catalyst (SAPO-34) for the one-pot conversion of CH_2Cl_2 into hydrocarbons. The destructive adsorption of chlorinated methanes and the dehydrochlorination of chlorinated ethanes were found to occur simultaneously when a mixture of these compounds is converted over La_2O_3-based catalysts. For the destructive adsorption reaction, the conversion of $CHCl_3$ and CCl_4 into CO and CO_2 dominate, whereas CH_2Cl_2 is hardly converted. The dehydrochlorination reaction of chlorinated ethanes, however is uninfluenced by the presence of other reactants. For the oxidative chlorination of methane over $LaCl_3$ in the presence of oxygen, CCl_4 has proven to be a good alternative for HCl. The chlorination of the catalyst via destructive adsorption of CCl_4 enables the regeneration of the chlorine which is lost in the reaction with CH_4, closing the catalytic cycle. Compared to HCl, CCl_4 offers the advantage of having a lower economic value and the fact that no H_2O is formed during reaction, which would make the reaction conditions more corrosive. The experiments on the consecutive conversion of CH_2Cl_2 via CH_3OH into hydrocarbons over La_2O_3 and SAPO-34, respectively, have shown that the combination of these two reactions in one reactor is difficult. The SAPO-34 material possesses very little activity under these conditions and coke formation results in plugging of the reactor. CH_2Cl_2 is converted into CO, CO_2, CH_4 and C_2H_4. After an induction period, an unassigned product is formed, after which the reactor rapidly becomes plugged. SAPO-34 is found to be active for the destructive adsorption of CH_2Cl_2, which could poison the material. Also, the desorption of H_2O from the La_2O_3 material may suppress the conversion of methanol to olefins.

Introduction

La-based materials have proven to possess great potential for the selective conversion of chlorinated hydrocarbons (CHCs) at relatively low temperature. Various reactions, such as destructive adsorption, dehydrochlorination and H/Cl exchange, occur over the catalytic surface of these materials. The versatility of the La-based catalyst opens new opportunities for use in commercially attractive reactions, such as the conversion of the light ends waste mixtures, the activation of methane into CH_3Cl and the one-pot conversion of chlorinated methanes (CHC_1) into hydrocarbons. These options will now be discussed consecutively.

First of all, the light ends waste mixture, which is formed as by-product during the production of vinyl chloride, contains various $CHC_{1\text{-}2}$. La_2O_3-based materials convert both chlorinated methanes and ethanes. The dehydrochlorination of chlorinated ethanes and the destructive adsorption adsorption of CHC_1 proceed over the same active sites on La_2O_3-based materials. The nature of these reactions, however, is markedly different: destructive adsorption of CHC_1 requires the presence of lattice oxygen, whereas dehydrochlorination of chlorinated ethanes is a catalytic reaction linked to an equilibrium surface composition. When these two reactions occur simultaneously in the same reactor, as would be the case for conversion of the light ends mixture, competitive adsorption between the reactants may result in inhibition of either reaction.

Secondly, $LaCl_3$ is an active catalyst for the activation of methane into CH_3Cl, which can be used as a reagent in the synthesis of silicone polymers.[1] The presence of oxygen is crucial for activation of methane into CH_3Cl over $LaCl_3$ using HCl.[2, 3] The catalytic cycle of this reaction is shown in Scheme 1.[2, 3] The key step results is the conversion of a La-Cl bond into a

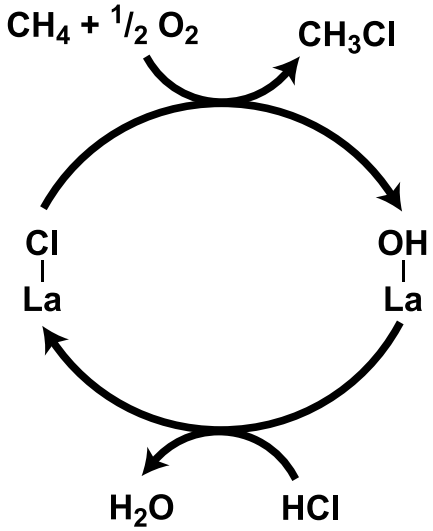

Scheme 1. Catalytic cycle for the oxidative chlorination of CH_4 over $LaCl_3$ in the presence of O_2 and HCl.[2, 3]

La-OH bond: oxygen and a surface Cl are proposed to form a hypochlorite (OCl^-) site, which converts methane into CH_3Cl consecutively. The role of HCl is limited to the regeneration of the La-Cl bond. Therefore, the destructive adsorption of CHC_1 could be used as an alternative for the regeneration step using HCl, since both reactions result in a net chlorination of the surface. The use of CCl_4 as a source of chlorine instead of HCl would be advantageous because of the lower economic value of CCl_4.

Finally, the destructive adsorption of chlorinated C_1 over La_2O_3-base materials results in the formation of oxygenated products, such as CO, CO_2 and CH_3OH. A catalyst which is able to convert these products into re-usable products and is active in the same temperature range would make the one-pot conversion of CHC_1 into chemical intermediates and/or transportation fuels possible. Silicoaluminophosphate materials (SAPO), specifically SAPO-34, are not only known to convert methanol into hydrocarbons[4, 5], but have also been used for the conversion of CH_3Cl into olefins.[6] They are relatively stable under the conditions required for destructive adsorption. CH_2Cl_2 can consecutively be converted into CH_3OH and hydrocarbons over La_2O_3 and SAPO-34, respectively. Therefore, a combination of La_2O_3-based materials and SAPO-34 could potentially be used for the one-pot conversion of CHC_1 into hydrocarbons.

In this chapter, these three possible applications of the La-based materials are pioneered to evaluate the potential of the catalyst. First, a mixture of several CHCs, namely CCl_4, $CHCl_3$, CH_2Cl_2, 1,1,2-$C_2H_3Cl_3$ and 1,2-$C_2H_2Cl_2$, is run over La_2O_3 and LaOCl to mimic the conversion of light ends mixtures. Next, CCl_4 and CH_4 are converted together with O_2 over $LaCl_3$ to explore the potential of CCl_4 as an alternative for HCl as a chlorinating agent. Finally, CH_2Cl_2 is led over a catalyst bed of La_2O_3 and SAPO-34 material. Both materials are present in the same reactor, with La_2O_3 closest to the reactor inlet, to evaluate the one-pot conversion of chlorinated CH_2Cl_2 into hydrocarbons. CH_2Cl_2 is first converted over La_2O_3 into CH_3OH, which is subsequently converted into hydrocarbons over SAPO-34. In all experiments, the reactor effluent was continuously analyzed using gas chromatography (GC).

Experimental

Chlorinated C_1/C_2 Mixtures over La_2O_3-Based Materials

The activity experiments for the conversion of the mixture of chlorinated C_1 and C_2 were performed in a tubular fixed-bed quartz reactor, which was discussed in detail in Chapter 2. The catalyst bed consisted of 1.0 g LaOCl-P or La_2O_3 (Acros Organics, 99.99 %) pressed in a 200-500 µm sieve fraction, pretreated in 10 mL/min He (Hoekloos, ≥ 99.996 %) at 550 °C. To find the initial reaction temperature, the reaction was carried out from 50 to 400 °C using a 10 mL/min flow with the total concentration of the reactants at 7-9 vol% reactant in He (Hoekloos, ≥ 99.996 %). The reaction was also performed at 400 °C over 1.0 g La_2O_3

(Acros Organics, 99.99 %). A bubbler containing a mixture of liquid chlorinated C_1 and C_2, namely CCl_4 (Acros Organics, 99.8 %), $CHCl_3$ (Acros Organics, 99.9 %), CH_2Cl_2 (Acros Organics, 99.9 %), 1,2-$C_2H_4Cl_2$ (Acros Organics, 98+ %) and 1,1,2-$C_2H_3Cl_3$ (Acros Organics, 98 %), was used to generate the reactant flow. Due to the difference in vapour pressure between the reactants, the relative concentrations steadily changed during the experiments. Especially for the relatively more volatile compounds, such as $CHCl_3$ and CH_2Cl_2, a strong decrease of the concentration was observed throughout the temperature programmed reactions. In Table 1 an overview is shown for the initial reactant concentrations in each experiment. Because the reaction as a function of time over La_2O_3 was expected to take longer than the temperature-programmed experiments, more $CHCl_3$ and CH_2Cl_2 was added to the reactant mixture to maintain all reactant concentrations until the end of the experiment.

Table 1. Initial reaction concentrations and experimental conditions for flow-gas experiments using mixtures of chlorinated C_1 and C_2.

Experiment	Material	T (°C)	[Reactant] in He (vol%)				
			CCl_4	$CHCl_3$	CH_2Cl_2	1,2-$C_2H_4Cl_2$	1,1,2-$C_2H_3Cl_3$
1	La_2O_3		2.6	1.5	0.7	1.5	1.6
2	LaOCl		2.5	1.6	1.0	1.4	1.7
3	La_2O_3	400	1.1	4.1	2.1	1.0	1.51

CCl_4/CH_4 and O_2 over $LaCl_3$

The activity experiments were performed in a tubular fixed-bed quartz reactor. The catalyst bed consisted of 0.5 g LaOCl-P 200-500 µm sieve fraction, pretreated in 10 mL/min He (Hoekloos, ≥99.996 %) at 550 °C. The catalyst was chlorinated for 4 h at 450 °C with 10 ml/min 10 vol% HCl in He (Hoekloos, ≥99.996 %). The setup possessed a by-pass line outside the reactor, which was kept at 150 °C. CCl_4 was added to the reactant flow by injecting liquid CCl_4 into a heated line (170 °C) using a syringe pump (0.1 ml/h). First, the reactor flow was stabilized over the by-pass to 10 vol% CH_4, 8-9 vol% CCl_4 and 12 vol% O_2 in He. All experiments were performed subsequently over the same catalyst bed and after each experiment the reactant flow was switched over the by-pass. First the reaction was run over the catalyst at 450 °C. Next, CCl_4 was removed from the reactant feed. The experiment with CCl_4 present was repeated after re-introduction of CCl_4 to the reactant feed. Finally, O_2 was removed from the feed. An overview of initial concentrations used for each experiment is provided in Figure 1.

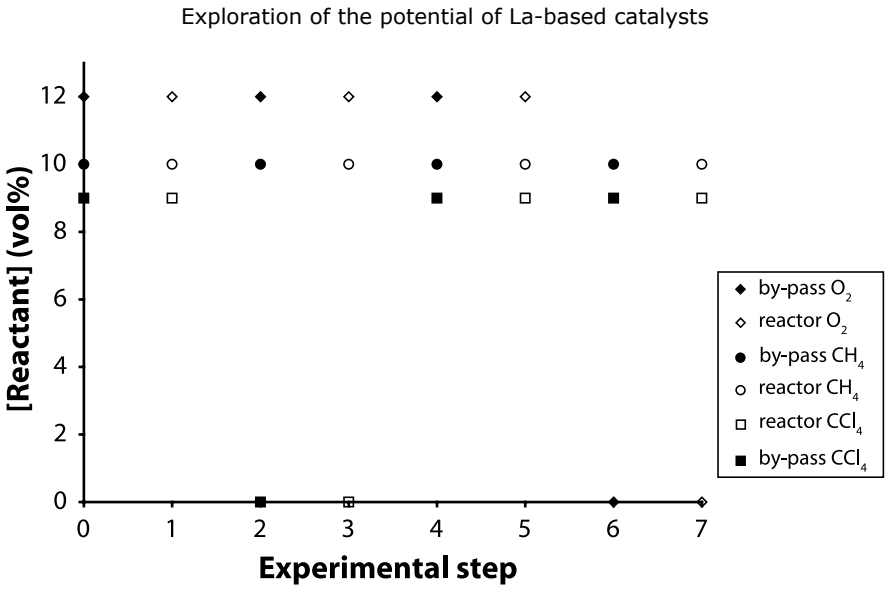

Figure 1. Reaction conditions and initial reactant concentrations throughout experiment with $CCl_4/CH_4/O_2$ over $LaCl_3$ (reactor temperature = 450 °C, by-pass temperature = 150 °C).

CH_2Cl_2 over La_2O_3 and SAPO-34

Details on the preparation of the SAPO-34 material used in this work can be found in literature.[6] In a blank experiment, CH_2Cl_2 (Acros Organics, 99.9 %) was led over 2.0 g of La_2O_3 (Acros Organics, 99.99 %) at 350 °C to test the stability of the conversion into CH_3OH. This temperature was chosen based on the activity results in Chapter 3 and results on the conversion of methanol into hydrocarbons over SAPO-34.[4, 5] The reactant flow consisted of 10 ml/min 6.1 vol% CH_2Cl_2 (Acros Organics, 99.9 %) in He (Hoekloos, ≥99.996 %). In a second series of experiments, 2.0 g La_2O_3 (Acros Organics, 99.99 %) and 0.5 g SAPO-34 200-500 µm sieve fractions were placed in the reactor in separate catalyst beds with La_2O_3 closest to the reactor inlet. The temperature and flow-rate were varied to find the optimal conditions for the consecutive conversion of CH_2Cl_2 over La_2O_3 and SAPO-34. Finally, the reactor was loaded with 1.0 g La_2O_3 (Acros Organics, 99.99 %) and 1.0 g SAPO-34, both pressed in sieve fractions of 200-500 µm. The reactant flow consisted of 5 ml/min 6.1 vol% (Acros Organics, 99.9 %) CH_2Cl_2 in He (Hoekloos, ≥99.996 %). The experiment was performed as a function of time at 400 °C to test the stability of the catalyst combination.

Results and Discussion

Three commercially attractive reactions for the conversion of CHCs are explored in a series of flow-gas experiments. In this section, the results of each reaction are discussed: 1)

the conversion of mixtures of $CHC_{1\text{-}2}$ over La_2O_3-based materials, 2) the oxidative chlorination of methane using CCl_4 as a source of chlorine and 3) the one-pot conversion of CH_2Cl_2 into hydrocarbons over a combination of La_2O_3 and SAPO-34 material.

Activity Results $CHC_{1\text{-}2}$ Mixtures over La_2O_3-Based Materials

In Figures 2 and 3, the conversion of the chlorinated C_1 and C_2 hydrocarbons is shown as a function of temperature over La_2O_3 and LaOCl, respectively. In both experiments, the chlorinated methanes are converted into CO and CO_2 and the chlorinated ethanes are converted into chlorinated ethenes. Two types of reaction occur simultaneously: destructive adsorption of CCl_4, $CHCl_3$ and CH_2Cl_2 (Reaction Eqs. (1)-(3)), and dehydrochlorination of 1,2-$C_2H_4Cl_2$ and 1,1,2- $C_2H_3Cl_3$ (Reaction Eqs. (4)-(7)). For La_2O_3 and LaOCl, destructive adsorption precedes the dehydrochlorination reaction. The initial temperature of conversion, however, is significantly lower over LaOCl than over La_2O_3 for both destructive adsorption and dehydrochlorination.

CCl_4 (g) + 2 La-O-La (s)	→	CO_2 (g) + 4 La-Cl (s)	(1)
$CHCl_3$ (g) + 2 La-O-La (s)	→	CO (g) + 3 La-Cl (s) + La-OH (s)	(2)
CH_2Cl_2 (g) + La-O-La (s)	→	1/2 CO (g) + 1/2 CH_3OH (g) + 2 La-Cl (s)	(3)
1,2-$C_2H_4Cl_2$ (g)	→	C_2H_3Cl (g) + HCl (g)	(4)
1,1,2-$C_2H_3Cl_3$ (g)	→	1,1-$C_2H_4Cl_2$ (g) + HCl (g)	(5)
	→	cis-1,2-$C_2H_4Cl_2$ (g) + HCl (g)	(6)
	→	trans-1,2-$C_2H_4Cl_2$ (g) + HCl (g)	(7)

Figure 2 shows that CCl_4 and $CHCl_3$ are converted via destructive adsorption into CO_2 and CO over La_2O_3, but the concentrations of these reactants increase towards the end of the experiment as a result of chlorination of the catalyst. The steady decrease of the concentration of CH_2Cl_2 is a result of the difference in vapour pressure between the compounds in the reactant mixture, which was previously discussed in the experimental section. Therefore, the conversion of CH_2Cl_2 is not significant. This is confirmed by the fact that no CH_3OH was observed. The results in Figure 3 show the same trend; CCl_4 and $CHCl_3$ react into CO_2 and CO, whereas CH_2Cl_2 is not converted.

In Chapter 4, it was found that during an induction period the catalytic surface becomes chlorinated until a specific degree of chlorination is reached. Once this specific surface composition is reached, the product distribution becomes stable. This is best observed in the dehydrochlorination of 1,1,2-$C_2H_3Cl_3$, which was converted over La_2O_3 at 400 °C as a function of time in a previous experiment. During an induction period, 1,1-$C_2H_4Cl_2$, cis-1,2-$C_2H_4Cl_2$, trans-1,2-$C_2H_4Cl_2$ and C_2HCl were formed. In addition, two product were formed which could not be assigned. When a stable product distribution was achieved, 1,1-$C_2H_4Cl_2$, cis-1,2-$C_2H_4Cl_2$ and C_2HCl were formed exclusively. In the experiment with the mixtures

of chlorinated C_1 and C_2, the formation of the two unassigned products is not observed, however, and trans-1,2-$C_2H_4Cl_2$ is only formed initially. The formation of C_2HCl could not be verified because this compound co-elutes with C_2H_3Cl, which is also formed from the dehydrochlorination of 1,2-$C_2H_4Cl_2$. It appears that the simultaneous conversion of chlorinated methanes and chlorinated ethanes shortens the induction period. Because lattice oxygen is exchanged for chlorine by the destructive adsorption reaction, the surface composition that is required for a stable product distribution is reached more rapidly. Moreover, the destructive adsorption occurs at lower temperature and therefore the catalytic surface becomes chlorinated before the dehydrochlorination reaction begins. This explains why the two unassigned products are not formed, because they are expected to be formed exclusively on an oxygen-rich surface, such as La_2O_3.

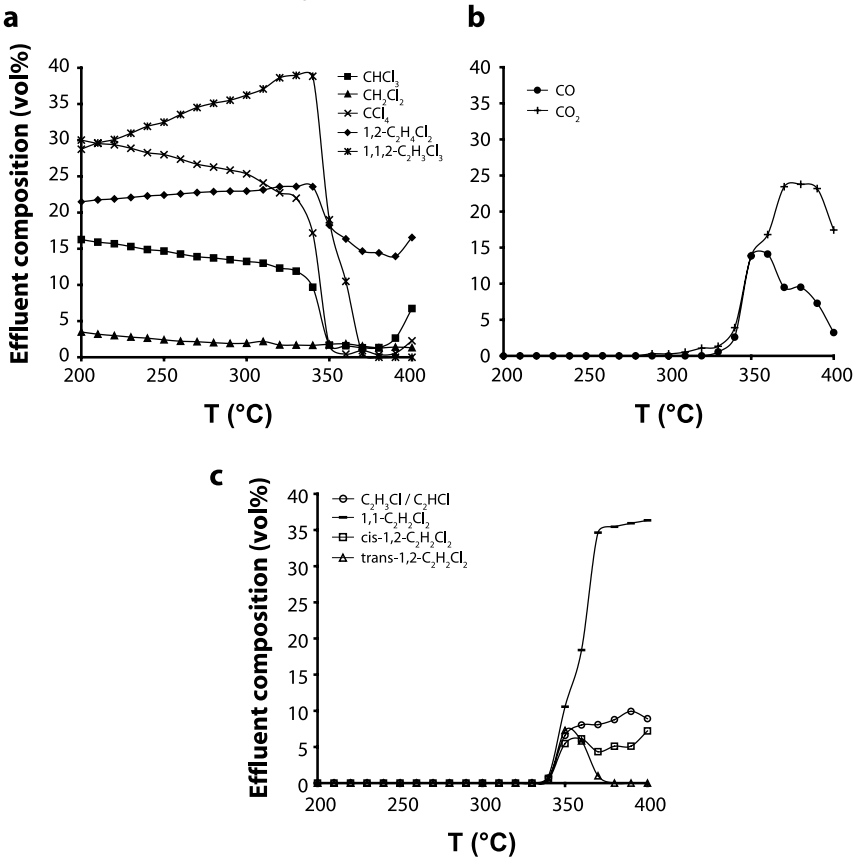

Figure 2. Effluent composition of a mixture of chlorinated methanes and ethanes over La_2O_3 as a function of temperature: a) reactant concentrations, b) concentrations of products formed as a result of destructive adsorption, and c) concentrations of products formed as a result of dehydrochlorination. The concentrations in the graph are calculated based on the reactants and products without He (inlet concentrations are shown in Table 1, GHSV = 800 h^{-1}).

The conversion of the reactant mixture at 400 °C over La_2O_3 as a function of time is shown in Figure 4. Initially, CCl_4 and $CHCl_3$ are fully converted, whereas no reaction of CH_2Cl_2 occurs. However, the activity towards $CHCl_3$ decreases more rapidly than in the case of CCl_4. The conversion and product distribution of the dehydrochlorination reactions with 1,2-$C_2H_4Cl_2$ and 1,1,2-$C_2H_3Cl_3$ are relatively stable throughout the experiment. The results show that the destructive adsorption and dehydrochlorination reaction can occur simultaneously on the same catalyst material. The conversion of CH_2Cl_2, however, appears to be hindered by the competitive adsorption of the other reactants. The destructive adsorption reaction is dependent on the presence of a certain amount of lattice oxygen. Once the catalytic surface

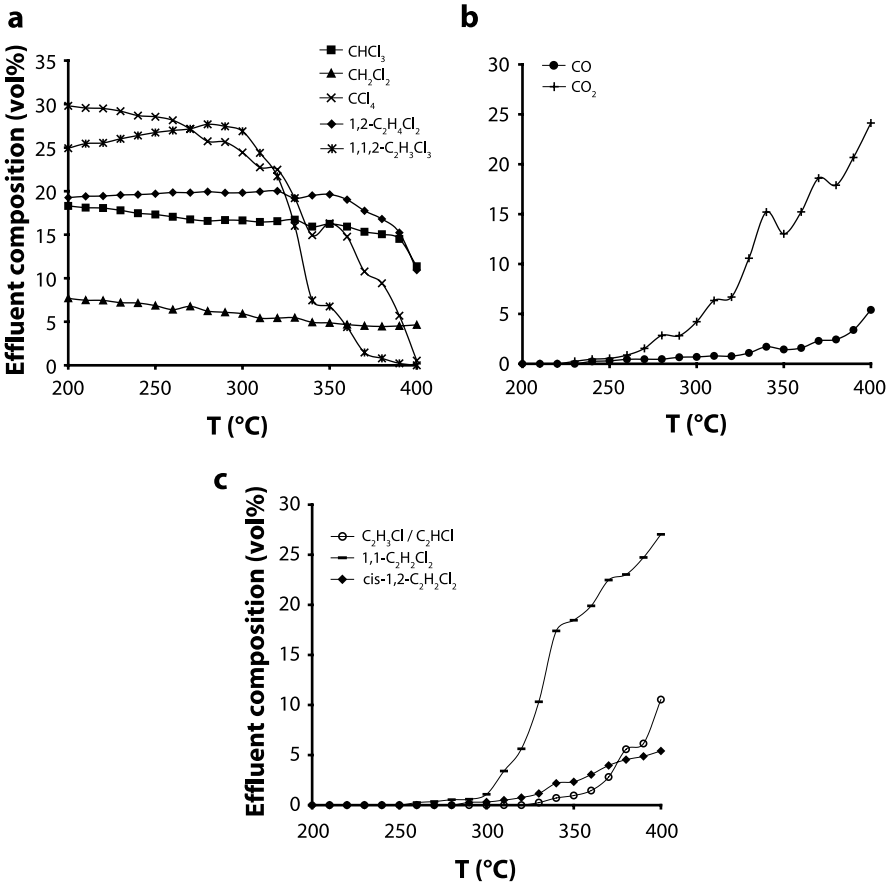

Figure 3. Effluent composition of a mixture of chlorinated methanes and ethanes over LaOCl as a function of temperature: a) reactant concentrations, b) concentrations of products formed as a result of destructive adsorption, and c) concentrations of products formed as a result of dehydrochlorination. The concentrations in the graph are calculated based on the reactants and products without He (inlet concentrations are shown in Table 1, GHSV =800 h^{-1}).

Exploration of the potential of La-based catalysts

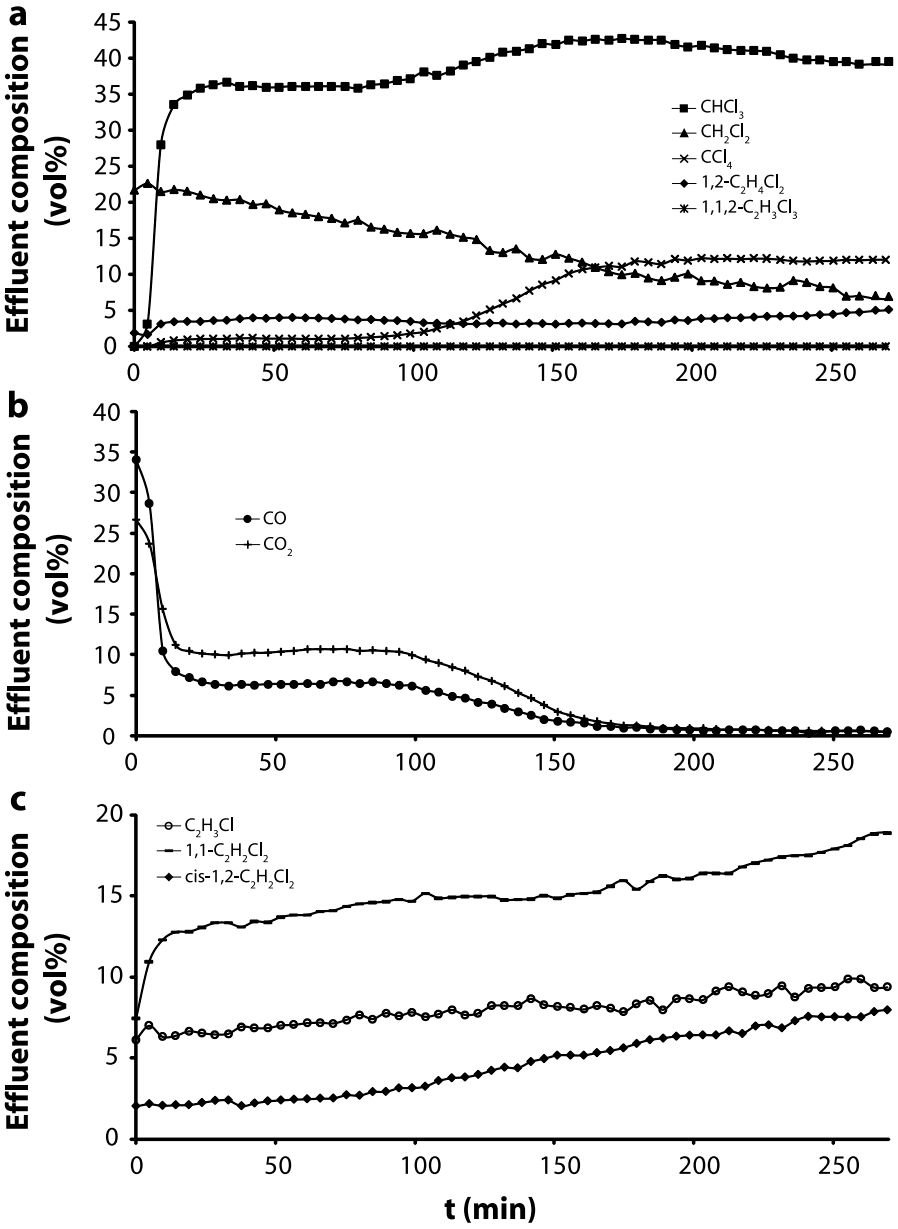

Figure 4. Effluent composition of a mixture of chlorinated methanes and ethanes over La_2O_3 at 400 °C as a function of time: a) reactant concentrations, b) concentrations of products formed as a result of destructive adsorption, and c) concentrations of products formed as a result of dehydrochlorination. The concentrations in the graph are based on the reactants and products without He (inlet concentrations are shown in Table 1, GHSV =800 h^{-1}).

becomes chlorinated, the reaction becomes limited by the solid-state diffusion of oxygen from the bulk of the material to the catalytic surface. This ultimately results in deactivation of the material for the destructive adsorption reaction. The dehydrochlorination reaction, on the other hand, is catalytic and shows no signs of deactivation throughout the experiment.

Activity Results CCl_4/CH_4 and O_2 over $LaCl_3$

The experiment with CCl_4/CH_4 and O_2 over $LaCl_3$ was performed under various reaction conditions as shown in Figure 5. First, the reactant concentrations were stabilized over the bypass (Figure 5, region 1). Then, the feed was switched to the reactor at 450 °C (Figure 5, region 2). When the feed is switched over the reactor, several products are formed, namely CO, CO_2, CH_2Cl_2 and CH_3Cl. The products are the result of two reactions: the oxidative chlorination of CH_xCl_{4-x} ($x > 0$) and the destructive adsorption of CH_xCl_{4-x} ($x < 4$).

The CH_4 molecule is chlorinated by the $LaCl_3$ material, as shown in Reaction Eq. (8)-(10). The chlorination reaction may be repeated when the formed chlorinated C_1 is re-adsorbed, which is described by Reaction Eqs. (9)-(11). As a result of this reaction, chlorine is removed from the catalyst material and hydroxyl groups are formed.[2, 3] The hydroxyl groups may react into H_2O or HCl according to Reaction Eqs. (12) and (13). Another possibility is that the $LaCl_3$ phase becomes partially hydrated ($LaCl_3 \bullet nH_2O$).

CH_4 (g) + 1/2 O_2 (g) + La-Cl (s)	→	CH_3Cl (g) + La-OH (s)	(8)
CH_3Cl (g) + 1/2 O_2 (g) + La-Cl (s)	→	CH_2Cl_2 (g) + La-OH (s)	(9)
CH_2Cl_2 (g) + 1/2 O_2 (g) + La-Cl (s)	→	$CHCl_3$ (g) + La-OH (s)	(10)
$CHCl_3$ (g) + 1/2 O_2 (g) + La-Cl (s)	→	CCl_4 (g) + La-OH (s)	(11)
2 La-OH (s)	→	La-O-La (s) + H_2O (g)	(12)
La-OH (s) + La-Cl (s)	→	La-O-La (s) + HCl (g)	(13)

Without a source of chlorine to regenerate the catalytic surface, the availability of chlorine would decrease and, consequently, the conversion of CH_4. The destructive adsorption reaction counterbalances the oxygenation of the catalytic surface. CCl_4 is abundantly present as a reactant, but re-adsorption of the chlorinated C_1 formed from methane also contributes to the destructive adsorption reaction. For CCl_4, $CHCl_3$ and CH_2Cl_2, the reaction equations for the destructive adsorption over La_2O_3-based materials are shown in Reaction Eqs. (1)-(3). CH_3Cl may also be converted according to Reaction Eq. (14) at the temperature used in this experiment (450 °C), but the activity is expected to be relatively low compared to the other chlorinated C_1. Based on the results with the mixture of chlorinated C_1 and C_2 (Figure 4), the contribution of the destructive adsorption of CH_2Cl_2 is also considered relatively low with CCl_4 and $CHCl_3$ present.

2 CH_3Cl (g) + La-O-La (s)	→	$(CH_3)_2O$ (g) + 2 La-Cl (s)	(14)

Exploration of the potential of La-based catalysts

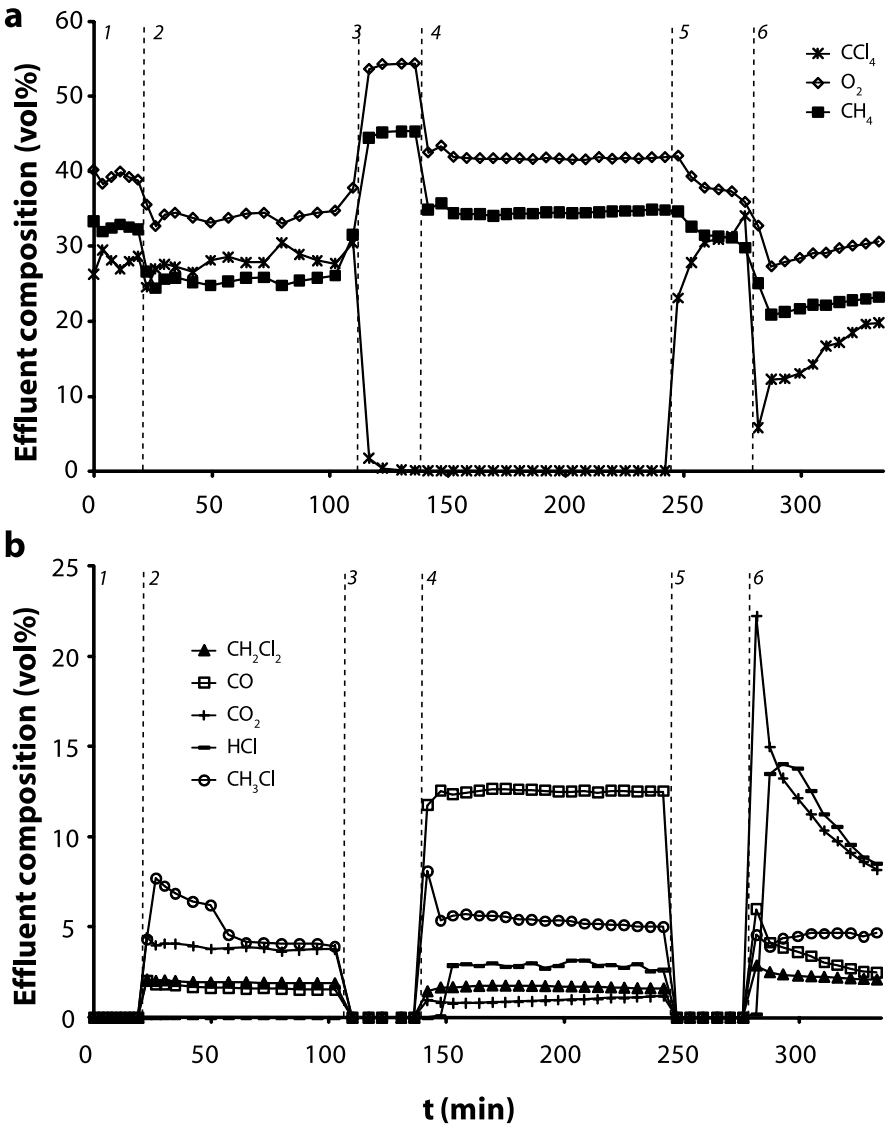

Figure 5. Effluent composition for a) reactants and b) products for the conversion of CH_4, CCl_4 and O_2 over $LaCl_3$ at 450 °C: 1) stabilization of CH_4, CCl_4 and O_2 over by-pass, 2) CH_4, CCl_4 and O_2 over reactor, 3) stabilization of CH_4 and O_2 over by-pass, 4) CH_4 and O_2 over reactor, 5) stabilization of CH_4, CCl_4 and O_2 over by-pass, 6) CH_4, CCl_4 and O_2 over reactor (Reaction conditions are shown in Figure 1, GHSV = 400 h^{-1}).

After some time the reactant flow was switched back to the by-pass (Figure 5, region 3). To evaluate the influence of CCl_4 on the stability and selectivity of the catalyst, the syringe pump containing CCl_4 was stopped, which resulted in an increase in concentration for CH_4 and O_2. Once stabilized, the feed was switched back to the reactor (Figure 5, region 4). Without CCl_4, the selectivity towards CO_2 decreases, whereas the selectivity towards CO increases. Also, without CCl_4 the formation of HCl is observed. The increase in CO indicates that the destructive adsorption of $CHCl_3$ and CH_2Cl_2 has become more pronounced without the presence of CCl_4. Consequently, less CO_2 is formed, since this is primarily formed via the destructive adsorption of CCl_4. The product distribution is relatively stable, even though the availability of chlorine at the catalyst surface is expected to decrease. A likely explanation is that solid-state diffusion of lattice oxygen occurs from the catalytic surface into the bulk phase of the material. The opposite has been observed in the destructive adsorption reaction over La_2O_3; the catalytic surface becomes chlorinated as a result of the chlorine/oxygen exchange between the gas phase and the catalyst material, respectively. To compensate for the difference in O/Cl ratio between the bulk phase and the catalytic surface, oxygen atoms diffuse from the bulk to the surface and the chlorine atoms vice versa. In the case of the reaction with CH_4 and O_2, the principle is the same, but the oxygen atoms diffuse in the opposite direction compared to the destructive adsorption, namely from the catalytic surface into the bulk phase of the material. This results in relatively constant surface composition, which explains the formation of HCl according to Reaction Eq. (13). This solid-state diffusion combined with the destructive adsorption of re-adsorbed chlorinated C_1 may result in a relatively constant conversion, but this effect is expected to be temporary. As the bulk phase also becomes oxygenated, the driving force for the regeneration of surface chlorine decreases and the catalyst becomes deactivated.

The reactant feed was switched to the bypass and CCl_4 was reintroduced (Figure 5, region 5). When the reactant concentrations were stable, the feed was switched back to the reactor (Figure 5, region 6). The strong increase in concentration of CO_2 compared to the CO_2 concentration in Figure 5b shows that the catalyst material has become oxygenated. The CO_2 concentration decreases gradually with time and is expected to stabilize to the level of Figure 5b. It should be noted that the concentrations of CH_3Cl and CH_2Cl_2 remain relatively stable throughout the experiment. Apparently, the oxidative chlorination of CH_4 is not strongly influenced by the absence of a chlorinating agent or the use of a chlorinating agent other than HCl.

Activity Results CH_2Cl_2 over La_2O_3 and SAPO-34

SAPO-34 is an active catalyst for the conversion of methanol into hydrocarbons at 300 °C and higher temperatures.[4] A reaction network has been proposed for the conversion of methanol over SAPO-34, which is shown in Scheme 2.[6] CH_3OH is converted into a primary product, $(CH_3)_2O$, which is subsequently converted into hydrocarbons. In ad-

dition, C_2H_6 and C_3H_8 are formed as tertiary products. Moreover, the formation of coke, which leads to deactivation, increases with increasing reaction temperature.[5] Therefore, the temperature at which CH_2Cl_2 is significantly converted into CH_3OH over La_2O_3 should match this temperature range, preferably at a relatively low temperature. The destructive adsorption of CH_2Cl_2 over La_2O_3 was tested at 350 °C as a function of time as shown in Figure 6. The experiment shows that CH_2Cl_2 is not fully converted under these conditions, but no deactivation is observed during 4 h. The formation of CH_3OH and CO is relatively stable throughout the experiment. The concentration of CO_2 steadily increases. During reaction carbonates are formed on the catalytic surface of the La_2O_3, which dissociate into CO_2 as the material becomes more chlorinated.

Next, the La_2O_3 and SAPO-34 were loaded in the same reactor as separate catalyst beds with the La_2O_3 closest to the reactor inlet. The reaction conditions were varied to find the optimal conversion as shown in Figure 7. First, the conversion of CH_2Cl_2 was performed over the La_2O_3-SAPO-34 combination at 350 °C (Figure 7a). Remarkably, more CH_2Cl_2 is converted over the catalyst combination than in the experiment with La_2O_3 only. Also, the sum of the reactant and products is the same in both experiments (not shown). This implies that the SAPO-34 is also active for the destructive adsorption of CH_2Cl_2, which might lead to the collapse of the SAPO-34 structure as a result of chlorination. However, SAPO-34 has been found to be relative stability in the presence of chlorine.[6]

Since no hydrocarbons were detected at 350 °C, the temperature was raised to 400 °C (Figure 7b). At this temperature, CH_2Cl_2 is fully converted over the catalyst combination. CH_3OH is no longer detected and low amounts of CH_4 and C_2H_4 are formed, indicating that the SAPO-34 catalyst is active for the methanol to hydrocarbon conversion at this temperature. The CO concentration first strongly increases and then steadily decreases, which is

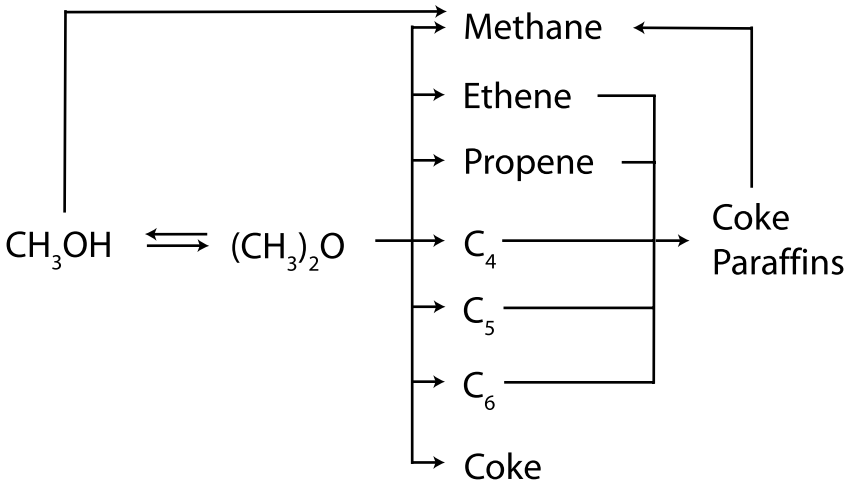

Scheme 2. Reaction network for methanol to olefin reaction over SAPO-34.

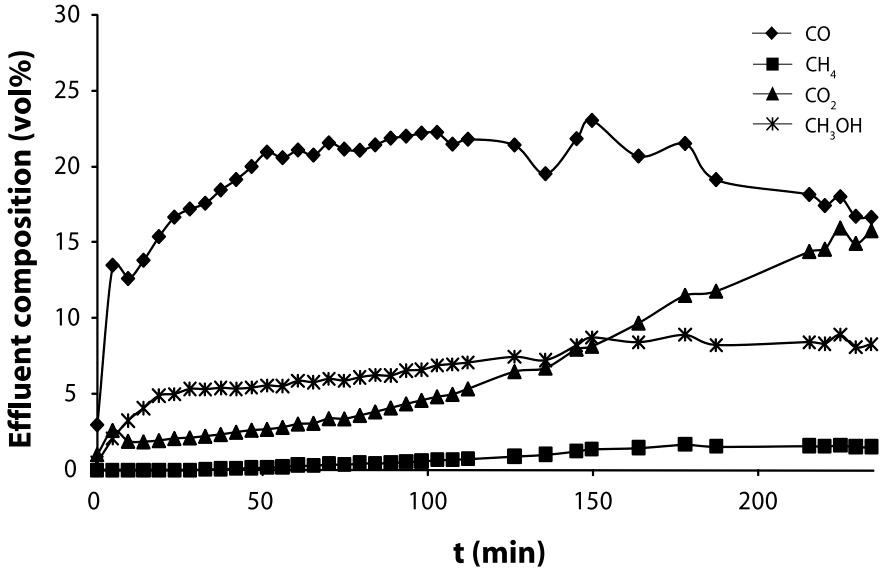

Figure 6. Effluent composition of CH_2Cl_2 at 350 °C over La_2O_3 as a function of time. The concentrations in the graph are based on the reactants and products without He ($[CH_2Cl_2]$ = 6.1 vol%, GHSV = 800 h^{-1}).

most likely due to the decreasing availability of lattice oxygen at the catalytic surface of the La_2O_3 material. The concentration of CO_2, on the other hand, is steadily increasing as a result of the dissociation of carbonates on La_2O_3.

When the temperature is raised to 450 °C, a lower selectivity towards CH_4 is observed. Finally, the flow-rate was lowered to increase the residence time (Figure 7d) of the reactant. After 105 min, the concentration of CO_2 is decreasing which is paralleled by the increase of the CO concentration. Possibly, the majority of the carbonates has dissociated as a result of the chlorination of La_2O_3. At this point, the product concentrations stabilize and an unassigned product is formed. This product is detected on the column for the chlorinated hydrocarbons (RL2 T5a, Table 1 Chapter 2). The retention time, which is close to that of CH_3OH and CH_3Cl, is low and in the same range as, for example H_2O, CH_3OH, CO, CH_4 and CO_2. For the conversion of CH_3Cl into hydrocarbons over SAPO-34, the material is activated with propene before reaction to overcome a slow induction period.[6] This induction period may also have occurred in the experiments here, since the stabilization of the product distribution is accompanied by the formation of a new product. This new product could be assigned to $(CH_3)_2O$, since this compound has been proposed to be an intermediate in the formation of hydrocarbons from methanol over SAPO-34 catalysts.[5] The proposed reaction network of CH_3OH over SAPO-34 is shown in Scheme 2. $(CH_3)_2O$ was formed together with CH_3OH during the destructive adsorption of CH_3Cl over LaOCl as shown by the infrared results in Chapter 3. It was, however, not detected in the flow-gas experiments in Chapter 3. If the retention time of $(CH_3)_2O$ is close to that of CH_3Cl and CH_3OH, its peak may have overlapped with the strong CH_3Cl peak,

Exploration of the potential of La-based catalysts

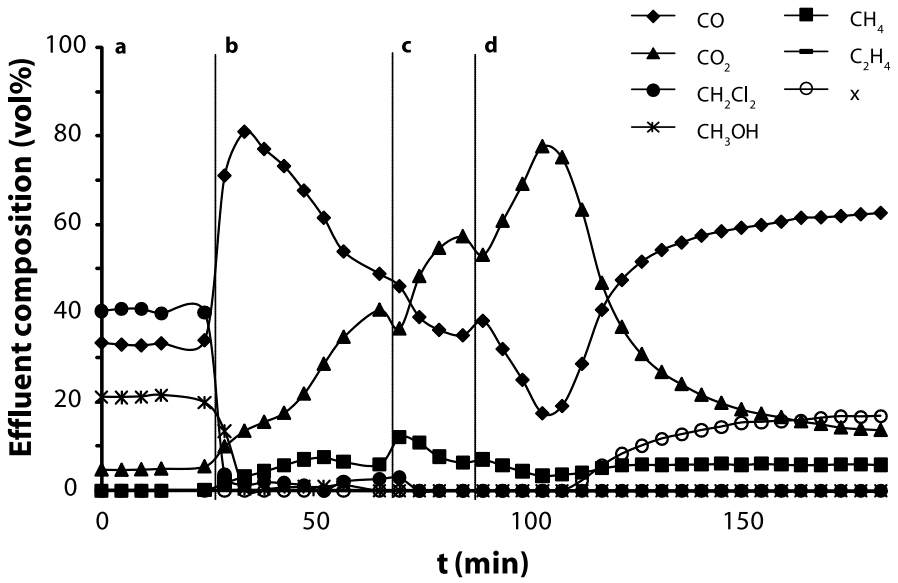

Figure 7. Effluent composition of CH_2Cl_2 over La_2O_3-SAPO-34 combination: (a) 350 °C, GHSV = 800 h^{-1}, (b) 400 °C, GHSV = 800 h^{-1}, (c) 450 °C, GHSV = 800 h^{-1} and (d) 450 °C, GHSV = 400 h^{-1}. The concentrations in the graph are based on the reactants and products without He (x represents an unassigned product, [CH_2Cl_2] = 6.1 vol%).

which was used as a reactant in that experiment. This would explain why $(CH_3)_2O$ was not observed in the previous experiment. It should be noted that the sum of the reactant and product concentrations strongly decreased when the temperature was raised to 450 °C (not shown), indicating the formation of coke. The reaction eventually was stopped because of the reactor bed became plugged. After reaction, both catalyst beds in the reactor indeed showed significant coke formation, while no coke formation was observed on the reactor walls or quartz wool.

Based on the results in Figure 7, a reaction temperature of 400 °C and GHSV of 400 h^{-1} was chosen as the optimum conditions for the conversion of CH_2Cl_2 over the La_2O_3-SAPO-34 combination. In addition, the amount of La_2O_3 material was halved while the amount of SAPO-34 was doubled in an attempt to increase the conversion of methanol into hydrocarbons. The results for the conversion of CH_2Cl_2 over the catalyst combination at 400 °C are shown in Figure 8. CH_3OH is initially observed, but its concentration rapidly decreases to zero. Similarly to the experiment shown in Figure 7, low concentrations of CH_4 and C_2H_4 are detected. In this experiment, a steady increase of the CO_2 concentration is also paralleled by a decrease in CO concentration. After approximately 100 min, the CO_2 concentration strongly decreases, while the concentration of CO increases. At the same time, the unknown product is formed. This induction period was also observed in Figure 7. The reaction was stopped when the reactor became plugged. In summary, no significant amounts of C_2 hydrocarbons were detected in the experiments described here. The low selectivity towards olefins may be

a result of H_2O desorbing from the La_2O_3 material, since H_2O is known to suppress the formation of olefins over SAPO-34.[7, 8] The desorption of H_2O is expected to be temporary, however, since desorption of HCl is more favourable on a more chlorinated catalyst surface.

Conclusions

It has been shown that a mixture of chlorinated methanes and ethanes, as in the case of the light ends mixtures, can be converted into oxygenated products and chlorinated ethenes, respectively. The destructive adsorption of chlorinated C_1 compounds results in the formation of CO and CO_2. The destructive adsorption of CH_2Cl_2 is, however, less favourable when CCl_4 and $CHCl_3$ are present. The destructive adsorption reaction is dependent on the presence of lattice oxygen and, as a result, the conversion decreases as the catalyst material becomes more chlorinated. The dehydrochlorination of the chlorinated ethenes is uninfluenced by the destructive adsorption reaction. In fact, a more chlorinated catalyst surface translates into higher selectivity towards chlorinated ethenes. Therefore, the chlorination of the catalyst as a result of the destructive adsorption of chlorinated C_1 benefits the selectivity of the dehydrochlorination reaction. With the right method to regenerate the lattice oxygen of thecatalyst material, the La_2O_3-based material could be used to selectively convert a mixture of chlorinated methanes, ethanes and ethenes into CO, CO_2 and chlorinated ethenes. This enables conversion of chlorinated C_1 compounds into combustion products at a significantly lower temperature than conventional incineration, and the recycling of chlorinated ethenes, such as C_2H_3Cl and 1,1-$C_2H_2Cl_2$, for the production of polyvinyl chloride (PVC) and poly vinylidene chloride (PVDC), respectively.

CCl_4 has proven to be an excellent substitute for HCl in the activation of methane over $LaCl_3$ in the presence of O_2. The hydroxyl groups, which are formed on the catalytic surface as a result of the chlorination of methane, react with HCl under formation of H_2O (Scheme 1). When CCl_4 is used as a chlorinating agent, the catalytic cycle is closed via an additional step: CCl_4 is converted into CO_2 resulting in chlorination of the catalytic surface after which the hydroxyl groups dissociate into HCl (Scheme 3). The advantage of using CCl_4 would be that this compound has a lower economic value compared to HCl and the fact that the highly corrosive mixture of HCl and H_2O is avoided when CCl_4 is used.

The one-pot conversion of CH_2Cl_2 into hydrocarbons was tested over a combination of a La_2O_3 and a SAPO-34 catalyst bed in the same reactor. First, CH_2Cl_2 is converted into CH_3OH over La_2O_3 and is then consecutively converted into hydrocarbons over the SAPO-34 catalyst. The results show that only a small amount of CH_2Cl_2 is converted into CH_4 and C_2H_4. It appears that the SAPO-34 material is also active for the destructive adsorption of CH_2Cl_2, which may lead to poisoning of the catalyst. In addition, the desorption of H_2O may temporarily suppress the formation of olefins over SAPO-34. The latter problem could be circumvented by using a more chlorinated material, such as LaOCl, which is less likely to release H_2O. The one-pot conversion of CH_2Cl_2 over a combination of a La_2O_3-based catalyst

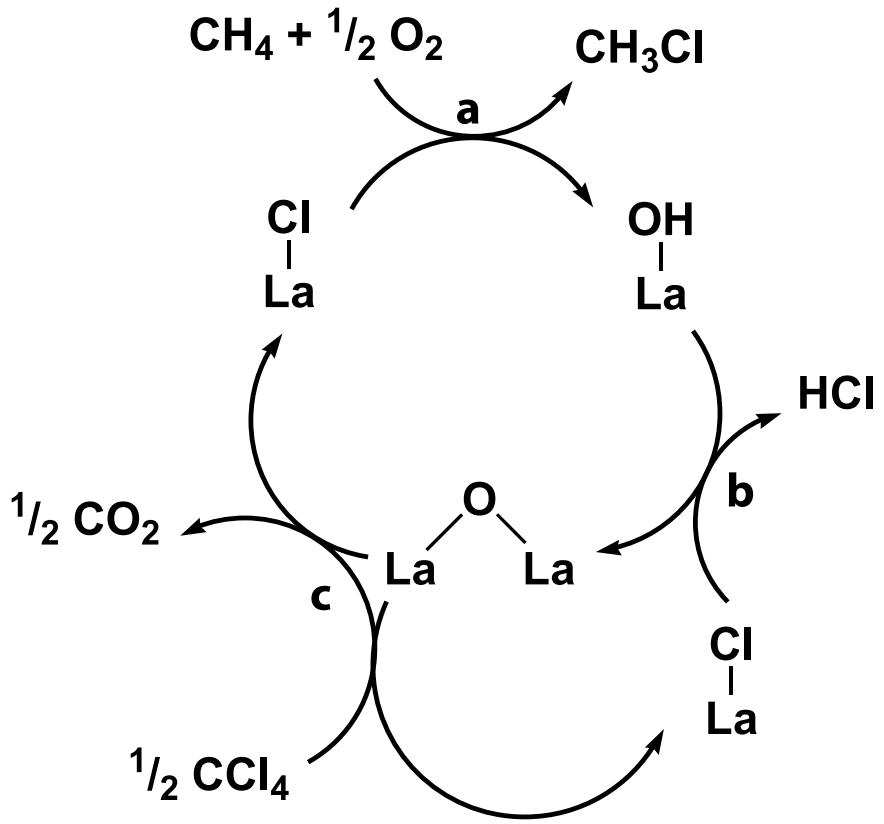

Scheme 3. Catalytic cycle for the oxidative chlorination of CH_4 over $LaCl_3$ in the presence of O_2 and CCl_4.

and SAPO-34 is possible in principle. However, a great challenge lies in the control of the reaction conditions and the properties of the La-based catalyst material that is used.

Acknowledgements

Elvira Peringer (Technical University of Munich, Germany) is thanked for performing the reactions of CH_4, CCl_4 and O_2 over $LaCl_3$ and for her help with the discussion of the results. Unni Olsbye (University of Oslo, Norway) is thanked for providing the SAPO-34 material for the experiments on the conversion of CH_2Cl_2. The exchange with the Technical University of Munich, where the results on the activation of methane were measured, was supported by the Integrated Design of Catalytic Nanomaterials for a Sustainable Production (IDECAT) network. This work was supported by the National Research School Combination Catalysis (NRSCC) and the Dutch Science Foundation (VICI/NWO-CW grant).

References

1. K. H. Brookes, M. R. H. Siddiqui, H. M. Rong, R. W. Joyner, G. J. Hutchings, *Appl. Catal. A* **2001**, 206, 257.
2. E. Peringer, S. G. Podkolzin, M. E. Jones, R. Olindo, J. A. Lercher, *Top. Catal.* **2006**, 38, 211.
3. S. G. Podkolzin, E. E. Stangland, M. E. Jones, E. Peringer, J. A. Lercher, *J. Am. Chem. Soc.* **2007**, 129, 2569.
4. Y.-J. Lee, S.-C. Baek, K.-W. Jun, *Appl. Catal. A* **2007**, 329, 130.
5. D. Chen, A. Gronvold, K. Moljord, A. Holmen, *Ind. Eng. Chem. Res.* **2007**, 46, 4116.
6. S. Svelle, S. Aravinthan, M. Bjørgen, K.-P. Lillerud, S. Kolboe, I. M. Dahl, U. Olsbye, *J. Catal.* **2006**, 241, 243.
7. A. J. Marchi, G. F. Froment, *Appl. Catal.* **1991**, 71, 139.
8. E. J. Munson, A. A. Kheir, N. D. Lazo, J. F. Haw, *J. Phys. Chem.* **1992**, 96, 7740.

7

Summary and concluding remarks

Chapter 7

More than one third of all chlorine consumption is used for the production of polyvinyl chloride (PVC). The monomer that is produced as precursor is C_2H_3Cl. This product is synthesized industrially by the chlorination of C_2H_4 into 1,2-$C_2H_4Cl_2$. The latter is subsequently cracked into C_2H_3Cl and HCl. Even though the production process of C_2H_3Cl is rather selective, several by-products are formed. Due to the scale of the process, the amount of by-products is relatively large, however. These by-products are mainly chlorinated C_1, e.g. CCl_4, $CHCl_3$ and CH_2Cl_2, and C_2, e.g. 1,1,2-$C_2H_3Cl_3$ and C_2H_5Cl, and are collected as a mixture known as the light ends. Regulation of the removal and production of chlorinated C_1 and C_2 demands for efficient disposal of the chlorinated by-products of the PVC industry. Currently, the preferred route of destruction is incineration. Though efficient, this is a costly process due to the high temperature that is required for the incineration of chlorinated hydrocarbons (CHCs). Furthermore, incineration results in the loss of feedstock.

La-based materials are active materials for the conversion of CHCs: they enable the destruction of CHCs at relatively low temperature, but also offer the possibility for recycling of some of the by-products. In this PhD thesis, the conversion of different chlorinated C_1 and C_2 compounds over La-based materials was studied to evaluate the potential of these catalyst materials and to gain more insight into the reactions that occur over the catalytic surface. Special attention has been devoted to the influence of the chlorination degree of the catalyst material, which is able to tune the catalyst selectivity and activity.

In **Chapter 2**, the destructive adsorption of CCl_4 over La_2O_3-based materials was studied to establish a link between activity and acid-base properties of the catalyst material. It was found that the synthesis method of LaOCl materials has a dramatic influence on the bulk as well as on the surface properties. In flow-gas experiments, the following activity trend was observed: $LaCl_3$ << La_2O_3 < LaOCl-S < LaOCl-P. CH_3OH probing shows that LaOCl-P contains a larger number of strong adsorption sites than LaOCl-S, more specifically sites that are likely used for the destructive adsorption of CCl_4. The larger amount of chlorine at the surface appears to increase the number of active Lewis acid sites at the surface of LaOCl-P. However, these differences in strength cannot be revealed by CO IR adsorption measurements. Nevertheless, we believe that the strength of the Lewis acid sites remains a key factor for activity and that stronger Lewis acid sites result in a higher intrinsic activity for CCl_4 destruction. Basic oxygen sites remain necessary to enable the conversion of CCl_4 to CO_2. In other words, the appropriate acid-base pair should be available at the catalyst surface to have an active material.

Chapter 3 dealt with the destructive adsorption of the H-containing chlorinated C_1 compounds, namely $CHCl_3$, CH_2Cl_2 and CH_3Cl, over La_2O_3-based catalysts. Two reaction pathways are established that lead to the formation of phosgene-like gas phase intermediates ($CH_xCl_{2-x}O$). It was found that a basic O site is able to abstract a H atom from the gas phase reactant, which is a new aspect for the destructive adsorption in comparison to the experiments with CCl_4. The $CH_xCl_{2-x}O$ intermediate can rapidly re-adsorb on the catalyst surface and form surface species, such as carbonates, formates and methoxy groups. The surface species can then interconvert and/or dissociate into gas phase products. The dissociation

of the surface species is dependent on the reaction temperature and the degree of surface chlorination. The flow-gas experiments showed that as the number of hydrogen atoms in the molecule increases, the initial temperature of reaction increases. This trend is believed to be a result of the decreasing polarization of the bonds in the C_1 molecule as a consequence of more hydrogen atoms. A second factor which influences conversion is the chlorination degree of the LaOCl surface. An optimum degree of surface chlorination exists, which translates to an optimal combination of Lewis acidic and basic surface sites. The surface chlorination is, in view of the proposed reaction scheme, of direct influence on the selectivity. A catalyst with ample O promotes the reaction pathway involving H/Cl removal. The removal of H results in less hydrogenated, and hence less desirable, surface intermediates and gas phase products. The surface chlorination also inhibits the formation of carbonates, which reduces the formation of CO_2. Therefore, a chlorinated catalyst is more selective than, for example, pure La_2O_3.

In **Chapter 4**, the focus is on the dehydrochlorination of chlorinated C_2 compounds, in particular C_2H_5Cl, 1,2-$C_2H_4Cl_2$ and 1,1,2-$C_2H_3Cl_3$, over La_2O_3-based materials. A hydrogen and chlorine atom is abstracted from the chlorinated ethane by the catalytic surface, resulting in the formation of a hydroxyl group and a lattice chloride. In the case of an O-rich surface, such as La_2O_3, the hydroxyl groups will react with other hydroxyl groups under formation of H_2O. However, when a specific degree of chlorination of the catalytic surface is reached, the elimination of H_2O becomes less pronounced and HCl is formed. After the induction period characterized by the formation of H_2O, the product distribution and conversion become stable and the chlorination degree of the catalyst surface also remains constant. In situ IR experiments have shown that at relatively high temperature, secondary reactions may occur, such as a second dehydrochlorination step resulting in the formation of an ethyne, or destructive adsorption leading to the formation of CO and CO_2. This indicates that the reaction temperature and chlorination degree are key factors to achieve optimal selectivity towards the formation of ethenes.

In **Chapter 5**, it has been shown that $LaCl_3$ is able to catalyze the H-Cl exchange reaction of CCl_4 with CH_2Cl_2 without the presence of oxygen atoms. To achieve high conversion both on weight and volume basis, $LaCl_3$ was supported on carbon nanofibers (CNF), thereby greatly increasing the surface area in comparison to bulk $LaCl_3$. As a support material, CNF have two main advantages for the H-Cl exchange reaction: 1) the support material is able to withstand the harsh pre-treatment with HCl, and 2) it contains no oxygen, which excludes the destructive adsorption of the reactants. DFT calculations have shown that weakly adsorbed H and Cl atoms exist on the catalytic surface as intermediates. The reaction is suited for the efficient conversion of CCl_4, which is a highly stable and toxic compound with low economic value. More importantly, this is the first time that no O atoms are involved in the exchange of H and Cl atoms between gas phase CHCs.

From the findings mentioned above it is clear that La-based catalysts are versatile catalysts, which are able to convert chlorinated C_1 and C_2 compounds via different reactions, such as destructive adsorption, dehydrochlorination and H-Cl exchange. Therefore, the use

of La-based materials in several relevant test cases has been explored in **Chapter 6**.

First of all, it has been shown that a mixture of chlorinated methanes and ethanes, i.e. CCl_4, $CHCl_3$, CH_2Cl_2, 1,1,2-$C_2H_3Cl_3$ and 1,2-$C_2H_4Cl_2$, as in the case of the light ends mixtures, can be converted into oxygenated products and chlorinated ethenes, respectively. The destructive adsorption of chlorinated C_1 compounds results in the formation of CO and CO_2. The destructive adsorption of CH_2Cl_2 is, however, less favourable when CCl_4 and $CHCl_3$ are present. The dehydrochlorination of the chlorinated ethanes is not inhibited by the destructive adsorption reaction. In fact, a more chlorinated catalyst surface translates into higher selectivity towards chlorinated ethenes. Therefore, the chlorination of the catalyst as a result of the destructive adsorption of chlorinated C_1 benefits the selectivity of the dehydrochlorination reaction.

In a second part, CCl_4 has proven to be a good substitute for HCl in the activation of methane over $LaCl_3$ in the presence of O_2. The hydroxyl groups, which are formed on the catalytic surface as a result of the chlorination of methane, conventionally react with HCl under formation of H_2O. When CCl_4 is used as a chlorinating agent, the catalytic cycle is closed via an additional step: CCl_4 is converted into CO_2 resulting in chlorination of the catalytic surface after which the hydroxyl groups dissociate into HCl.

Finally, the one-pot conversion of CH_2Cl_2 into hydrocarbons was tested over a combination of a La_2O_3 and a SAPO-34 catalyst bed in the same reactor. The results show that only a small amount of CH_2Cl_2 is converted into CH_4 and C_2H_4. It appears that the SAPO-34 material is also active for the destructive adsorption of CH_2Cl_2, which may lead to catalyst poisoning. The one-pot conversion of CH_2Cl_2 over a combination of a La_2O_3-based catalyst and SAPO-34 is in principle possible. However, a great challenge lies in the control of the reaction conditions and the La-based catalyst material that is used.

This PhD thesis has shown that the chlorination degree of La-based catalyst materials is of direct influence on their activity and selectivity for the conversion of CHCs. However, the degree of chlorination also changes as a result of the reactions with CHCs. Therefore, the next challenge lies in the control of the chlorination degree during reaction. Steam has been used to make the destructive adsorption of CCl_4 catalytic over La_2O_3-based materials, but the influence of steam on the destructive adsorption of H-containing chlorinated C_1 compounds and the dehydrochlorination of chlorinated ethanes has not been studied so far. Further investigation on the regeneration of oxygen, and hence the dechlorination of the catalyst material, is needed to enable control of the catalyst composition and the reactions of CHCs over the catalyst. Furthermore, research on new combinations of catalytic materials and reactions, as illustrated in Chapter 6, can be used to make the conversion of chlorinated waste streams more efficient and less costly. Even though more complex technological systems are needed to facilitate catalytic conversion of chlorinated waste compounds, the La-based material could be highly advantageous for applications using microreactor technology. This technology offers the advantage of detailed optimalization for the conversion of CHCs with minimal risks of exposure.

Samenvatting en conclusies

De productie van polyvinylchloride (PVC) is verantwoordelijk voor meer dan een derde van alle chloorconsumptie. C_2H_3Cl is de monomeer die gebruikt wordt als precursor hiervoor. Dit product wordt industrieel gesynthetiseerd via de chlorering van C_2H_4 tot 1,2-$C_2H_4Cl_2$. Het laatstgenoemde product wordt vervolgens gekraakt tot C_2H_3Cl en HCl. Ook al is het productieproces van C_2H_3Cl selectief, toch worden een aantal bijproducten gevormd. Gezien de grote schaal waarop het proces plaatsvindt, is de hoeveelheid bijproducten echter relatief hoog. Deze bijproducten zijn voornamelijk gechloreerde C_1, bv. CCl_4, $CHCl_3$ and CH_2Cl_2, en C_2, bv. 1,1,2-$C_2H_3Cl_3$ and C_2H_5Cl, en worden verzameld als een mengsel dat bekend staat als de light ends. De regulering voor de verwijdering en productie van gechloreerde C_1 en C_2 eist een efficiënte afbraak van de gechloreerde bijproducten uit de PVC-industrie. Momenteel heeft verbranding de voorkeur als afbraaktechniek. Hoewel dit een efficiënte techniek is, zijn de kosten voor dit proces hoog vanwege de hoge temperaturen die nodig zijn voor de verbranding van gechloreerde koolwaterstoffen (CKWs). Bovendien heeft verbranding het verlies van grondstoffen tot gevolg.

La-gebaseerde materialen zijn actief voor de omzetting van CKWs: ze zijn in staat deze op lagere temperaturen af te breken, maar bieden ook de mogelijkheid tot hergebruik van sommige bijproducten. In dit proefschrift wordt de omzetting van verschillende gechloreerde C_1 en C_2 op La-gebaseerde materialen bestudeerd om het vermogen van deze katalysatormaterialen te evalueren en om meer inzicht te verkrijgen in de reacties die plaatsvinden over het katalytisch oppervlak. De aandacht wordt met name gericht op de invloed het chloorgehalte van het katalysatormateriaal, welke in staat is om de activiteit en selectiviteit van de katalysator te bepalen.

In **Hoofdstuk 2** is de destructieve adsorptie van CCl_4 op La_2O_3-gebaseerde materialen bestudeerd om een verband te vinden tussen de activiteit en de zuur-base eigenschappen van het katalysatormateriaal. De synthesemethode voor de LaOCl-materialen bleek van grote invloed te zijn op zowel de bulk- als oppervlakte-eigenschappen. In de experimenten met gasstromen werd de volgende trend in activiteit waargenomen: $LaCl_3$ << La_2O_3 < LaOCl-S < LaOCl-P. Het gebruik van CH_3OH als probe-gas liet zien dat LaOCl-P een hoger aantal sterke Lewis-zure plaatsen bevat dan LaOCl-S, in het bijzonder plaatsen die waarschijnlijk gebruikt worden voor de destructieve adsorptie van CCl_4. De hogere hoeveelheid chloor aan het oppervlak lijkt het aantal actieve Lewis-zure plaatsen aan het katalytisch oppervlak van LaOCl-P te verhogen. Dit verschil in sterkte van Lewis-zure plaatsen komt echter niet tot uiting in de CO adsorptie metingen met infrarood (IR) spectroscopie. Desalniettemin, geloven we dat de sterkte van de Lewis-zure plaats een belang-rijke factor is voor activiteit en dat sterkere Lewis-zure plaatsen resulteren in hogere intrinsieke activiteit voor de destructie van CCl_4. Basische zuurstof-plaatsen blijven nodig om de omzetting van CCl_4 tot CO_2 mogelijk te maken. Met andere woorden, een actief materiaal vereist een geschikt zuur-base paar op het katalytisch oppervlak.

Hoofdstuk 3 behandelt de destructieve adsorptie van H-bevattende gechloreerde C_1, namelijk $CHCl_3$, CH_2Cl_2 and CH_3Cl, over op La_2O_3-gebaseerde materialen. Twee reactiepaden zijn aangetoond, die resulteren in de vorming van fosgeen-achtige tussenproducten in de

gasfase ($CH_xCl_{2-x}O$). De basische zuurstof-plaats is in staat een H te ontrekken aan de reactant in de gasfase. Dit is een nieuw aspect voor de destructieve adsorptie in vergelijking met de experimenten met CCl_4. Het $CH_xCl_{2-x}O$ tussenproduct kan heradsorberen op het katalytisch oppervlak en door middel van chemisorptie worden verschillende oppervlaktestructuren gevormd, zoals carbonaten, formaten en methoxygroepen. De oppervlaktestructuren kunnen in elkaar omgezet worden en/of dissociëren tot gasvormige producten. De dissociatie van de oppervlaktestructuren is afhankelijk van de reactietemperatuur en het chloorgehalte van het katalytisch oppervlak. De gasstroomexperimenten toonden dat de initiële reactietemperatuur toeneemt met een afnemend aantal chlooratomen in het molecuul van de reactant. Deze trend is mogelijk het gevolg van de afnemende polarisatie in de bindingen van het C_1 molecuul als gevolg van het toenemende aantal H atomen. Een tweede factor van invloed is de mate van chlorering van katalytische oppervlak van LaOCl. Er bestaat een optimaal niveau van chlorering van het katalytisch oppervlak, wat zich vertaalt naar een optimale combinatie van Lewis-zure en basische oppervlakte-plaatsen. De chlorering van het oppervlak is, met betrekking tot het voorgestelde reactieschema, van directe invloed op de selectiviteit. Een materiaal met voldoende O bevordert het reactiepad waarbij H/Cl verwijderd wordt van het reactantmolecuul. Als H van het molecuul verwijderd wordt, dan worden minder gehydrogeneerde, en dus minder aantrekkelijke, tussenproducten en eindproducten gevormd. De chlorering van het katalytisch oppervlak gaat ook de vorming van carbonaten en CO_2 tegen. Daarom is een gechloreerde katalysator selectiever dan bijvoorbeeld zuiver La_2O_3.

In **Hoofdstuk 4** wordt de aandacht verlegd naar de dehydrochlorering van gechloreerde C_2, in het bijzonder C_2H_5Cl, 1,2-$C_2H_4Cl_2$ and 1,1,2-$C_2H_3Cl_3$, op La_2O_3-gebaseerde materialen. Een H en Cl atoom worden door het katalytisch oppervlak afgesplitst van het gechloreerde ethaanmolecuul, wat resulteert in de vorming van een hydroxylgroep en een roosterchloorion. Wanneer het oppervlak O-rijk is, zoals bij La_2O_3, zullen de hydroxylgroepen met elkaar reageren tot H_2O. Wanneer echter een specifiek chloreringsniveau van het katalytisch oppervlak is bereikt, dan neemt eliminatie van H_2O af en wordt HCl gevormd. Na een inductieperiode die gekenmerkt wordt door de vorming van H_2O, worden de conversie en product-verdeling constant. Ook de chloreringsgraad van het katalytisch oppervlak blijft dan constant. In situ IR experimenten hebben aangetoond dat op een relatief hoge temperatuur secundaire reacties kunnen plaatsvinden, zoals een tweede dehydrochloreringstap leidend tot de vorming van een ethyn, of destructieve adsorptie wat resulteert in de vorming van CO en CO_2. Dit geeft aan dat de reactietemperatuur en chloreringsgraad belangrijke factoren zijn om een optimale selectiviteit te verkrijgen voor de vorming van ethenen.

In **Hoofdstuk 5** is aangetoond dat $LaCl_3$ in staat is de H-Cl uitwisselingsreactie tussen CCl_4 en CH_2Cl_2 te katalyseren zonder de aanwezigheid van O-atomen. Om een hoge conversie op zowel volume- als op gewichtsbasis te bewerkstelligen, werden kooldraden als dragermateriaal voor $LaCl_3$ gebruikt. Het doel hiervan was om het katalytisch oppervlak sterk te vergroten in vergelijking met bulk $LaCl_3$-katalysatoren. Kooldraden hebben twee grote voordelen als dragermateriaal voor de H-Cl uitwisselingsreactie: 1) het is in staat de

agressieve voorbehandeling met HCl te weerstaan, en 2) het bevat geen O-atomen, wat destructieve adsorptie van de reactanten voorkomt. Density functional theory (DFT) berekeningen geven aan dat zwakgeadsorbeerde H- en Cl-atomen op het katalytisch oppervlak voorkomen als overgangstoestand. De reactie is geschikt voor de efficiënte omzetting van CCl_4, wat een stabiele en giftige stof is met een lage economische waarde. Nog belangrijker is het feit dat dit de eerste reactie is waarbij geen O-atomen betrokken zijn bij de uitwisseling van H- en Cl-atomen tussen CKWs in de gasfase.

Uit de bovengenoemde bevindingen blijkt dat op La-gebaseerde materialen veelzijdige katalysatoren zijn, die in staat zijn gechloreerde C_1 en C_2 via verschillende reacties om te zetten, zoals destructieve adsorptie, dehydrochlorering en H-Cl uitwisseling. Daarom is in **Hoofdstuk 6** het gebruik van op La-gebaseerde materialen in een aantal relevante toetsprocessen verkend.

Allereerst is aangetoond dat een mengsel van gechloreerde methanen en ethanen, nl. CCl_4, $CHCl_3$, CH_2Cl_2, 1,1,2-$C_2H_3Cl_3$ en 1,2-$C_2H_4Cl_2$, kan worden omgezet tot O-bevattende producten en gechloreerde ethenen, respectievelijk. De destructieve adsorptie van CH_2Cl_2 is minder gunstig indien CCl_4 en $CHCl_3$ ook aanwezig zijn. De dehydrochloreringsreactie wordt niet gehinderd door de destructieve adsorptie reactie. Sterker nog, een in meerdere mate gechloreerde katalysator vertaalt zich naar hogere selectiviteit voor gechloreerde ethenen.

Het tweede gedeelte bewijst dat CCl_4 een goede vervanger is voor HCl in de activering van methaan over $LaCl_3$ in aanwezigheid van zuurstof. De hydroxylgroepen die gevormd worden op het katalytisch oppervlak als gevolg van de chlorering van methaan, reageren in de conventionele reactie met HCl tot H_2O. Wanneer CCl_4 gebruikt wordt als chloreringsmiddel dan wordt de katalytische cyclus gesloten door een extra reactiestap: CCl_4 wordt omgezet tot CO_2 wat resulteert in chlorering van het katalytisch oppervlak, waarna de hydroxyl groep dissocieert naar HCl.

Als laatste werd in een enkele reactor de conversie van CH_2Cl_2 naar koolwaterstoffen getest over een La_2O_3 en een SAPO-34 katalysatorbed. De resultaten tonen dat slechts een kleine hoeveelheid CH_2Cl_2 wordt omgezet tot CH_4 and C_2H_4. Het lijkt erop dat SAPO-34 ook actief is voor de destructieve adsorptie van CH_2Cl_2, wat zou kunnen leiden tot een irreversibele deactivering van de katalysator. De conversie van CH_2Cl_2 naar koolwaterstoffen over een combinatie van een op La_2O_3-gebaseerd materiaal en SAPO-34 is in principe mogelijk. Er ligt echter een grote uitdaging in het controleren van o.a. de reactieomstandigheden.

Dit proefschrift heeft laten zien dat de chloreringsgraad van La-gebaseerde materialen van directe invloed is op de activiteit en selectiviteit bij de conversie van CKWs. De chloreringsgraad verandert echter als gevolg van de reacties met de CKWs. Daarom ligt de volgende uitdaging in het controleren van de chloreringsgraad tijdens reactie. Stoom is al gebruikt om de destructieve adsorptie van gechloreerde CCl_4 op La_2O_3-gebaseerde materialen katalytisch te maken, maar de invloed van stoom op de destructieve adsorptie van H-bevattende gechloreerde C_1 en de dehydrochlorering van gechloreerde ethanen is nog niet bestudeerd. Verder onderzoek naar de terugwinning van rooster-O, en dus de dechlorering van het katalysatormateriaal, is nodig voor controle van de samenstelling van de katalysator en reac-

ties die plaatsvinden op de katalysator. Verder kan onderzoek naar nieuwe combinaties van katalysatormaterialen en reacties, zoals toegelicht in Hoofdstuk 6, worden gebruikt om de omzetting van gechloreerde afvalstromen efficiënter en goedkoper te maken. Er zijn wellicht complexe technologische systemen nodig om de katalytische omzet-ting van CKWs te faciliteren, maar de op La-gebaseerde materialen kunnen voordelig zijn in toepassingen waarbij microreactortechnologie gebruikt wordt. Deze technologie heeft als voordeel dat de omzetting van de CKWs tot in detail geoptimaliseerd kan worden waarbij de risico's van blootstelling minimaal zijn.

List of Abbreviations

CHCs	Chlorinated hydrocarbons
CHC_1	Chlorinated C_1 hydrocarbons
CHC_{1-2}	Chlorinated C_1 and C_2 hydrocarbons
CHC_2	Chlorinated C_2 hydrocarbons
CKWs	Gechloreerde koolwaterstoffen
CNF	Carbon nanofibers
DFT	Density functional theory
DMP	Dimethyl pyridine
DNP	Double numerical with polarization
EN	Electronegativity
FEG	Field emission gun
GHSV	Gas hourly space velocity
GC	Gas chromatograph(y)
IR	Infrared
IRCH	Indiana relative chemical hazard
LUMO	Lowest unoccupied molecular orbital
MFC	Mass flow controller
na	Not applicable
PE	Polyethylene
PVC	Polyvinyl chloride
PVDC	Polyvinylidene chloride
RT	Room temperature
SAPO	Silicoaluminophosphate
SEM	Scanning electron microscopy
STM	Scanning tunnelling microscopy
TCD	Thermal conductivity detector
TPD	Temperature programmed desorption
XPS	X-ray electron spectroscopy
XRD	X-ray diffraction

List of Publications and Presentations

Publications

Destructive Adsorption of CCl_4 over La-Based Solids: Linking Activity to Acid-Base Properties
A. W. A. M. van der Heijden, V. Bellière, L. Espinosa Alonso, M. Daturi, O.V. Manoilova and B. M. Weckhuysen, *J. Phys. Chem. B* **2005**, 109, 23993-24001.

Intermediates in the Destruction of Chlorinated C_1 Hydrocarbons on La-Based Materials: Mechanistic Implications
A. W. A. M. van der Heijden, M. Garcia Ramos and B. M. Weckhuysen, *Chem. Eur. J.* **2007**, 13, 9561– 9571.

Dehydrochlorination of Intermediates in the Production of Vinyl Chloride over La_2O_3-Based Catalysts
A. W. A. M. van der Heijden, A. J. M. Mens, R. Bogerd and B. M. Weckhuysen, *Catal. Lett.* **2008**, DOI 10.1007/s10562-008-9436-2.

Catalyzed Hydrogen-Chlorine Exchange between Chlorinated Hydrocarbons under O-Free Conditions
A. W. A. M. van der Heijden, S. G. Podkolzin, M. E. Jones, J. H. Bitter and B. M. Weckhuysen, *Angew. Chem. Int. Ed.* **2008**, in press.

Patent applications

Metathesis of Chlorinated Waste Compounds
A. W. A. M. van der Heijden, J. H. Bitter and B. M. Weckhuysen, patent filed.

Oral presentations

LaOCl: Linking Activity to Structure
A. W. A. M. van der Heijden, V. Bellière, L. Espinosa Alonso, M. Daturi, O. V. Manoilova and B. M. Weckhuysen
Netherlands' Catalysis and Chemistry Conference
Noordwijkerhout, the Netherlands, March 2005

Destructive Adsorption of CCl_4 on La-Based Solids: Linking Activity to Acid-Base Properties
A. W. A. M. van der Heijden, V. Bellière, L. Espinosa Alonso, M. Daturi, O. V. Manoilova and B. M. Weckhuysen
Combined Workshops NIOK - NRSC-Catalysis
Utrecht, the Netherlands, October 2005

Mechanistic Studies on Conversion of Chlorinated C_1 Hydrocarbons over La-based Catalysts
A. W. A. M. van der Heijden, M. Garcia Ramos and B. M. Weckhuysen
Combined workshops NIOK - NRSC-Catalysis
Utrecht, the Netherlands, November 2006

Mechanistic Studies on Chlorinated C_1 Hydrocarbon Conversion over La-based Catalysts
A. W. A. M. van der Heijden, M. Garcia Ramos and B. M. Weckhuysen
Netherlands' Catalysis and Chemistry Conference
Noordwijkerhout, the Netherlands, March 2007

In- en ex-situ IR spectroscopie metingen aan recycling reacties van CKW's met lanthaan-oxide katalysatoren
A. W. A. M. van der Heijden, M. Garcia Ramos and B. M. Weckhuysen
Infrarood & Raman Discussie Groep Voorjaars bijeenkomst 2007
Delft, the Netherlands, April 2007

De Zoektocht naar de Perfecte Katalysator om Schadelijke Stoffen Af te Breken
A. W. A. M. van der Heijden
Academisch Café
Utrecht, the Netherlands, November, 2007

Poster presentations

Destructive Adsorption of CCl_4 on La-Based Solids: Linking Activity to Acid-Base Properties
A. W. A. M. van der Heijden, V. Bellière, L. Espinosa Alonso, M. Daturi, O. V. Manoilova and B. M. Weckhuysen
Netherlands' Catalysis and Chemistry Conference
Noordwijkerhout, the Netherlands, March 2006

Catalytic Destruction of CCl_4 on La-Based Solids: Linking Activity to Acid-Base Properties
A. W. A. M. van der Heijden, V. Bellière, L. Espinosa Alonso, M. Daturi, O. V. Manoilova and B. M. Weckhuysen
Second International Congress on Operando Spectroscopy
Toledo, Spain, April 2006

Destructive Adsorption of CCl_4 on La-Based Solids: Linking Activity to Acid-Base Properties
A. W. A. M. van der Heijden, V. Bellière, L. Espinosa Alonso, M. Daturi, O. V. Manoilova and B. M. Weckhuysen
Second Conference of the Coordination Action CONCORDE
Thessaloniki, Greece, January 2006

Destructive Adsorption of Chlorinated Hydrocarbons over Alkaline Earth Metal Oxides: Linking Basicity and Lewis Acidity to Catalyst Performances
A. W. A. M. van der Heijden, M. Garcia Ramos and B. M. Weckhuysen
20th North American Catalysis Society Meeting
Houston, United States, June 2007

Mechanistic Insight into the Catalytic Removal of Chlorinated C_1 Hydrocarbons over La-Based Materials
A. W. A. M. van der Heijden, M. Garcia Ramos and B. M. Weckhuysen
Europacat VIII
Turku, Finland, August 2007

Dankwoord

Dit is het laatste stuk tekst uit dit proefschrift wat ik schrijf. Bij iedere letter die ik tik begin ik meer te beseffen dat het bijna voorbij is. Het zijn 4 jaar van ontdekken, leren en zwoegen geweest die ik niet zou willen of kunnen missen. Hoewel het een korte periode lijkt te zijn geweest, kijk ik met trots en plezier terug op de vele ontdekkingen die we gedaan hebben. Natuurlijk heb ik op allerlei manieren hulp gehad van de mensen om mij heen. Ik wil iedereen hartelijk bedanken voor hun bijdrage en hier bij een aantal mensen in het bijzonder stilstaan om hen toe te spreken.

Bert, ik wil jou ten eerste bedanken voor de mogelijkheid die je me hebt gegeven om dit onderzoek te doen. Jouw positieve en enthousiaste manier van begeleiden heeft mij veel zelfvertrouwen gegeven en me in staat gesteld veel te leren. Ik heb je openhartigheid in persoonlijke gesprekken over wetenschappelijke en niet-wetenschappelijke zaken altijd erg gewaardeerd en heb ook altijd het gevoel gehad dat ik volledig open tegen jou kon zijn. Vooral de momenten dat ik nieuwe resultaten had, die we na vijven met de voeten op het bureau bespraken, waren inspirerend en motiverend. Jouw snelle nakijkwerk en steun voor mijn ontdekkingstocht in de wetenschapscommunicatie hebben ook van de afronding van dit proefschrift een prettige periode gemaakt. Bedankt voor alles wat ik geleerd heb in de afgelopen jaren.

It has been my pleasure to have worked with so many talented people in these past years. I would like to thank all the members of "Team Lanthanum". Olga, thank you for helping me get started with the research and making my first months a lot easier. Virginie, your endless energy and ability to party with anyone made you a great contribution to the research and the working atmosphere. Thank you for everything. Guinevière, you were only with us for a while, but I enjoyed your open way of speaking and will remember the interesting discussions we had. Leti, I can only admire the continuous growth you have shown since I first met you. You were excellent as an Erasmus student and have continued to be so as a PhD student and colleague. I wish you all the best with your own PhD research. I also want to thank Maria for all her hard work on her master's research. Even though I knew it was difficult for you sometimes, you kept working hard with a nice publication as a result. Good luck with you work in the "corporate jungle". René, je enthousiasme en leergierigheid tijdens zowel het tweedejaarsproject en je bacheloronderzoek waren erg plezierig. Veel succes met afronden van je studie en je toekomstige plannen. Ik wil Bart bedanken voor zijn literatuurscriptie die mede de basis heeft gelegd voor de experimenten van Hoofdstuk 6. Ik wens jou ook alle succes met je promotieonderzoek. Ik wil verder nog alle studenten die in het kader van het tweedejaars-project hebben meegewerkt aan dit onderzoek: David, Esther, Johnny, Rob, Hans, Suzanne, Arjan, René, Peter, Anke en Anoeska.

Tijdens metingen in het buitenland heb ik de hulp gehad van diverse experts. Ik wil Joeri Rogiers van Tessenderlo Chemie danken voor de ervaring met de chloorexperimenten en het gebruik van hun faciliteiten toen mijn eigen opstelling nog in opbouw was. I thank Marco Da-

turi of the University of Caen for helping me get settled in Caen and for his contributions to the measurements and the discussion of the results. I also thank Phillipe Bazin for his practical help with using the IR vacuum cell. Simon Podkolzin of the Dow Chemical Company is thanked for all the valuable discussions and the time he invested in the DFT calculations. You were always kind and patient with me, especially when I was just getting familiar with this topic. Elvira, I want to thank you in particular for the period of the IDECAT exchange. The results that we obtained in Munich were very nice and I thank you for the wonderful time with you and your colleagues in- and outside the lab. I still think you should become an ambassador for Bavaria (the region, not the beer).

Natuurlijk kan dit dankwoord niet zonder het noemen van alle mensen die werkzaam zijn bij en rondom onze groep in Utrecht. Ik wil Ad^{M} bedanken voor alle problemen die hij opgelost heeft en die hij mij heeft leren oplossen. Je zat een kamer verder van mijn opstelling en ik kon altijd binnenlopen als ik advies of gereedschap nodig had. Ik waardeer het enorm dat je ondanks je drukke bezigheden altijd tijd voor me wist vrij te maken. Natuurlijk ook bedankt voor het uitvoeren van de N_2-fysisorptie en XPS-metingen. Tom, de discussies met jou betreffende mijn IR resultaten maakten me altijd weer wijzer, ondanks dat we niet altijd tot een definitieve conclusie konden komen. Ook Fouad wil ik bedanken voor alle keren dat hij me heeft geholpen met spectroscopieperikelen. Jullie ontspannen houding en de subtiele pracht van spectroscopie maakten voor mij de derde verdieping in het Went een heerlijke plek om te werken. Harry, ik wil jou bedanken voor de gemoedelijke werksfeer waarin we samengewerkt hebben op het gebied van de kooldraden en de $LaCl_3$ katalysator. Fred, ik denk dat van alle keren dat ik de groeten van je kreeg via Kees, de eerste toch altijd het mooist zal blijven. Bedankt voor al je hulp en goede zorg. Dymph en Monique, jullie flexibiliteit en zorgen om alles zo goed mogelijk voor ons te regelen kunnen niet genoeg benadrukt worden. Heel erg bedankt. Verder wil ik Ad^{E} (XRF), Marjan (SEM/XRD), Vincent (TPD/ICT), Cor van der Spek (TEM), de glasblazerij en de instrumentmakerij bedanken voor hun assistentie.

Natuurlijk wil ik al mijn collega's bedanken voor alle leuke tijden die we meegemaakt hebben tijdens en naast het werk. De BBQs, borrels, sporttoernooien, etentjes en barhangavonden waren een welkome afwisseling van de wetenschap. Ik wil met name de mensen die mij op de kamer hebben moeten doorstaan bedanken voor hun geduld. Kees en Jelle, het is ongelofelijk hoe drie mensen die zoveel gezamenlijke interesses hebben zomaar bij elkaar kunnen komen te zitten in een werkkast in het Went. Ik denk dat we geen betere combinatie van persoonlijkheden hadden kunnen hebben en wil jullie bedanken voor alle humor, discussies en gezelligheid van de laatste jaren. Hoewel de (mid)dagen soms te snel voorbijvlogen op onze kamer, was de sfeer altijd fantastisch. Ik hoop gauw weer naar een SUWU3 optreden te komen Kees! En Jelle, kun jij misschien voor mij ook zo'n ereburgerschap regelen van Bergeijk? Maakt vast indruk bij de familie… Cynthia, thank you for the short time we were "workroomies" and your love for small talk (like me). Best of luck with your postdoc!

Tenslotte wil ik de mensen bedanken die achter de schermen geholpen hebben om dit promotie-onderzoek tot een goed einde te brengen. Ik wil mijn vrienden en familie bedan-

ken voor hun steun en geduld in de laatste maanden toen ik wat minder in de gelegenheid was om af te spreken. In het algemeen wil ik alle mensen van de Zeister tafeltennisvereniging bedanken voor alle gezelligheid en sportiviteit. Mijn buurman Davorin, bedankt voor de gezellige gesprekken als ik pauze nodig had van het schrijven. Sander, een ferme ruzie toen we elkaar voor het eerst ontmoetten en sindsdien zijn we in verschillende fases van ons leven be-vriend gebleven. Bedankt voor al je hulp en vriendschap. Ruud en Laurens, ik noem jullie samen omdat we sinds ons 14^{e} jaar altijd contact met elkaar hebben gehouden. We hebben alle drie het pad van de promotie gevolgd en ik hoop dat ons contact er altijd zal blijven. Lai Mei, je bent een (studie)vriend door dik en dun en ik ben dan ook erg blij met jou als paranimf. Het feit dat je bereid bent van de andere kant van de wereld ervoor terug te komen vereert me. Natuurlijk is mijn naaste familie ook een vaste steun voor me geweest. Ik wil mijn beiden oma's bedanken, mijn ooms en tantes, neven en nichten. De familiegelegenheden zorgen altijd voor warmte, zelfs als we elkaar lang niet hebben gezien. Mijn opa's kunnen hier helaas niet meer bij zijn, maar de invloed van hun sterke en vriendelijke karakter heeft mij mede gevormd en mag hier niet vergeten worden. Ik wil mijn broer, Ron, bedanken dat hij paranimf wil zijn en dat hij bereid is een pak aan te trekken hiervoor (knipoog). Ik wil ook mijn ouders bedanken voor het feit dat ze van jongs af aan mijn nieuwsgierigheid hebben gestimuleerd en mij geleerd hebben vol te houden en door te zetten. Hierdoor heb ik mezelf kunnen ontplooien en mijn eigen keuzes leren maken.

Mijn laatste regels zijn voor de liefde van mijn leven: Lai Ting. Jij hebt de volledige promotie periode meegemaakt en de laatste twee jaar zelfs van zeer dichtbij. Ik kan je niet genoeg bedanken voor al het goede dat je me hebt gebracht. Je bracht rust, liefde en steun in mijn leven, iets wat onmisbaar was en is. Om nog maar te zwijgen over alle hulp met het grafische werk die je gegeven hebt aan deze soms gefrustreerde wetenschapper. We gaan nu allebei een nieuwe toekomst tegemoet. Ondanks dat we niet precies weten hoe die eruit gaat zien, heb ik er het volste vertrouwen in omdat het samen met jou zal zijn.

Alwies

Curriculum Vitae

Alwies van der Heijden werd geboren op 14 juni 1980 te Bergeijk. In 1998 behaalde hij het VWO-diploma aan Scholengemeenschap Were Di Locatie Merendreef te Valkenswaard. Ditzelfde jaar ging hij ook Scheikunde studeren aan de Universiteit Utrecht. In maart 2004 studeerde hij met genoegen af bij de sectie Anorganische Chemie en Katalyse onder begeleiding van Dr. D.E. Keller en Prof. Dr. Ir. B.M. Weckhuysen. Vanaf februari 2004 werkte hij als assistent in opleiding (AiO) in de groep Anorganische Chemie en Katalyse van de Universiteit Utrecht. De promotie werd gedaan onder supervisie van Prof. Dr. Ir. B.M. Weckhuysen. De bevindingen van het onderzoek zijn beschreven in dit proefschrift.

Alwies van der Heijden was born on the 14th of June 1980 in Bergeijk. In 1998 he obtained his diploma of secondary school at Scholengemeenschap Were Di Locatie Merendreef in Valkenswaard. In the same year he started with a study of Chemistry at Utrecht University. In March 2004 he received his master's degree with credit in the section Inorganic Chemistry and Catalysis under supervision of Dr. D.E. Keller and Prof. Dr. Ir. B.M. Weckhuysen. In February 2004, he started working as a PhD student in the group Inorganic Chemistry and Catalysis at Utrecht University. The research was performed under supervision of Prof. Dr. Ir. B.M. Weckhuysen. The findings of the research are described in this PhD thesis.